Volume Changes during Fracture Injection of Biosolids

by

Guowei Xia

A thesis
presented to the University of Waterloo
in fulfillment of the
thesis requirement for the degree of
Master of Applied Science
in
Civil Engineering

Waterloo, Ontario, Canada, 2007

AUTHOR'S DECLARATION

I hereby declare that I am the sole author of this thesis. This is a true copy of the thesis, including any required final revisions, as accepted by my examiners.

I understand that my thesis may be made electronically available to the public.

Abstract

The term biosolids refers to the nutrient-rich organic materials resulting from the treatment of domestic sewage at a wastewater treatment facility. It is a widely acceptable term for sewage sludge that has been treated at a wastewater treatment plant and is beneficially recycled. Biosolids inherently come from sewage sludge, so they have the same origin and biological nature, but a different applicability. The quantity of municipal biosolids produced increases annually in the United States. The production of biosolids has increased because of both the advance of sanitation and wastewater treatment and the growth of population.

Sludge or biosolids are contaminated by varying amounts of heavy metals or hazardous organic compounds from industrial and commercial wastewater. Therefore, society has to face the potential for increased negative impacts on the environment from the increasing volume of biosolids being produced. Public concerns about applied biosolids treatment or reuse methods are potential health, environmental, or aesthetic impacts (such things as disease, odors), because of the pollutants in the biosolids.

The most commonly used methods for biosolids treatment and recycling are briefly reviewed in the first two chapters of this thesis. However, the current biosolids treatment or recycling options have their own defects. A new and innovative technology, deep biosolids injection, is proposed for the treatment of biosolids and is to be implemented by Los Angeles where the City has been granted underground solids injection control permits under Class V wells by the US Environmental Protection Agency.

Deep biosolids injection is a process referred to as one type of several deep underground injection techniques. It shares many similarities with slurried solids injection above the fracture pressure, which has been successfully used for the treatment of slurried non-hazardous solid materials produced in the oil industry such as drill cuttings, viscous emulsions with clay, oily sand, NORMs (naturally occurring radioactive materials), pipe scale, tank bottoms, soil from spill clean-up, and so on.

The distinctive biosolids properties result in injection mechanisms different from other slurry injection processes. Filtration and consolidation processes occur simultaneously along with injection of biosolids, and these must be understood in order to properly design and manage a biosolids injection operation. Hydraulic fracture mechanisms, filtration theory and consolidation principles provide the basis for the interpretation of biosolids injection process.

A semi-analytical hydraulic fracture model for injection of a compressible substance (biosolids) is developed as a modification of the Perkins-Kern-Nordgren (PKN) hydraulic fracture model. The PKN model is modified with a pseudo-dynamic leak-off function that describes the deposition of biosolids (filtration) and plugging effect of biosolids on the fracture wall in a porous medium. The pseudo-dynamic leak-off function is given in terms of the net pressure and the resistance of the filter cake to flow. The hydraulic fracture model is employed to compute the volume of biosolids slurry remaining in an open induced fracture. The consolidation process in the closure phase of deep biosolids injection is described using the biosolids properties under different stress conditions. A Terzaghi-type

relationship is used to compute the volume change in the closure phase using compressibility data available from published literature.

In contrast to the conventional PKN leak-off model, simulation results using the new model show that the induced fracture volume is much larger because of the impaired leak-off and because of the volumetric effects and consolidation of the biosolids in the fracture. Solids contents and biosolids compaction behavior have significant impacts on the geometry of fracture (width, length, volume) over time. The model was developed to help guide large-scale injection of municipal and animal biosolids as an environmentally more secure method of treatment than surface approaches.

Acknowledgements

I would first like to thank my supervisor Dr. Maurice Dusseault, for his valuable guidance and financial support. I also appreciate Dr. Leo Rothenburg and Dr. Giovanni Cascante for their worthwhile comments and review of this thesis.

I would also like to thank Roman Bilak, President Terralog Techonogies Inc for the valuable ideas on slurry fracture injection and for the generous access to the company's data archives.

To many friends I have made, I give thanks for their part in making the M.A.Sc. experience both pleasurable and memorable. These thanks will go to all persons at University of Waterloo and Terralog Technologies Inc who provided me support and helped me to spend my time in a memorable way, especially Dr. Baoci Xu, Betty Dusseault, Dr. Gang Han, and Suzanne Olmstead.

To Mom, Dad, I am grateful for your endless support for me to pursue my interest.

Finally, I acknowledge with thanks the financial support I received over the course of my graduate program from Terralog Technologies Inc (Calgary) and the faculty of engineering of the University of Waterloo.

Table of Contents

List of Figures

List of Tables

SYMBOLOGY

$[\cdot]$	tensor, as in $[\sigma ij]$ or $[kij]$
$\{\cdot\}$	vector of values, e.g. {p} pressures at points
Δ	change in X, e.g.: ΔV = volume change
A	fracture face area (L^2), m^2
A_c	fracture cross-section area (L^2), m^2
c_l	leak-off coefficient ($L/t^{1/2}$), ($m/s^{1/2}$)
C_c	compression Index (Lt^2/M), kPa^{-1}
C_s	coefficient of secondary compression
C_v	coefficient of consolidation (L^2/t), mm^2/d
e	void ratio
E	Young's modulus (M/Lt^2), MPa or GPa
G	Shear modulus (M/Lt^2), GPa
G_s	specific gravity of solids
h	height of fracture (L), m
k	permeability (L^2), darcy D
K	hydraulic conductivity or coefficient of permeability (L/t)
m	Dry mass of solids (M), Kg
m_v	coefficient of volume compressibility (Lt^2/M), kPa^{-1}
P_b, P_f, P_{bore}	breakdown & fracturing injection pressure, bore hole pressure (M/Lt^2), kPa, MPa
P_p, P_w, P_{prop}	far-field pore pressure or initial formation pressure, well bore net pressure, fracture propagation pressure (M/Lt^2), kPa, MPa
P_L, P_S	liquid pressure, solid pressure (M/Lt^2), kPa, MPa
P_i	reference pressure (M/Lt^2), kPa, Mpa
p_0	pore pressure (M/Lt^2), kPa, MPa
L	fracture half length (L), m
q	rate of flow through a cross-section of the fracture (L^3/L^2 t), m/s
q_l	rate of flow leaking off from the fracture face area (L^3/L^2 t), m/s
q_{Leak}	rate of leak-off flow per unit fracture length (L^3/L t), m^2/s
q_L, q_S	liquid flow rate, Solids flow rate (L^3/t), m^3/s
Q	injection rate (L^3/t), m^3/s
Q_l	leak-off rate or filtration loss rate (L^3/t), m^3/s

R_0	reference resistance for the formation (L^{-2}), m^{-2}
S_P	spurt loss coefficient (L^2), m^2
S_g	specific gravity of slurry (dimensionless)
SC	solids content %
t_c	characteristic time (t), s
u	pore water pressure (M/Lt^2), kPa, MPa
u_L, u_S	velocity of the liquid, velocity of the solids (L/t), m/s
V	volume (L^3), m^3
W, $\overline{w}$	maximum width of the fracture, averaged width (L), m
w_i	water content unit in percentage
Y	thickness of filter cake (L), m
α, α_{av}, α_i	specific resistance, averaged specific resistance, reference resistance (L-2), m^{-2}
β, n, δ	compatibility parameters dimensionless
β_T	linear thermal compressibility ($\Delta L/LT$), $°C^{-1}$
ε	strain, compressive positive ($\Delta L/L$)
ε_s, ε_{sav}	volume fraction of solids, averaged volume fraction (defined as solidosity) in percentage units
μ	viscosity (M/Lt), centipoises cP
μ_f	growth-rate of the fracture length (L/t), m/s
ν	Poisson's ratio
σ, σ'	total, effective compressive stress (M/Lt^2), MPa
σ_1, σ_2, σ_3	principal compressive stresses (M/Lt^2), MPa
σ_v, σ_h	total vertical stress, total horizontal stress (M/Lt^2), MPa
σ_{hmin}, σ_{hmax}	minimum, maximum total horizontal stress (M/Lt^2), MPa
σ_T	tensile failure stress of the rock, (M/Lt^2), MPa
γ	unit weight (MN/m^3)
ϕ	porosity unit in percentage
ν	Poisson's ratio
τ	time at which fluid leak-off begins at position x (t), s
ω	volume of inert solids per unit area (L^3/L^2), m^3/m^2
ρ	density (M/L^3), kg/m^3

Chapter 1
Introduction

1.1 General

Biosolids refers to the nutrient-rich organic materials resulting from the treatment of domestic sewage at a wastewater treatment facility. As by-product at wastewater treatment plants, the quantity and quality of biosolids are dependent on the treatment standard and amount of wastewater required to be treated. Since more stringent regulations were issued and population of US has increased, biosolids present quantitative and qualitative problems. Nowadays, most biosolids in the US are currently managed by application to farmland, lagoons, or landfills. As the rapid suburbanization of farmland, this practice becomes increasingly difficult and restricted. Biosolids are also contaminated by varying amounts of heavy metals or hazardous organic compounds from industrial and commercial wastewater. Therefore, public concerns about applied biosolids treatment or reuse methods are potential health, environmental, or aesthetic impacts (such things as disease, odors), because of the pollutants in the biosolids. This thesis introduced an alternative technology to inject biosolids into the deep subsurface. In that high temperature environment, the biosolids will undergo a naturally accelerated process of biodegradation which is increased by the high temperature. Deep biosolids injection is a process referred to as one type of several deep underground injection techniques. It shares many similarities with slurried solids injection above the fracture pressure, which has been successfully used for the treatment of slurried non-hazardous solid materials produced in the oil industry such as drill cuttings, viscous emulsions with clay, oily sand, NORMs (naturally occurring radioactive materials), pipe scale, tank bottoms, soil from spill clean-up, and so on.

The major research objective is to estimate the amount of biosolids injected into underground reservoirs. Because, first, large amounts of injected biosolids emplaced underground near the well bore could affect the *in situ* stress profile, in order to maintain safety operation, operators should have a basically understand of the operation procedures which is in compliance with the volume of injected slurry. Second, the amount of methane produced is dependent on the *in situ* volume of biosolids. In addition, the recycled methane has economic value that could offset the operation costs. For the biosolids injection, the distinctive biosolids properties result in injection mechanisms different from other slurry injection processes. Filtration and consolidation processes occur simultaneously along with injection of biosolids, and these must be understood in order to properly design and manage a biosolids injection operation. Hydraulic fracture mechanisms, filtration theory and consolidation principles provide the basis for the interpretation of biosolids injection process. In addition, most hydraulic fracture models are developed to simulate the hydraulic fracture processes with regular fracture fluids without solids contents in them. So those models could not provide suitable simulation results.

A semi-analytical hydraulic fracture model for injection of a compressible substance (biosolids) is developed as a modification of the Perkins-Kern-Nordgren (PKN) hydraulic fracture model. The PKN model is modified with a pseudo-dynamic leak-off function that describes the deposition of biosolids (filtration) and plugging effect of biosolids on the fracture wall in a porous medium. The pseudo-

dynamic leak-off function is given in terms of the net pressure and the resistance of the filter cake to flow. The hydraulic fracture model is employed to compute the volume of biosolids slurry remaining in an open induced fracture. The consolidation process in the closure phase of deep biosolids injection is described using the biosolids properties under different stress conditions. A Terzaghi-type relationship is used to compute the volume change in the closure phase using compressibility data available from published literature.

In contrast to the conventional PKN leak-off model, simulation results using the new model show that the induced fracture volume is much larger because of the impaired leak-off and because of the volumetric effects and consolidation of the biosolids in the fracture. Solids contents and biosolids compaction behavior have significant impacts on the geometry of fracture (width, length, volume) over time. The model was developed to help guide large-scale injection of municipal and animal biosolids as an environmentally more secure method of treatment than surface approaches.

1.2 Goals and Methodology

The main goals of this study are as follows:

- Summarize current biosolids management practices
- Introduce hydraulic fracture injection of biosolids
- Identify impacts of biosolids filter cake on the induced fracture geometry
- Estimate volume changes during one cycle-injection
- Design and develop a model with can couple filtration of biosolids with hydraulic fracture injection
- Evaluate the model by adjusting different input parameters to determine their sensitivities to the model results

To achieve these goals, the published and unpublished literatures on hydraulic fracture, filtration of highly compactable material and consolidation of sludge were reviewed. The available professional papers discussing deep biosolids injection and biodegradation of biosolids were referenced. A semi-numerical model was developed to evaluate the volume changes during one-cycle injection of biosolids. Numerical codes programmed by Matlab are used to test the model and to estimate the volume changes during the fracture injection of biosolids. A Terzaghi-type relationship is used to compute the volume change in the closure phase using compressibility data available from published literature

1.3 Thesis Organization

This thesis consists of six chapters and one appendix. After the general introduction and the description of goals and methodologies for this research, Chapter 2 begins with the introduction to biosolids.

Chapter 2 first introduces the background of biosolids. It includes the source of municipal biosolids, current systems for the treatment or recycling of sewage sludge and biosolids, characteristics of biosolids and factors in biosolids management. The term biosolids is widely accepted for sewage sludge that has been treated at a wastewater treatment plant and is beneficially recycled. With the annual increase of biosolids production, biosolids present quantitative issues. In addition, the composition of biosolids will add qualitative issues to the society. Therefore, biosolids impose their impacts on human life and environment. Their impacts and factors in biosolids management are discussed in detail.

Chapter 3 describes the conventional municipal biosolids treatment practices and one innovative technology for biosolids management. A brief summary of current biosolids management methods demonstrates their advantages and disadvantages. A comparison table listing widely used management methods clearly shows their adaptabilities, costs and environmental risks and safety.

In Chapter 4, mechanisms for deep underground injection of biosolids are discussed. Since the operation of deep injection incorporates hydraulic fracture process with filtration of biosolids and consolidation process, literature reviews on mechanism of hydraulic fracture, filtration theory of highly compactable material and consolidation principles are conducted.

In Chapter 5, a physical model is developed to estimate the volume changes during one cycle-injection. The model is divided into two parts in terms of active injection phase and closure phase. For the active injection phase, a semi-analytical hydraulic fracture model for injection of a compressible substance (biosolids) is developed as a modification of the Perkins-Kern-Nordgren (PKN) hydraulic fracture model. The consolidation process in the closure phase of deep biosolids injection is described using the biosolids properties under different stress conditions. A Terzaghi-type relationship is used to compute the volume change in the closure phase using compressibility data available from published literature. And model results and discussion are presented in Chapter 6.

Chapter 7 indicates the implication and future work.

Appendix A presents the numerical codes that are used to compute the fracture propagation with filtration of biosolids, which is written by Matlab.

Chapter 2
Introduction to Biosolids

2.1 Sewage Sludge and Municipal Biosolids

The term sewage sludge is widely known by the public and it is also commonly used in the wastewater profession. It refers to bioactive slurry with a combination of water, microorganisms for the treatment of wastewater, organic matter and inorganic matter. Sludge must be recycled or disposed of properly by following a set of regulations. The alternative term biosolids for municipal sewage sludge is starting to prevail, as it indicates the biological nature of the waste slurry.

The term biosolids is defined as: "nutrient-rich organic materials resulting from the treatment of domestic sewage at a wastewater treatment facility" (National Biosolids Partnership 2005a). Its distinction from sludge can be deduced from the definition of biosolids by the US Environmental Protection Agency (EPA 1994): "Biosolids are a primarily organic solids product produced by wastewater treatment processes that can be beneficially recycled." The Water Environmental Federation (WEF) emphasizes this distinction (NEBRA 2005). From the definition given by WEF, we find that the biosolids and sludge have the same origin and biological nature, but different applicability. The term biosolids for sewage sludge is widely accepted and the word "treated" generally is emphasized so that it is clear that the material meets regulations for future land application, recycling or reuse.

Many other organic residuals like paper mill sludges and animal manure (e.g. from cattle, fowl, and pigs) are also of biological origin and could be classified as biosolids.

2.1.1 Source of municipal biosolids

Biosolids are by-product at wastewater treatment plants. The wastewater, primarily composed of domestic sewage, is usually treated at a publicly-owned municipal treatment plant. Meanwhile, industrial and commercial wastewater will discharge into sewer networks connected to the municipal wastewater treatment plant. Hence, the biosolids will contain some amount of contaminants such as heavy metals or organic compounds depending in part on the ratio of domestic sewage to other sewage.

The predominant wastewater treatment processes used are primary and secondary treatment. Tertiary treatment may be required to achieve the lower levels of risk needed for the discharge of effluent in certain environmentally sensitive areas. The solids removed during the primary and secondary treatment in a wastewater treatment plant are preliminarily called sewage sludge or raw sludge, which can be disposed by incineration, landfills, or further treatment. Biosolids are produced when sewage sludge undergoes further treatment such as digestion, composting or alkaline

stabilization. The nature of domestic wastewater results in sludge rich in organic matter that can be ameliorated with the widely used biological treatment process in wastewater treatment plants.

Biosolids have inherently similar compositions to wastewater sludge; they are mostly water, and much of the non-water particles are of biological origin. Biosolids consist of both biological and inert solids in the wastewater as well as perhaps some substances added for the purpose of treatment.

This thesis uses information on waste treatment in the United States. Canadian data and treatment approaches are generally similar, but the American data are more easily accessed therefore they are used.

The annual production of municipal biosolids in United States has increased since 1972. The quantity increased dramatically from 4.6 million dry tons in 1971 (Bastian 1997) to 6.9 million dry tons in 1998. When the Clean Water Act, the minimum treatment requirements for wastewater, was issued in 1974, the quantity of biosolids increased by 50% from 1972 and, meanwhile, the population increased by 29% from 1972 to 1998 (US EPA 1999). The amount of biosolids will continue to increase in the United States because the population is growing, and more and more municipalities are using treatment facilities. Figure 2.1 shows the quantities and distribution of biosolids use and disposal in the USA in 1998.

Generally speaking, the amount of biosolids and its quality are highly dependent on the level of wastewater treatment, as well as the sources of the wastewater. The cleaner the water obtained from the wastewater treatment, the larger the amount of biosolids generated. Furthermore, the concentrations of pollutants in the biosolids will be increased because of the higher efficiency of removal of constituents in the wastewater. Wastewater treatment uses additional chemicals to increase the efficiency of treatment; chemicals such as ferric chloride, alum and lime used to settle solids will finally end up in the biosolids (e.g., aluminum hydroxide for phosphorus removal).

Industrial discharge into the sewage system has a significant impact on the quality and quantity of biosolids because it mixes at the municipal wastewater treatment plant with the domestic sewage. Since the federal and state governments in the United States enforce certain regulations relating to the pretreatment of the industrial discharge, pollutants such as heavy metals or organic compounds in the industrial waste streams must be reduced before discharge. Consequently, the characteristics of biosolids are related to the pretreatment of the industrial discharge as well as the municipal wastewater treatment process.

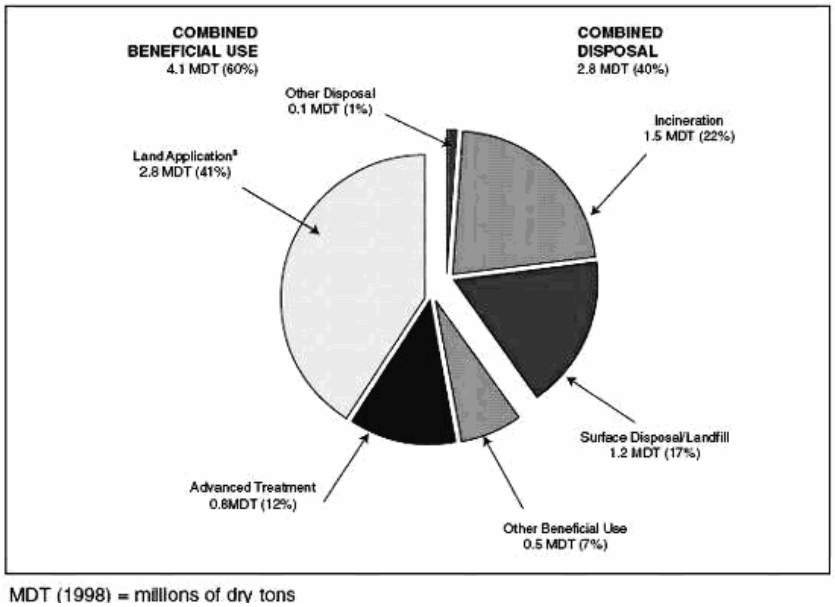

Figure 2.1 Estimation of biosolids use and disposal 1998 (US EPA, 1999)

2.2 Systems for the Treatment or Recycling of Sewage Sludge and Biosolids

The treatment or recycling of sewage sludge is regulated under federal environmental statutes in all major industrialized countries. All biosolids (or slurried solid streams) are required to be treated or recycled in a safe and environmentally acceptable manner.

Biosolids management practices primarily involve land application and land surface disposal. In land application, the biosolids can be recycled or reused with compost or other highly treated organic materials for beneficial use such as landfill cover or land reclamation. Other biosolids management options include landfill, surface spreading and incineration.

Options for the treatment or utilization of biosolids are:

- Direct land application
- Composting and land application
- Heat drying and land application
- Incineration
- Landfilling

2.3 Characteristics of Biosolids

The characteristics of biosolids can be grouped into three categories: physical, chemical and biological. The physical properties will affect the method of treatment. The chemical and biological properties will profoundly impact environmental and social issues. Public concerns mostly arise from the chemical and biological properties.

Physical properties of biosolids:

- Solid content/water content
- Organic matter content
- Shear strength properties
- Compactibility

For the application of biosolids to the ground surface, the physical properties will affect the method of application to some extent as the soil's physical and chemical properties can be altered by the biosolids applied.

The physical properties of biosolids are critical to make decisions on the selection of sites for landfills, especially for enhanced bioreactors and composting sites. The settlement of biosolids in the landfill is also an important factor affecting the stability or performance of the landfill site.

Chemical properties of biosolids:

- pH
- Soluble salts content and type
- Plant nutrients - macroscopic and microscopic
- Essential and non-essential trace elements for humans and animals, particularly heavy metals
- Organic chemicals

Biosolids contain trace elements and heavy metals coming primarily from industrial, commercial and residential discharges in the wastewater system. Many of the regulated heavy metals are essential to animals and humans and plants, but only in trace amounts. Some trace elements like zinc are often deficient in soils and may also be vital to human development. Other heavy metals or trace elements are toxic to animals, humans and plants. Plant nutrients such as P or N can supply necessary materials for growth, but an excess of them will negatively impact the environment (e.g.: groundwater nitrification, algae bloom on run-off water courses).

Biological properties of biosolids:

Biological characteristics of wastes may affect human health and the environment. All biosolids contain a wide variety of microbes. Many of these are beneficial, while others can be harmful to humans, animals, or plants. The microbial population in biosolids is also important to the decomposition of organic matter (Epstein 2002).

2.4 Factors in Biosolids Management

Odor, pathogens (e.g. disease-causing bacteria and viruses), biodegradable toxins (e.g. hydrocarbons), biological vectors (e.g. rodents and flies) as well as heavy metals should be taken into consideration for biosolids management. Part 503 Rule (US EPA 1994) defines two types of biosolids with respect to pathogen reduction: Class A (no detectable pathogens) and Class B (a reduced level of pathogens). It also imposes a vector attraction reduction requirement as well as providing many alternatives for meeting the requirement. Hence, the characteristics and classification of biosolids can affect biosolids management decisions in several ways. Biosolids can be used as any other fertilizer or soil amendment product only when those factors meet the "Class A" pathogen level, the vector attraction reduction requirements, and the high-quality pollutant concentration limits for metals (or any other specified material). The composition of the biosolids may have a significant impact on their management, but other physical and social factors such as cost of management, site location, and transportation of biosolids are also important. Table 2.1 shows the major management control points for the successful management of biosolids.

Table 2.1 Overview of management control points for biosolids (US EPA,2002a)

Issues	Self-Monitoring Checklist	Control Options
1. Biosolids Generating Facility		
Odors and aesthetics Consistency of biosolids Biosolids treatment	Assess biosolids to determine 503 treatment criteria for pathogens and vector attraction reduction Degree of stability and odor potential includes factors such as volatile solids content; lime, polymer and iron usage, and pH Physical consistency Ratio of primary to secondary Cleanliness of equipment Time of retention after treatment	Generator, storer and land applier communicate about status of biosolids treatment or problems Reduce post-treatment retention Have options to divert unacceptable loads Reevaluate treatment and handling practices to address chronic issues Provide further treatment Provide vehicle cleaning station
2. Transportation		
Odors and aesthetics Traffic and safety	Proper equipment in compliance with State and Federal Transportation Regulations Regular inspections and maintenance of vehicles and equipment Suitable haul routes Vehicles and equipment kept clean	Train drivers Plan/inspect haul route, minimize time in transport Emergency spill plan and supplies in place Maintain and clean trucks and equipment regularly
3. Field Storage Site		

Odors and aesthetics Water quality and environmental protection Safety and health protection	Proper site location & suitability Proper design of field storage or constructed facility - run-on and run-off controls - accumulated water control - buffers Biosolids quality vs. length & amount in storage Operations and maintenance plan Odor prevention and mitigation plan Spill control and response plan Safety plan	Regular self inspections of site and operations Consistent implementation of management plants Self monitoring of biosolids quality and condition Revision of management plants when necessary - change amount or length of storage - implement odor control and mitigation measures - implement additional structural or site management practices Remove stored biosolids when atmospheric conditions are conductive to low odor impacts on neighbors

2.4.1 Social and environmental issues

Public opposition in some areas of the United States and Canada has hindered the beneficial use of biosolids. Most concerns from the public are about potential health, environmental, or aesthetic impacts (e.g., risk of disease, odors) because of the pollutants in the biosolids. Furthermore, the public's perception can have a large impact on the possibility of biosolids treatment and application as well as the location of the treatment site. Although public perception often does not rely on science, it can be voiced irrespective of the degree of risk, and must be taken into account.

Society must face the fact that there are increased volumes of biosolids produced in part because of the advance of sanitation and wastewater treatment (higher levels of treatment generate more wastes), which in combination with population growth has resulted in larger volumes of sewage sludge and biosolids.

2.4.1.1 Land use and water quality issues

After stabilization treatments, biosolids are allowed to be beneficially used. Land use is still a big concern for surface disposal of biosolids because this may involve a large land area for a large city. For example, large cities such as Toronto, Los Angeles and Vancouver have severe problems in finding enough land area for biosolids application and often must seek other solutions.

Although biosolids can be beneficially applied to agricultural land or to forested or grass lands through careful and controlled application, the demand from agriculture alone can not balance the locally variable supply in many cases; and the long-term contamination potential for water bodies by leachate from the biosolids is still in question.

Constituents such as nutrients, organic matter, pathogens and metals which inevitably exist in biosolids have potential impacts on water quality. These constituents can contaminate water bodies through management practices such as landfill storage on or application to soil. These constituents are conveyed by seepage flow of the leachate into groundwater, streams and other water bodies. If significant amounts of the negative constituents are present in the biosolids, and possible transport pathways exist for surface water and groundwater, contaminants in leachate can negatively impact groundwater resource.

Landfills have served as the main method for surface disposal, and this method has potential for constituents moving out of site, driven by precipitation events or seepage. When run-off or leachate containing soluble and particulate components is generated, it constitutes an attack on the surrounding water body or groundwater. Nitrogen and phosphorus are present in significant amounts in biosolids and this must be taken into consideration when biosolids are applied as soil amendment or fertilizer, as well as in surface landfill disposal. Nutrients such as nitrogen or phosphorus enter into surface waters in runoff or seep into groundwater; this may provide excess amounts of nutrients for crops or other organisms, as well as contaminating the groundwater. The surplus of nitrogen and phosphorus

mainly contributes to the eutrophication of surface water (consumption of all the oxygen), which impairs use for fisheries, recreation, industry and drinking water sources. The leachate from landfill or land application is a primary concern for long-term impacts on groundwater as it has the potential, for example, to give excess soluble nitrate – NO_3 – in drinking water sources. High nitrate levels in wells have resulted in some cases of methemoglobinemia in susceptible infants. This serious condition reduces the blood's ability to carry oxygen efficiently; hence the condition's other name "blue baby syndrome". Elevated nitrate levels in water can have the same effect on immature horses and pigs and can also cause abortions in cattle (US EPA 2000a).

2.4.1.2 Odor issues

Odors are a major reason why the public is reluctant to accept local biosolids recycling and treatment projects. However, if projects are operated properly, they have positive effects on the people's lives where biosolids are applied as agricultural fertilizers. Odor management is therefore a high priority for environmental protection. Detectable odorous compounds are generated and emitted from the biosolids during biosolids treatment, storage and use. The main odorants are ammonia, amines, and sulfur-containing compounds. US EPA's documents report that "ammonia is the most commonly-found odor agent in the emission from biosolids. It is not detectable as easily as reduced sulfur compounds, but at high concentrations it is so intense that it strongly masks odors from other compounds, such as those containing reduced sulfur groups."(US EPA 2000a). Amines are easily detected when it is generated through high-temperature treatment processes and are usually accompanied by ammonia emissions. The sulfur compounds, however, draw the most attention and are reported to be detectable in small amounts from various treatment processes. Other odorants includes dimethylsulfide, dimethyl disulfide and methyl mercaptan" (US EPA 2000a).

Odors may also under some conditions be linked with the emission of aerosol pathogens; pathogens are a particular threat to human health and must be controlled or eliminated. Other public concerns linked with odors include aesthetic issues and nuisance issues.

Offensive odors can hinder public acceptance of beneficial use of biosolids because the bad smell and any potential relation with toxic residues from municipal and industrial waste trigger public concerns. In some areas, rapid suburbanization of former farmland makes land application no longer feasible because sites for land application are fewer and are closer to denser human habitats. This reduces the quantity of farmland for biosolids use as fertilizer or soil amendment. Appropriate treatment and good management practices can control most odor problems; however, even the best operations may occasionally emit offensive odors. Hence, odor-control methods are needed for good management of biosolids and are implemented through cooperative efforts with others (i.e., generator, transporter, storer, and applier). There are a number of suitable ways available for solving this problem such as biofilters or neutralizing solutions.

Success in controlling odor is largely dependent on the degree of stabilization of biosolids achieved at the wastewater treatment plant prior to delivery to sites for further treatment (e.g. composting), direct application (e.g. spraying on pasture land), or immediate disposal (e.g. landfills). If the organic matter and nutrients are present in forms that microbes readily use, odorous emissions likely occur as

the nitrogen and sulfur in the organic matter are converted by the microbes into gaseous products. Therefore, to fully eliminate such problems, the raw sludge must undergo digestion, composting, alkaline and chlorine treatment, or passage through drying beds or thermal drying processes.

During the process of transporting biosolids from the generating facility to the storage or application site, odor emissions are controlled through appropriate conveyance, such as well-maintained sealed trucks. USDA (1997) suggested that odors can be controlled by treating malodorous biosolids with lime prior to shipping to an application site, minimizing the possibility of anaerobic decomposition conditions, maximizing the ability of microbes to break down substances rapidly, injecting biosolids into the soil (e.g., 10-15 cm deep) rather than spreading them on the land surface, and collecting, treating, and dispersing any odors that are formed (Walker 1998).

2.4.1.3 Health concerns

Pathogens and heavy metals in biosolids are the primary factors that may affect public health, as these agents, when in significant concentrations, are well-known for their toxic effects. Viruses, bacteria, and animal and human parasites may cause various human diseases and illnesses. This is a significant reason why there is persistent public opposition for biosolids applications for agricultural purposes and for surface land disposal. Even though the wastewater residuals must be subjected to additional pathogen reduction treatment prior to land application of biosolids, the liability associated with incidents of infectious disease spreading through either direct exposures or food or water pathways remains the primary public concern.

2.4.2 Treatment costs

Because of population growth, urbanization, higher levels of treatment of wastewater in more municipalities, and volumes of generated sludge have increased. It is clear that higher levels of treatment for wastewater are required and larger quantities of wastewater must be treated; hence, larger sewage sludge volumes are generated over time. Regulatory requirements in some jurisdictions have mandated higher levels of wastewater treatment which in turn increase the cost of biosolids management as well. Thus, as a city grows, the unit (per capita) costs may rise much more rapidly that the population growth because of greater transportation distances for sludge disposal, stricter treatment requirements, and less public acceptance, among other factors.

Usually, the beneficial use or disposal of biosolids is not cost-effective in that it does not generate any revenue whatsoever. Furthermore, the unit cost of treatment of biosolids is quite high in many urban centers. Although surface disposal is considered as the least expensive management option for biosolids, the additional costs of surface disposal processes imposed by the regulation of municipal solid waste landfill of Part 503 (The EPA's 40 CFR Part 503, *Standards for the Use and Disposal of Sewage Sludge*) have generally increased disproportionately in comparison to thermal treatment, chemical treatment and incineration. Land application has also faced increased cost because of the general trend toward suburbanization.

Besides, the treatment costs of biosolids, i.e. the average cost for manufacture, distribution and marketing of biosolids products, is three times more expensive than the costs of the least expensive treatment methods. As in the case of composted biosolids, for example, although there is an offset value from the sale price of composted biosolids, the total cost still remains high. In addition, the cost of compost is dependent on scale and performance of the facility. A large-scale operation usually reduces unit cost, and the co-composting of biosolids and other municipal organic waste such as yard trimmings can also become a more cost-effective option in some areas.

High cost of disposal, compounded with the difficulties in finding large enough land area suitable for disposal, is leading to solutions such as long-distance transportation. At the same time, high costs (trucks, trains, loading fees, etc) are also generated during the transportation of biosolids to far areas where needed.

Transportation of biosolids is also a substantial cost element, and it can have the most significant effect on the total costs of land application if the distances to the treatment sites are great. (For example, New York City transports large amounts of sludge to locations as far away as West Virginia because of the lack of close-by application sites.) The biosolids volume needing transportation is inevitably the controlling factor on the total cost, so that volume reduction through thickening, dewatering, conditioning, and drying at wastewater treatment plants increases the efficiency of transportation, and in turn reduces the total costs.

Therefore, not only regulatory compliance issues have led to consideration of new approaches to sewage sludge recycling or treatment, but also in some cases the rising transportation and labor costs have stimulated changes in sewage sludge management. Wastewater treatment authorities have been faced with dramatic increases in sewage sludge treatment costs. For example, in the 1970s, costs for sewage sludge treatment generally were almost invariably less than $100 per dry ton, whereas recent short-term private contracts to implement land based sewage sludge disposal alternatives have been reported to be as high as $800 per dry ton (McFarland 2000), although the average costs are far less.

Table 2.2 Capital, operating and maintenance costs for different types of composting (US EPA, 1999)

Type of Composting Method	Capital Costs	Operation and Maintenance Costs
Aerated Static Pile	$36,000 - $20 million	$12 - $500/ dry ton
In-Vessel	$850,000 - $33 million	$18.24 - $540/ dry ton
Windrow	$50,000 - $8 million	$2.15 - $245/ dry ton
Aerated Windrow	$450,000	$50 - $325/ ton
Static Pile	Not reported	$25 - $165/ ton

(1997 data from 100 composting facilities)

Chapter 3
Biosolids Treatment Options

3.1 Conventional Municipal Biosolids Treatment

Biosolids can be used beneficially (soil amendment), recycled (e.g. as compost) or disposed of in surface facilities (landfills) only when regulatory requirements regarding public health and environmental protection are met. Hence, it is common that further treatment on site is required before the solids are conveyed to the final destination, and the biosolids' characteristics can help decide the applicability of a particular treatment processes. For instance, pathogens, potential vector attraction and metal content in biosolids must be reduced to required levels to meet beneficial recycling criteria (e.g. field spreading). Even the biosolids for landfill disposal must meet a set of regulatory requirements so that risks are reduced. Also, the biosolids volume intimately impacts the biosolids management process and likewise the treatment cost, as discussed in Section 1.4.2.

The treatment methods for biosolids are partially dependent on the nature of the wastewater treatment process; in other words, the type and level of wastewater treatments affect the type, quantity, and quality of biosolids generated. These can be adjusted to some extent when industrial discharges are mixed at wastewater plants because pretreatment of wastewater by industry can improve biosolids quality considerably (US EPA 1999).

The stabilization and dewatering stages are major biosolids treatment processes.

Stabilization is the process of reduction of pathogens, odor and volatile substances in the biosolids, and this is achieved through various processes. Thereafter, stabilized biosolids that meet the federal and state regulations can further be used or recycled directly. The most common methods of stabilization are alkali stabilization, anaerobic or aerobic digestion, composting, thermal treatment, and drying.

Dewatering is a method used to remove excess water from biosolids. This process is usually a critical step that must be done before a stabilization process like composting, drying or incineration. The water content of the biosolids (i.e. the solids concentration) can determine whether the stabilization process will function properly or not. For example, excessive water contents could drive costs of thermal drying upward to unacceptable levels. Non-thermal dewatering processes involve methods such as belt filter press dewatering, centrifuge dewatering, recessed chamber press dewatering, flocculation and settlement.

3.1.1 Aerobic digestion vs. anaerobic digestion

Aerobic digestion is a biological degradation process with oxygen supply. The biosolids are stored in an open or closed vessel or lagoon, and the organic solids are gradually degraded into carbon dioxide,

water and nitrogen through the action of aerobic bacteria. Meanwhile, pathogens and odors are reduced in the process. Hence, objectives of reducing biosolids volume and production of stabilized biosolids are fulfilled at the same time. Aerobic digestion is commonly recommended for smaller wastewater treatment in the form of an aerated lagoon. The advantage of aerobic digestion is its simple operation, which is largely self-sustaining. However, high energy consumption is its disadvantage, as high energy for oxygen transfer is required during the process.

Recently, aerobic digestion under higher temperature operation is becoming more popular because it can produce biosolids with lower pathogen levels and higher solids content, and at higher temperature the bio-decomposition processes take place more rapidly.

Anaerobic digestion can achieve the same objectives as aerobic digestion such as mass reduction, volume reduction, and pathogens sterilization. The organic content of biosolids, odor and pathogen content are reduced through continued decomposition until regulatory requirements are met. In contrast to aerobic digestion, anaerobic digestion is a biological degradation process occurring in a closed vessel under strict oxygen-free condition. Oxygen can impede this operation because the relevant microorganisms in this process are killed by oxygen. Carbon dioxide and methane are mainly produced through the anaerobic digestion of biosolids. Anaerobic digestion is a popular treatment practice because most wastewater treatment is of large scale and methane produced from anaerobic bio-reaction vessels at warm temperatures (more rapid) has economic recovery value.

Chemical processes of anaerobic digestion are typically described as a multiple-stage reaction, and three basic stages are defined by the Water Environment Federation (WEF, 1995). In the first stage, large molecular weight compounds hydrolyze into fatty acids, alcohols or even ammonia and carbon dioxide. In stage two, the products from the previous stage are converted into acetic acid and other compounds. In stage three, methane is produced, mainly from two sources: the combining of hydrogen and carbon dioxide directly into methane, and the degrading of acetate into methane. Usually, the anaerobic digestion operates at about 35°C, but some thermal anaerobic digestion is proposed and operated in practice at around 55°C. The advantages of thermal anaerobic digestion are speed, as well as a higher degree of pathogen reduction and further stabilization. Anaerobic digestion is sensitive to operational conditions such as pH, loading rate, detention time, scale of reaction vessel and agitation, temperature, etc (National Biosolids Partnership 2005b). These controlling points must be considered in planning and during the operation.

3.1.2 Compost

Composting is one alternative for biosolids stabilization. In the process, microorganisms degrade the organic content of biosolids to achieve mass reduction and pathogens sterilization under specific high-temperature environments. The end product from composting is in a humus-like form with high content of organic matter and nutrients like nitrogen. Because of the relatively strong effect of high temperature on pathogen reduction, a Class A biosolids without detectable levels of pathogens is produced; hence, the end product has a high degree of applicability.

During the composting process, bulking agents such as yard trimmings, wood chips, and bark are commonly added into the biosolids to supply carbon sources. These agents also increase the porosity to maintain the oxygen level in the biosolids in order to sustain the aerobic environment for composting, so the biosolids mass is increased correspondingly.

Composting is typically operated as windrow composting, aerated static piles, or in-vessel composting (US EPA, 1999). In a piled form or in a vessel, the feedstock undergoes decomposition by microbes at a high temperature. High-temperature composting is favorable for the destruction of pathogens and for the production of high quality stabilized biosolids for further use or recycling. Hence, the specific temperature for different methods of composting and use of end products must be reached and sustained to achieve successful operation. Furthermore, in order to keep a suitable oxygen level for composting, air supply is critical in the process. In an aerated static pile, perforated aeration pipes are used, mechanical turning is used for windrows, and in a vessel, air is blown into the feedstock (US EPA 2002b).

Physical work is needed for adding bulking agents, monitoring turning, and implementing process control. Meanwhile, feed and finished material must be moved with mechanical equipment and storage piles must be maintained for curing and distribution, so composting is a labor intensive operation, therefore it is costly (US EPA 2002b).

Odor is another issue in the operation of composting. Odor-control measures must be combined into the design for composting, but measures such as frequent turning in the composting would generate more odors. In these cases, timing the turnings to occur when conditions are ideal is used to minimize odors as well as collecting and scrubbing the off-gasses chemically or biologically through packed towers, mist towers, or constructed biofilters (US EPA 1999). Control of odors is discussed in detail in the fact sheet entitled: Odor Management in Biosolids Management (US EPA 2000c).

With the ease of storage and handing, the use of composting in combination with various land applications makes it widely applied.

Composting with organic MSW such as yard trimmings, paper, and wood chips, simultaneously increases the scale of the composting process, which in turn decreases the pre-capital cost of its operation. On the other hand, the end products have wide usage in land application such as soil amendment for mine reclamation and forest land. The higher quality composted biosolids are also available to landscapers for landscaping projects and parks, and to homeowners for lawn and home gardens. Nevertheless, besides odor, we also have to pay attention to the level of nutrients in composted biosolids. Nutrients such as nitrogen or phosphorous present in the biosolids for land application would contaminate the ground water through percolation with rain fall. It could be one of the negative points for application of composted biosolids.

Although a large amount of the carbon from animal and human biosolids is returned back to the soil and has beneficial effects, the composting process generates atmospheric CO_2 and lesser amounts of CH_4, both greenhouse gases.

The cost is another constraint with regard to processing. In-vessel composting is less labor intensive, but it has higher capital cost than both aerated static pile and windrow configurations. The capital costs of in-vessel systems are around $33,500 per dry metric ton per day processing capacity.

A typical aerated static pile facility costs nearly $33,000 per dry metric ton per day processing capacity (Harkness *et al.* 1994). Typical operation and maintenance (O&M) costs for in-vessel systems range from $150 per dry ton per day to greater than $200 per dry ton per day. Aerated static pile O&M costs are on average $150 per dry ton per day (Harkness *et al.* 1994). Costs for windrowing fit between the costs for in-vessel and aerated static pile methods

3.1.3 Alkaline stabilization

Alkaline stabilization, like other stabilization processes, works well for reducing odors and for reducing the potential of vector attraction and pathogen levels. The stabilized biosolids from this process can be handled easily through further recycling and treatment. Alkaline stabilization also can neutralize and improve acid soils by adding alkaline materials.

The end product from alkaline stabilization can at least achieve Class B biosolids rank. With larger amounts of alkaline material applied and longer exposure time at higher temperature, Class A biosolids are produced.

The materials commonly used for alkaline stabilization are hydrated lime, quicklime (calcium oxide), fly ash, lime and cement kiln dust, and carbide lime (US EPA 2000b). Quick lime has a strong ability to destroy pathogens because of its high heat of hydration. However, easily obtained fly ash, lime kiln dust, and cement kiln dust are cheaper and this has made them more commonly used. Other chemical additives may be added to alkaline stabilization. The chemical additives in the stabilization can increase solids content and granularity, can reduce mobility of heavy metals, can increase the agricultural lime value, and can achieve a higher degree of pathogen reduction. This kind of biosolids product contains pathogens below detectable levels, and has a long-term stability, allowing for storage with minimum potential for odor production or re-growth of pathogens (US EPA 1999).

The products of alkaline stabilization are also widely acceptable in many circumstances (e.g., agriculture, landscaping, and mine reclamation), and have special use as a substitution for fertilizer. They also perform better than other amendments for land reclamation, especially at acid mine spoils or mine tailings sites.

Alkaline stabilization is a simple technology with reliable operation and small land area required. However, the volume of material produced is increased by approximately 15% to 50% in comparison with other stabilization techniques, such as digestion (US EPA 2000c). The larger biosolids volume results in higher cost, such as in transportation. Several other points including odor generated during the alkaline stabilization, end use, and re-growth of pathogens contribute to possible negative impacts on the environment.

3.1.4 Air drying and thermal drying

Drying systems mainly reduce the water content in the biosolids rather than being a real stabilization process. The air drying process serves as an extra stabilization step for stabilized dewatered biosolids

for further volume reduction. The most common types of air drying are the “Two Summer Method” and the “Rapid Drying Method”. The requirements for the successful operation of these two types of air drying are outlined by the US EPA Pathogen Equivalency Committee (PEC) (National Biosolids Partnership 2005b). Thermal drying involves heating the biosolids in order to draw moisture from the biosolids, leaving the solids content behind; consequently, a reduction of volume and pathogens is achieved. The product of thermal drying is used as fertilizer or soil conditioner. Nevertheless, significant odor is generated by drying raw solids, which is a disadvantage for the process.

3.2 Biosolids Disposal or Reuse

3.2.1 Land application

Because of the nature of biosolids, rich in organic matter, they can be beneficially used in agriculture, forestry, and land reclamation after suitable stabilization methods such as digestion, composting, alkaline treatment, heat treatment etc. The land application of biosolids can be performed as direct surface land spreading of biosolids or by injecting biosolids into the soil.

The degree of stabilization of biosolids such as digestion, composting or alkaline stabilization before spreading depends on the biosolids end use under the guidance of the US EPA Regulations, and the degree of stabilization can proportionally affect the cost of land application.

Biosolids stabilized by composting lead to various types of applications, like applications to agricultural lands, forests, and mine reclamation sites. Meanwhile, highly treated biosolids are widely accepted by landscapers for home garden or lawn use.

Biosolids used for direct land application or land reclamation are relatively cheaper than other commercial enrichment agents, and the demands for commercial enrichment agents for reclamation sites can be alleviated. Another advantage of land spreading is that biosolids can be composted (recycled) with other organic MSW materials directly at a landfill or a spreading site, which could reduce the composting cost for use as a soil amendment and fertilizer, and the composted material can be used as a daily cover or as part of a final landfill cover. As biosolids are also produced in liquid form with low solids content or as a semisolid that contains a large amount of water, they are often applied at place not too distant from its production site.

The accumulation level of trace elements and pathogens is the most stringent rule in the regulations for the consideration of land application of biosolids so as to ensure the health of humans, animals and plants. Meanwhile, the nutrient components in the biosolids are limited to guarantee that there can not be excess nitrogen passing the root zone of crops to the ground water when composted biosolids is used as soil enrichment. In addition, the reduction of vector attraction must be achieved to meet the required levels. Nevertheless, the soil can only accept a limited amount of loading with heavy metals, and there always remain concerns that pathogens and viruses are not fully deactivated. “The National Academy of Sciences of the USA concluded that while there is no documented

scientific evidence that sewage sludge regulations have failed to protect public health, there is persistent uncertainty on possible adverse health effect." (Epstein 2002).

3.2.2 Incineration of biosolids

Incineration generally is defined as the high temperature combustion of biosolids within an enclosed vessel. There are two primary technologies used to incinerate biosolids, Multiple Hearth Furnaces (MHF) and Fluidized Bed Incinerators (FBI) (National Biosolids Partnership 2005b).

Incineration dramatically reduces biosolids to a small amount of residue primarily consisting of ash at 20% of its original volume, and virtually all the volatile solids and pathogens are destroyed (US EPA 1999). Unlike land application and surface disposal, biosolids incineration takes advantage of the inherent energy value of the solids fraction of biosolids and takes up a small land area. Those points are considered as advantages of incineration processes.

Although there is energy recovered from the biosolids, the final product ash from incineration of biosolids is not an environmentally friendly material, and the by-products of air emission affect the atmosphere. The trace elements such as heavy metal in the biosolids are concentrated by incineration, and compounds such as dioxin may be formed. Therefore, air pollution control devices are required to protect air quality. If non-hazardous ash (low levels of heavy metals) is produced, it could be co-disposed of in a MSW landfill. Incineration is probably an alternative process for land disposal where the land is scarce or improper for land application, but only when incineration achieves successful energy recovery as well as required air emission level can it be accepted in terms of economical and environmental points of view.

3.2.3 Surface disposal or landfilling

Disposal of biosolids commonly occurs in MSW landfills, and ash from biosolids incineration might also be disposed of in MSW landfills. The major types of surface disposal are landfilling of biosolids in monofills, permanent piles or lagoons, and dedicated surface disposal practices (US EPA 1999).

Surface land disposal is an activity in which biosolids are placed on land for final disposal. Monofills are defined as only biosolids placed in the landfill, and note that in the United States, even though biosolids was in the past placed with MSW, this is now prohibited by the US EPA. Although the methane produced in the landfill can generate additional economic value for municipal sludge treatment, the cost of methane capture systems is quite high because of low efficiency. Methane is a strong greenhouse gas which has 20 times the impact of CO_2 when it emits to the atmosphere. The low efficiency of capture systems usually results in a high risk of atmospheric emissions of CH_4.

Monofills of biosolids are common engineering methods for the surface disposal of biosolids. Because of their high risk for environmental contamination, monofills are also now stopped and no new sites are allowed for monofills in the US. Such sites for biosolids also require higher levels of environmental monitoring. As discussed in Section 2.4.1.1, leachate and run-off from landfill sites

carry great potential to contaminate the surrounding water resource, so the regulations for surface disposal of biosolids are stringent.

3.3 Deep Underground Injection

Alternatively, an innovative technology for biosolids treatment and recycling is achieved by deep underground injection, which involves disposal through deep injection of slurry under hydraulic fracturing conditions into porous, permeable strata at depths greater than 300 - 400 m (Bruno 2000). This approach could eliminate most of the public concerns about environmental pollution and health attack from biosolids because it can adequately destroy or isolate all heavy metals, contaminants, and pathogens, as well as avoid air pollution, odors and contamination of ground water or surface water bodies. In addition, the deep environment can capture the carbon dioxide gas emission, the generated methane can be beneficial used for other purposes, and the degraded organic residues along with other materials would be permanently sequestered underground safely.

In contrast to other methods of treatment of biosolids, deep injection could perpetually entomb the solids materials underground. There is no further process required for residual matter disposal after the biodegradation and thermal treatment taking place at depth. In other treatment processes, such as incineration, composting or digestion, no matter what kind of end products are produced, like the ash from incineration, composted biosolids and digested biosolids, they still must be subjected to further disposal or recycling activities. Hence, deep underground injection can minimize the impacts on the environment that arise from traditional practices of biosolids treatment. This provides full protection for surface and shallow groundwater, as well as reduces greenhouse gas emissions to the atmosphere.

Because all toxic substances which inherently exist in biosolids are buried underground deeply without any risk of being accessed by human activities, deep injection eliminates public concerns about the reuse of biosolids. Suitable sites selected for deep biosolids injection minimize or eliminate the risk of contaminating shallow groundwater by biosolids products. The high temperature in the subsurface also sterilizes the biosolids. Then, the biosolids material placed deep underground can undergo a natural process of continuing anaerobic biodegradation, much as naturally deposited organic layers undergo diagenesis over geological time after deposition and burial. The indigenous active bacterial organisms can consume these organic materials during burial in natural sedimentary strata. The fact of acetate concentration increasing at depths below 150 m at two sites in Atlantic Ocean indicates this significant bacterial activity (Wellsbury *et al*. 1997). Because acetate is the necessary substrate for acetoclastic methanogenesis and is an important precursor for methane production, this may be a mechanism for formation of the enormous reservoirs of methane in gas hydrate found globally in sub-sea floor sediments (Kvenvolden 1995). Hence, methane could be generated by bacterial methanogenesis based on the burial of and acetogenic decomposition of organic carbon in sediments. Through geothermal biodegradation processes *in situ*, carbon dioxide emissions produced by this process are preferentially absorbed by formation waters because of high carbon dioxide solubility in water. Hence, carbon dioxide is captured in solution and high purity methane can be subsequently recovered for beneficial use.

The capital cost and land surface area required for a disposal facility is less than for an equivalent capacity conventional treatment facility. For the economical operations of deep biosolids injection, large-scale operations are preferred rather than small-scale operations because the amount of methane produced can partly offset the cost of operations if recovered, and this is more feasible in large-scale operations. If animal waste or other organic wastes are to be co-disposed with sanitary waste, the facility could be feasible even at a smaller scale of operation than that projected by the population of the region served by an injection facility. Hence it provides a local solution for a large metropolis, reducing long distance truck transportation, which also reduces risk and environmental impacts of additional traffic. Although additional costs such as pipelining would be taken into account for those cities without suitable geological conditions, it appears that pipelining biosolids is a reliable and cost effective method of transport to a treatment site.

The disadvantages of this method, other than technical difficulties, seem to be the requirements of right geology strata (Nadeem 2003), of special permission from regulatory agencies that is not necessarily easy, of public acceptance for a method that requires a great deal of education and knowledge sharing, and of knowledge of the implementation of oilfield technology by municipal sanitary engineers.

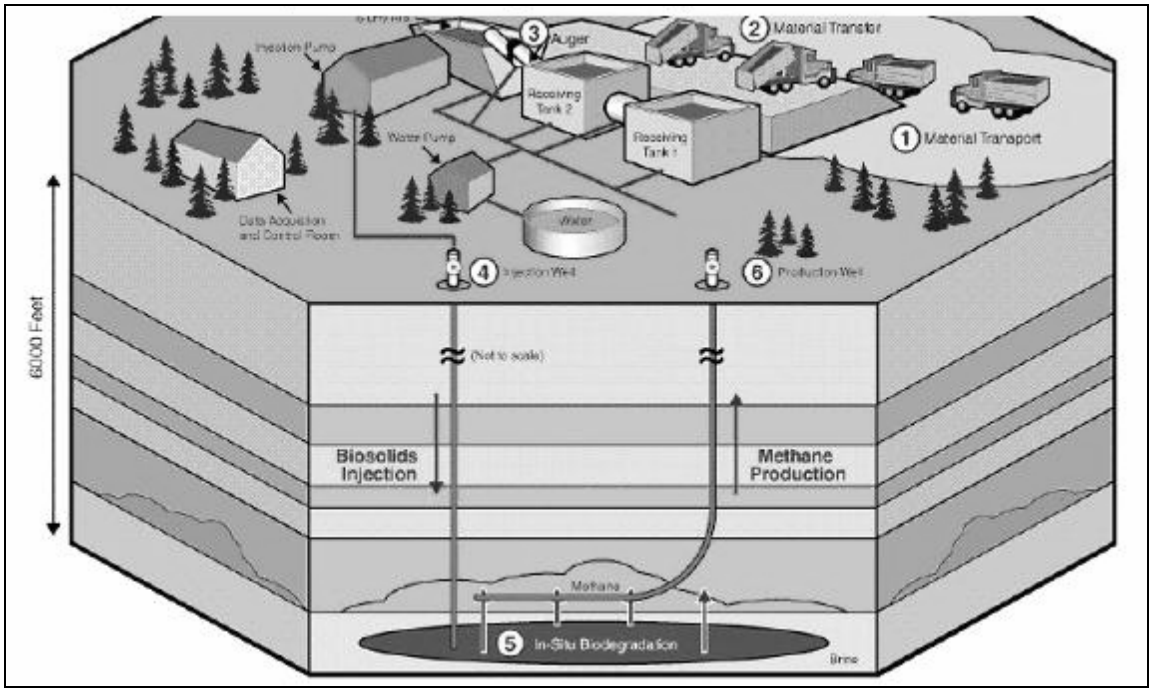

Figure 3.1 Deep biosolids injection system for waste treatment (Terralog Technology Inc. website)

Table 3.1 Comparison of various biosolids treatments

Process	Environmental risk and safety			Final products adaptation	Cost
	Contamination potential to Groundwater	*Odors and Air pollution*	*Possible attacks to environment*		
Compost and land application	Yes	Yes	Excess nutrients and amounts of heavy metal in end products; contamination through rain fall	High degree of acceptability for land application including home garden or lawn	High cost for compost process; low for land application
Alkaline and land application	Yes	Yes	Increased biosolids volume and possible re-growth of pathogens	For agriculture use; landscaping; mine reclamation site	Low cost and the most reliable operation
Incineration	Low potential	Yes	Concentrated heavy metal and dioxin produced; potential of air pollution	Final products end in landfilling sites	Very high
Surface disposal or landfilling	High potential	Yes	Contamination of pathogen and of excess nutrients; odors and CH_4, CO_2 emission	Forbidden	High*

Deep biosolids injection	Low**	No**	Waste migration and site instability	CH_4 harvest and CO_2 sequestration	Low for short distance transport and large scale operation

*Regulation (The EPA's 40 CFR Part 503) imposed additional cost

** Under competent operation conditions which are assumed for all of the processes.

Chapter 4

Mechanism for Deep Underground Injection of Biosolids

4.1 Introduction to Deep Underground Injection of Waste

Deep underground injection of waste dates back to the 1930s. Originally, oil and gas exploration and production companies began to inject saltwater by-products back into the oil production strata. With the development of safe disposal of these wastes, other industries began to inject industrial liquid waste underground by this same technique. It provided a good option for disposal of waste from industries such as the petrochemical industry (Texas Center for Policy Studies 2006)

Underground injection of hazardous waste is restricted to liquid state injection by the US EPA (no solids permitted). Most of such wastes are injected into depleted oil-producing formations or deep permeable zones with no resources. There have been great numbers of injection wells classified as Class I and II (see below) located in Texas for hazardous liquid waste and brine water injection into oil-producing formations (Texas Department of Water Resources 1984). The legal and regulatory requirements are well defined and the underground injection control program established by US EPA acts as the main yard stick for all underground injection. Table 3.1 shows the injection wells classification defined by the US EPA. Officials agree that waste disposal through properly constructed and operated injection wells is safer and less likely to contaminate surface water or potable ground water than landfills and other forms of land treatment (Office of Technology 1983). Currently in the United States, there are over 9 billion gallons of hazardous waste injected every year, over 2 billion gallons of brine from oil and gas operations injected every day; and large volumes of wastewater from automotive, petrochemical, sanitation and other industrial processes are also injected into deep aquifers (US EPA 2002a).

Since the deep underground injection technique is historically used for disposal of both hazardous and non-hazardous liquid waste, it is proposed for the treatment of biosolids or raw sludge after sterilization in compliance with EPA regulations for pathogens. Biosolids injection is granted a special exemption at the present time under the Class V wells designation in the USA (US EPA 2006).

The injection of slurry consisting of water with a considerable amount of solids is different from regular deep underground injection of liquids such as brine water from oil production. It requires a higher injection pressure to fracture the underground formation continuously, in contrast to other deep liquid injection processes which are generally operated below the formation fracture pressure. An injection process above fracture pressure attracts concerns about possible negative impacts on the environment because of possible loss of containment of the liquids at depth. However, experience from injection activities for non-hazardous oil field wastes in many geological environments above the fracture pressure gives confidence that it can be used safely for biosolids in a low-risk operation (Tsang and Apps 2005). Based on extensive experience, deep injection of slurry is technically feasible for large-scale disposal of solid wastes (sand, sludge, non-clarified water) using properly

engineered designs and careful control. The critical feasibility factor for deep injection of solids is the availability of a suitable geological site that has sufficiently thick sedimentary strata of high permeability and porosity.

Table 4.1 EPA injection well classification system (US EPA 2002a)

Well Class Injection	Well Description	Approximate Inventory
Class I	– Inject hazardous wastes beneath the lowermost USDW – Inject industrial non-hazardous liquid beneath the lowermost USDW – Inject municipal wastewater beneath the lowermost USDW	500
Class II	– Dispose of fluids associated with the production of oil and natural gas – Inject fluids for enhanced oil recovery – Inject liquid hydrocarbons for storage	147,000.
Class III	– Inject fluids for the extraction of minerals	17,000.
Class IV	– Inject hazardous or radioactive waste into or above a USDW. This activity is banned. These wells can only inject as part of an authorized cleanup.	40 sites.
Class V	– Wells not included in the other classes. Inject non-hazardous liquid into or above a USDW.	Range from 500,00 to >685,000

An appropriate geological site must have the ability to accept large volumes of slurred biosolids, the ability to rapidly dissipate pressures, the stratigraphic conditions to protect groundwater resources, and, if possible, a suitable gas-trapping geometry for eventual methane recovery.

Large amounts of non-hazardous oilfield wastes (NOW) such as produced sand, tank bottom sludges, drill cuttings, and drilling mud are treated on site through injection of a slurried form of these wastes into geological formations. The first demonstration project of solids injection in the oil industry originated in the off-shore environment for drilling cuttings and waste drilling mud disposal about 1986-88 (Veil and Dusseault 2003). Thereafter, this approach has been successfully used world-wide at various locations like Alaska, the North Sea and California (Schmidt *et al.* 1999, Schuh *et al*. 1993, Hainey *et al.* 1997, Srinivasan *et al.* 1998). Slurry fracture injection (SFI) has been used to dispose of naturally occurring radioactive material (NORM) offshore and onshore in the Gulf of Mexico, Louisiana (Malachosky *et al*. 1991, Reed *et al*. 2001). It has also been applied to dispose of

exploration and production wastes in Alberta and Saskatchewan, Canada (Srinivasan *et al*. 1997, Dusseault *et al*. 1997) and Duri oilfield, Indonesia (Arfie *et al*. 2005).

4.1.1 Geological site characteristics for biosolids injection

Solid wastes in slurry form have now been successfully disposed through slurry fracture injection at many sites. The appropriate geological site characteristics have been outlined for slurry fracture injection operation. These characteristics can serve as guidelines for site selection for deep biosolids injection, as deep biosolids injection is similar to the SFI process.

Generally speaking, the ideal geologic sequence for successful waste injection is a thick (>10 m), laterally extensive, highly porous (>25%), and permeable (>1 Darcy) zone of horizontally strafified unconsolidated sandstones and shales at moderate depths (400 m~1500 m) (Srinivasan *et al.* 1997). These types of geological sites can ensure the following key conditions for the slurry fracture injection process:

- Fluid bleed-off is rapid, allowing reservoir pressure decay and strain relaxation between injection episodes;
- A laterally extensive target stratum assures the necessary reservoir storativity to accommodate fluids;
- Low permeability overburden such as a ductile shale provides hydrologic isolation from overlying groundwater zones;
- Solids waste remain close to the injection point because of the high permeability induced fracture bleed-off
- Stress barriers exist to minimize the potential for vertical migration of slurry or liquid and fractures

Nadeem (2005) proposed a geological site assessment model that considered key conditions of sites for SFI processes; the model is used to locate suitable sites for injected materials quantitatively and qualitatively. In his study, he chose the parameters permeability, porosity, depth, area extent, thickness, mechanical strength, and compressibility of a reservoir, thickness and flow properties of the cap rock, geographical distance between an injection well and a waste source or collection centre, regional and detailed structural and tectonic setup of an area. Additional factors affecting the security level of a site include the details of the lithostratigraphic column overlying the target reservoir and the presence of overlying fracture blunting horizons.

This geological site assessment model is divided into two components: a decision tree and a numerical calculation system. The decision tree is used to evaluate the most critical parameters, giving a result of unsuitable or suitable site, but of unspecified quality. The numerical calculation gives a score to a prospective injection site based on the rank numbers and weighting factors for the various parameters.

4.1.2 Biosolids injection system

A biosolids injection system is shown in Figure 4.1, and a simple description is given. The slurry is produced in a homogeneous state through various steps. Vibrating screens using high velocity water jets are the first step used; then, slurry for injection at the desired uniform density is achieved in a highly agitated mixing and averaging tank with added waste water. Finally, using a high-pressure oil-field pump, the injectate is forced down a steel-cased well bore and through perforations into the target formation.

A slurry injection system, including water storage tanks and all support facilities, requires a surface area no larger than 10,000 m^2, where the system can be easily enclosed. The surface area of each injection well would not exceed 250-300 m^2 of surface area (Srinivasan *et al.* 1998). The injection wells are connected to the injection pump by high pressure tubing lines that can be buried if desired.

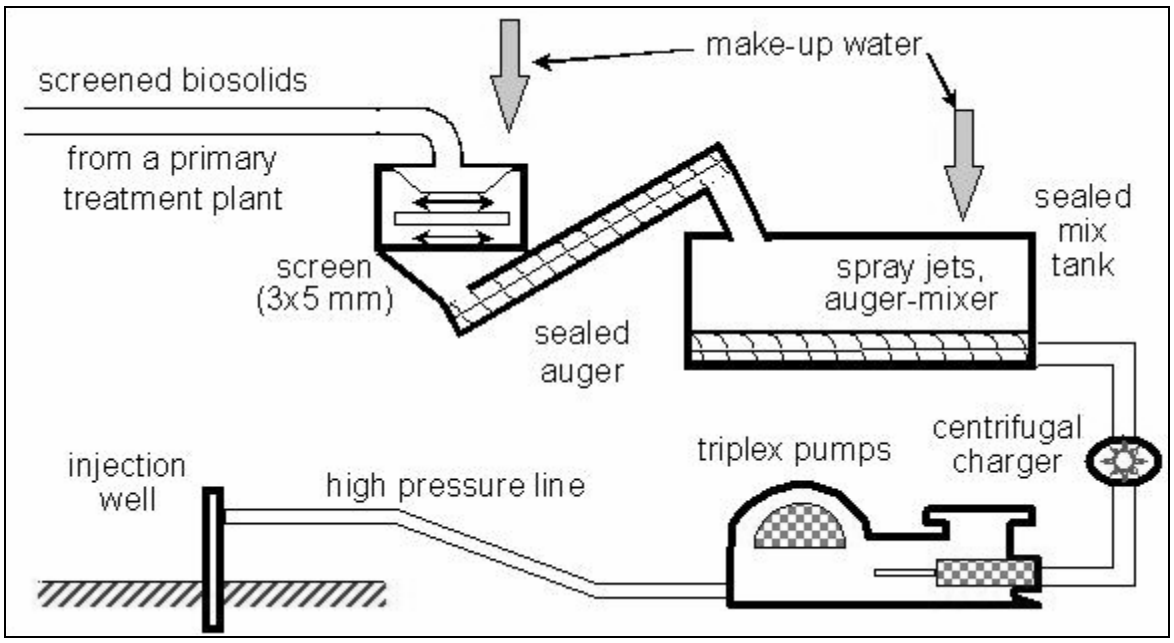

Figure 4.1 Slurry injection system (Dusseault, 2003)

4.1.3 Deep injection procedure:

The procedure for injection is described here, although there would be changes for different situations. Several steps are involved (Srinivasan *et al*. 1997, Bruno 2000):

1) Clear water injection stage

At the beginning of injection, clear water (generally waste water that also must be disposed) is used for injection. The pressure in the liquid is increased by pumping until it is high enough to

hydraulically fracture the formation at depth. At this time, all the system components can be ensured to function properly (e.g., Figure 4.2).

2) Waste injection stage

After a short period of time under steady-state water injection, solid granular material or biosolids are introduced into the injection system at a rate that is built up until the desired slurry density is achieved. During the injection, the feed rate of the solids material and the added water is kept in a steady-state condition. Nevertheless, it is not a completely steady state, because there can be small variations in the slurry density, or the injection rate could be changed during the injection period. The injection operation details depend on the monitored pressure response of the well, as well as the nature of the material being injected. Typically, one cycle of operation for a single disposal well can last for 6 to 10 hours, depending on the project strategy.

3) Solids content decreasing stage

This is a transient period after the solids feed ceases, so that content of solids in the injectate decreases to zero gradually as they are cleaned from the mixing and pumping system. This period of time is about 20 minutes, but can be longer as required to make sure the surface system is absolutely clean of solids.

4) Clear water flushing stage and closure stage

Clear water is continued for the flushing so that the wellbore is fully cleaned and the solids material pushed away from the wellbore perforations at depth. Then, the well is shut down under pressure by a surface valve so there is no possibility of liquid back-flow into the wellbore. The down-hole pressure in the shut-in well is accurately recorded over the entire closure phase, which may last for 12 to 48 hours in a typical cyclic operation, or longer if there is a long-term shut-down for maintenance or repairs.

There are several controlling factors critical to successes of SFI field operations. These critical parameters are injected slurry volumes, injection rates and pressure, and sustainable slurry solids concentrations. In addition, the operation strategy in terms of injection cycle duration, shut-in durations, injection rates and pressures, and daily injection volumes must be ensured to confine the containment injection zone within the target formation.

4.1.4 Biodegradation and methane production phase

After many days and months of injection, large amounts of biosolids have been placed underground. Biodegradation begins under the favorable *in situ* environment at depth, and this biodegradation takes place through the feeding and growth of the natural bacteria that are known to exist in a dormant state in underground reservoirs (Wellsbury *et al*. 1997).

Some research shows that rapid anaerobic biodegradation of the biosolids slurry would generate gases containing mainly CO_2 at 10-15% and CH_4 at 85-90% (Bruno *et al.* 2005). When the gas being generated by the bio-decomposition reaches the saturation condition within the biosolids mass, free

gas would flow out of the mass when the pressure rises to the fracturing level within the biosolids to develop a flow path for free gas. Biodegradation of the biosolids ceases when all the substrate and oxygen are depleted. The huge volume reduction of the biosolids after initial compaction could be up to 70% of the initial solids volume depending on the organic content. The remnants after biodegradation are essentially carbon and inert mineral materials. The whole process of biodegradation is analogous to the formation of coal. The Deep Biosolids Injection (DBI) treatment process is like temperature-accelerated generation of coal through the anaerobic decomposition of organic matter instead of natural methanogenesis and carbon formation. DBI facilitates the coalification process to be completed in a few years because of immediate deep burial (higher T) and possibly also bioengineered design for optimum biodegradation.

4.1.5 Biosolids injection mechanisms

Injection is dominated by the hydraulic fracture mechanism necessary to inject the solid particles in a slurry form. Since a fracture is developed during this process, a large net pressure, the difference between the fluid pressure in the fracture and the far-field pore pressure ($P_f - P_p$), drives the water phase outward through the porous medium. This bleeds off the water in the fracturing fluid as it flows outward into the surrounding formation, displacing the existing formation water, and depositing solids on the fracture wall. Hence, a process of high pressure gradient biosolids filtration occurs along with the fracture process. This filtration is part of the fluid leak-off aspects of hydraulic fracture operations. While the filter cake is composed of biosolids, its distinct properties lead to different fracturing processes, compared to fracture processes with clear liquids. The highly compactable properties of the biosolids contribute to the formation impairment (reduction of permeability in the fracture wall), and to an increase in the bottom-hole pressure required to extend the fracture. Hence, the fracture is propagating under a dynamic (changing) leak-off condition in which the properties of formation such as permeability and flow resistance are changing with time. Therefore, the biosolids have a significant impact on the geometry of the fracture domain. After active fracture injection, when the higher injection pressure is gradually dissipated by water dispelled from the fracture, the large overburden force starts to act on the solid components directly, causing the consolidation of remnant slurry in the fracture. In this case, the consolidating stress is eventually equal to the total minimum horizontal stress minus the far-field pore pressure ($\sigma_v - P_p$).

The typical profile of bottom-hole pressure for a slurry fracture injection (Figure 4.3) is divided into three phases. The first phase is an active injection process; in this step, a fracture is created by continuous fluid injection at a pressure higher than the minimum formation stress, σ_3. The slurry is continuously injected and solids that are carried by the fracturing fluid move along the fracture. During this process, solids can deposit on the fracture face because of the high pressure gradient across the solids cake between the flowing fracture and the formation. When the injection process ceases, the pressure in the fracture drops instantaneously to a level which is referred to as the instantaneous shut-in pressure. When the injection stops, a period of transient pressure decline in the closed fracture zone begins. At this point, the pressure in the fractured region is still higher than the formation pressure because the remnant slurry sustained a certain amount of energy required to

maintain the fracture open. As the remained fluid is dispelled from the fracture, the higher energy is finally dissipated and the fracture closes. The pressure in the fracture domain then slowly returns to the initial pressure of the formation (pore pressure P_p). Filtration is the predominant process in the fracture propagation phase, the first phase. After closure of the fracture, the solids are consolidated under the large overburden stress, which further decreases the volume of the injected biosolids. As the biosolids become fully compacted, biodegradation begins, generating further volume decrease, but this phase does not affect the hydraulic fracture and filtration phases.

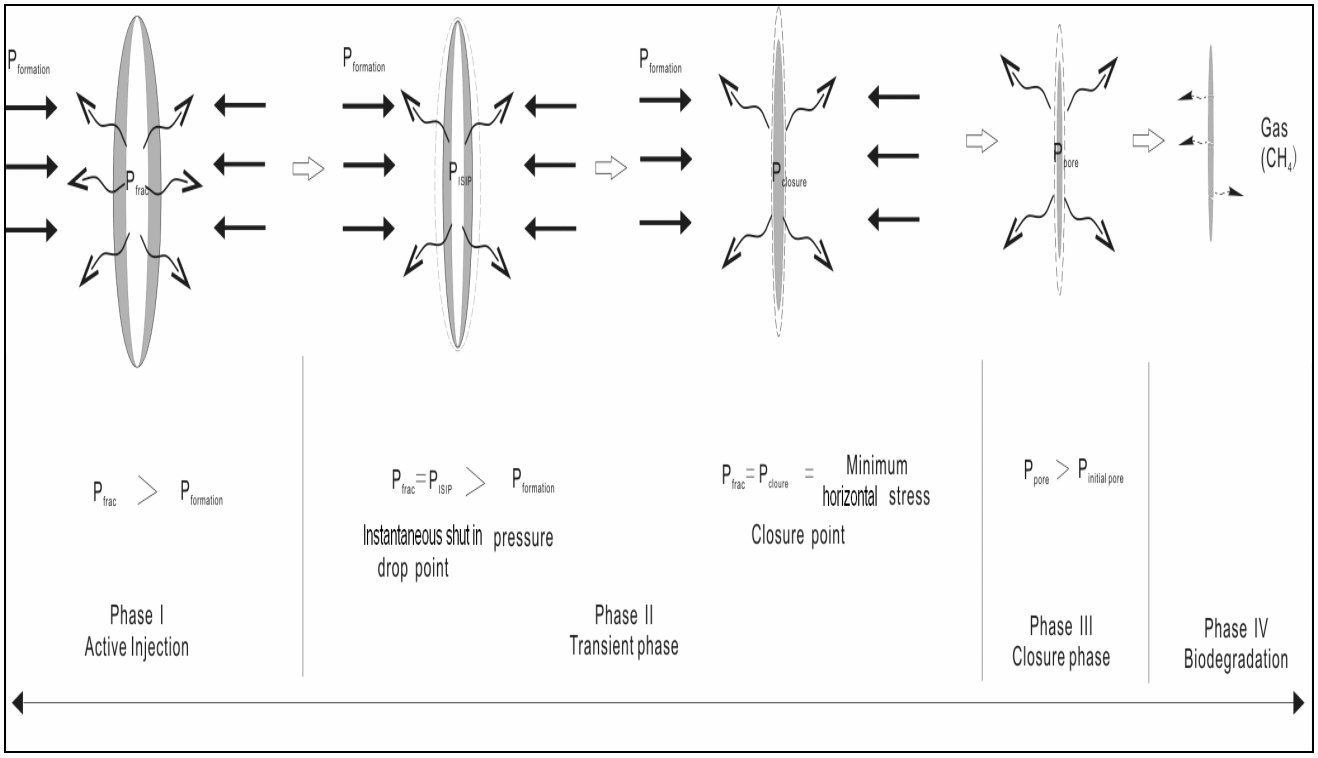

Figure 4.2 Evolution of volume of injected biosolids in a fracture

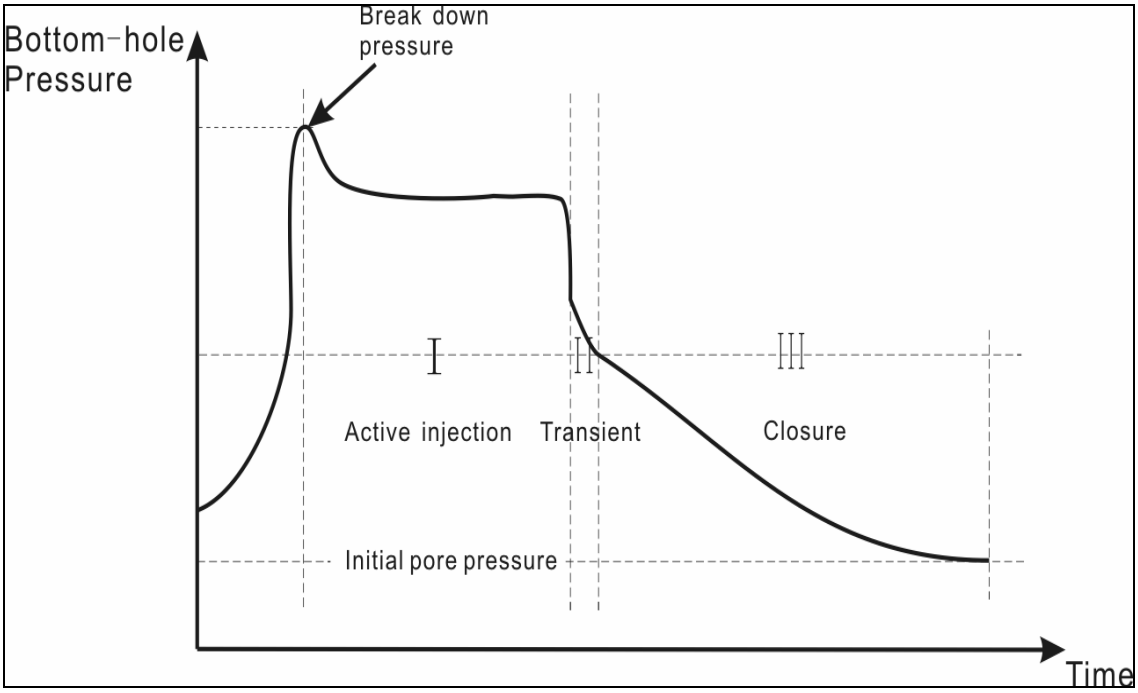

Figure 4.3 Bottom-hole pressures for one injection cycle

As biosolids sludge and other fine-grained solid wastes in slurry form are injected down hole above the formation fracture pressure into appropriate sandstone formations, the filtration of solids during the injection process as well as the consolidation of solids have significant effects on the total volume injected and the behavior. Hence the mechanics of simultaneous solids filtration, fracture propagation, and biosolids consolidation are clearly of basic interest to this process.

4.2 Hydraulic Fracturing Mechanisms

The mechanics of hydraulic fracture involve the rock response, the fracture process, and fluid mechanics. Fracture mechanics theory and practice indicate that underground stress and stress (and pressure) distribution, elastic rock properties, and fluid flow behavior control the created fracture geometry. Therefore, parameters like *in situ* stress, Poisson's ratio and Young's modulus, and permeability are all important in affecting the behavior during the hydraulic fracture treatment. Also, it can be expected that local stress fields, variations in the stress between adjacent formations, and changes in the stress fields induced by the hydraulic fracturing operation (pressure and temperature effects) also influence the geometry of the hydraulic fracture.

The rock is confined by stresses, and the stress configuration is expressed by three principal stress values and their directions. Figure 3.4 illustrates the local stress state at depth for an element of the formation. In Figure 3.4, σ_1 is the maximum stress, while σ_3 is the minimum horizontal stress, and σ_2 is the intermediate stress, between these two in magnitude. Depending on the geologic condition, the

vertical stress could be the maximum stress σ_1. However, in some cases, especially at shallow depth, the maximum stress σ_1 could be the maximum horizontal stress (shown as σ_2 in Figure 3.4), because of plate tectonics effects or erosion. The magnitude and direction of the principal stresses control the fracture geometry.

A hydraulic fracture propagates by opening up against the minimum principal stress (σ_3) direction because this costs a minimum of energy expenditure. If the minimum principal stress (σ_3) is horizontal, the fracture is vertical. In contrast, a horizontal (or approximately horizontal) fracture is generated when the minimum principal stress (σ_3) is in the vertical direction.

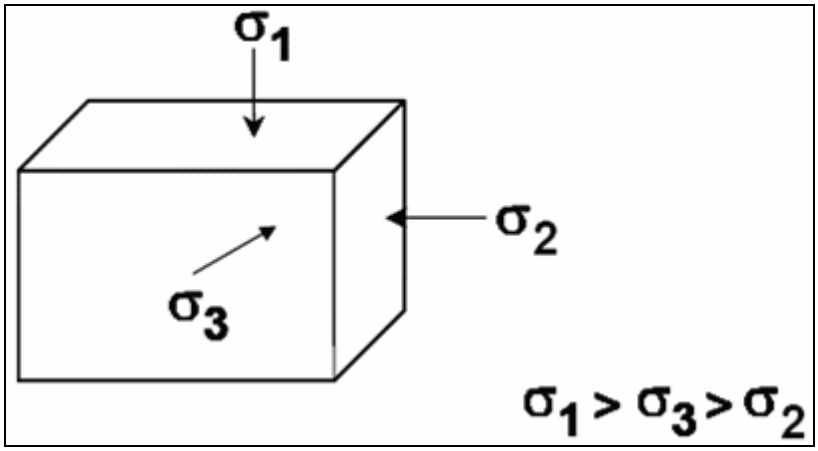

Figure 4.4 Local *in situ* stresses at depth

The state of *in situ* stresses in an ideal circumstance assumes that the stress field is entirely the result of gravity with no tectonic or erosion effect. Hence, the vertical stress is proportional with the depth, because of the overburden and can be estimated from equation 3.1a. Usually, a coefficient of from 21 kPa to 25 kPa per meter of depth can be used to compute the vertical total stress. Most of the measured vertical stresses indicate that equation 4.1a is reasonably valid for engineering purposes, except near mountains or deep valleys.

$$\sigma_V \cong \gamma Z \tag{4.1a}$$

$$\sigma_H' \cong \frac{\nu}{1-\nu}\sigma_V' \tag{4.1b}$$

where: σ_v = total vertical stress

σ_H = total horizontal stress (*in situ* stress)

σ'_v = effective vertical stress

σ'_H = effective horizontal stress (*in situ* stress)

ν = Poisson's ratio

γ = unit weight (MN/m^{-3})

If only gravity is acting, based on elastic theory, the effective horizontal stress can be estimated by equation 3.1b under the assumptions that there is no horizontal strain and that the material is isotropic, giving two horizontal stresses that are equal. Hence, the ratio between the effective horizontal and effective vertical stress is a function of Poisson's ratio. However, the total stress exerted on the deep formation is divided into two parts; those are pore pressure and effective stress. From the back calculation, the horizontal stress can be obtained by adding pore pressure to effective horizontal stress. Thus only in a relatively uniform formation that is free from tectonic effects, erosion, faults and shear zones, jointed rocks etc., can equation 3.1b represent the characteristic state of horizontal stress.

Poisson's ratios for most rocks lie between 0.2 and 0.33; hence, the ratio of the horizontal to vertical stress calculated form Eq.4.1b should be 0.25 to 0.5. However, most *in situ* measured values of this ratio could lie between 0.5 and 0.8 for hard rock, and between 0.8 and 1.0 for soft or inelastic rock such as shale or salt, even greater than 1.0 in some areas (Obert 1967). This is because over long periods the formation has been exposed to a large degree of geological tectonic force, and substantial differences between the principal stresses were generated.

In this circumstance, the measured field stresses are more reliable for engineering design. Equation 3.1b can not provide precise estimation of stress profiles, because of significant tectonic effects on the horizontal stress and stress orientation. Hence, several methods of stress determination are available to obtain *in situ* stresses for geological engineering projects. The major methods include flatjack, hydraulic fracturing, USBM overcoring torpedo, and CSRIO overcoring gauge (Eberhardt 2004), but only hydraulic fracturing is commonly used at depth in sediments.

It is known that the stresses carried by the solid phase contribute significantly to deformation, yield, or rupture. In order to produce a fracture, the injected fluid must first balance the pore pressure and then overcome the effective stress to generate the deformation. Therefore, the threshold stress for the induced fracture is equal to the sum of minimum effective stress and pore pressure. For example, at a great depth with the minimum stress in a horizontal direction, the break down pressure must exceed the minimum total horizontal stress, which is the sum of the pore pressure and the minimum effective stress.

The rock elastic properties are also important for hydraulic fracture design; they represent the rock's reaction to stress changes. Linear elasticity is used to predict fracture dimensions, and the stiffness of the formations is one of the key parameters in this theory. Young's modulus is defined as "the ratio of stress to strain for uniaxial stress" (Gidley *et al.* 1989). This modulus expresses the properties of material stiffness. Stiff material has a large Young's modulus that results in a narrow fracture. In contrast, a wider fracture is generated for more porous rock with a lower Young's modulus. The modulus of a rock is a function of the lithology, porosity, and other variables.

The azimuth of orientation of a vertical fracture depends upon the azimuth of the minimum and maximum horizontal stresses (Gidley *et al.* 1989).

Figure 4.5 shows a vertical wellbore under the action of horizontal *in situ* stresses σ_{hmin} and σ_{hmax}.

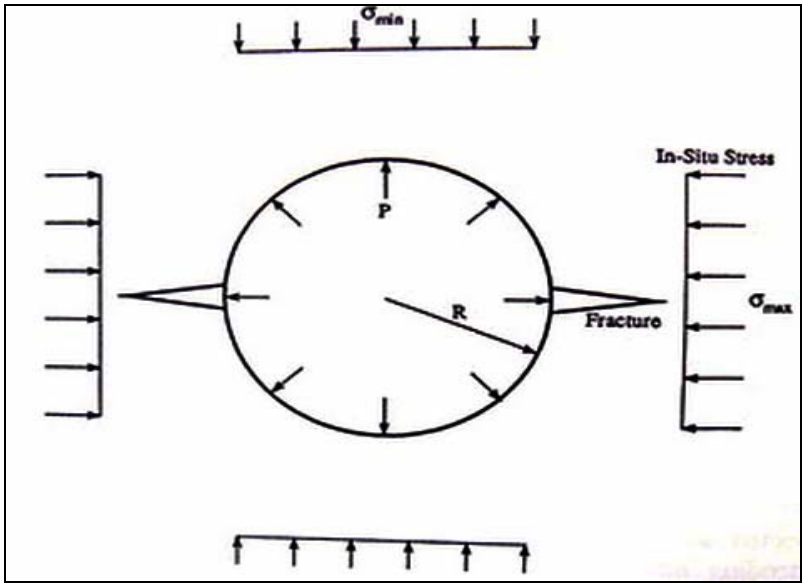

Figure 4.5 Horizontal section of a vertical well bore under the in situ stresses and pore pressure (Yew, 1997)

Assume that the rock is an elastic medium and has a tensile failure stress σ_T. Also, assume a vertical borehole parallel to the vertical stress which is also a principal stress, in this case either σ_1 or σ_2, such that σ_3 is also σ_{hmin}. Timoshenko and Goodier (1951) first applied elasticity theory to compute breakdown pressure P_b for initiating a fracture at the surface of the hole. The equation is:

$$P_b = 3\sigma_{h\min} - \sigma_{h\max} + \sigma_T \tag{4.2}$$

Where σ_{hmin} = minimum *in situ* stress

σ_{hmax} = maximum *in situ* stress

σ_T = tensile failure stress of the rock

In practice, there are also effects of pore pressure and flow in the porous reservoir; Schmidt and Zoback (1989) modified the breakdown pressure equation for a porous medium under the influence of the pore fluid:

For a formation impermeable to the fracturing fluid,

$$P_b = 3\sigma_{h\min} - \sigma_{h\max} + \sigma_T - \phi P_P \tag{4.3}$$

For a formation permeable to the fracturing fluid,

$$P_b = \frac{3\sigma_{h\min} - \sigma_{h\max} + \sigma_T - \alpha P_P\left(\frac{1-2\nu}{1-\nu}\right)}{1+\phi-\alpha\left(\frac{1-2\nu}{1-\nu}\right)} \tag{4.4}$$

where P_p = pore pressure

ϕ = porosity

ν = Poisson's ratio of dry rock, and

$$\alpha = 1 - \frac{\text{bulk of modulus of dry rock}}{\text{bulk of modulus of skeleton material}}$$

A typical bottom-hole pressure record is sketched in Figure 3.6. It is clear that the applied well bore pressure first balances the reservoir pressure or pore pressure, then as it increases, it could overcome the circumferential stress and the tensile failure stress of the rock medium, which can then lead to a tensile failure on the hole surface. Hence, a fracture is initiated in this case, usually with the fracture departing at 90° to the vertical hole wall and in a direction normal to σ_3. The hydraulically induced fracture propagates in the reservoir as pumping continues, and at the same time, the fracturing fluid leaks off through the fracture surface into the surrounding rock medium. It is important to notice that the pressure difference between the fluid pressure in the fracture and the minimum *in situ* stress, σ_3, maintains the open fracture, while the difference between the fracture pressure and the far-field pore pressure controls the rate of fluid leak-off from the fracture surface.

As shown in Figure 3.6, an initial breakdown pressure P_b (the maximum pressure) is first achieved; then, the pressure in the fracture drops to a propagation pressure, driving fracture growth outward from the hole. The flat portion of the pressure curve is the propagation pressure P_{prop}, where P_{prop} is significantly larger than σ_3 because of the additional frictional losses of pressure in the fracture aperture, as well as the value of σ_3. When injection stops, the pressure drops suddenly to a lower value but continues to decrease slowly to the reservoir pressure, as shown in Figure 3.6, because of the fluid leaking off from the fracture. In the decreasing section of the curve, the pressure in the borehole first drops to the instantaneous shut-in pressure (ISIP) which is still larger than σ_3, but smaller than P_{prop}. This is the transition point where fluid flow inside the fracture ceases and there is no friction loss; however, the fracture remains open. With the fluid leaking off through the fracture face, fluid pressure in the fracture declines, resulting in the closure of the fracture. At this point, the closure pressure is slightly lower than the instantaneous shut-in pressure (ISIP) and the closure pressure is considered to be equal to the minimum *in situ* stress (σ_3). Then, the fluid pressure inside the fracture declines gradually; eventually, it reaches equilibrium with the reservoir pressure (P_p).

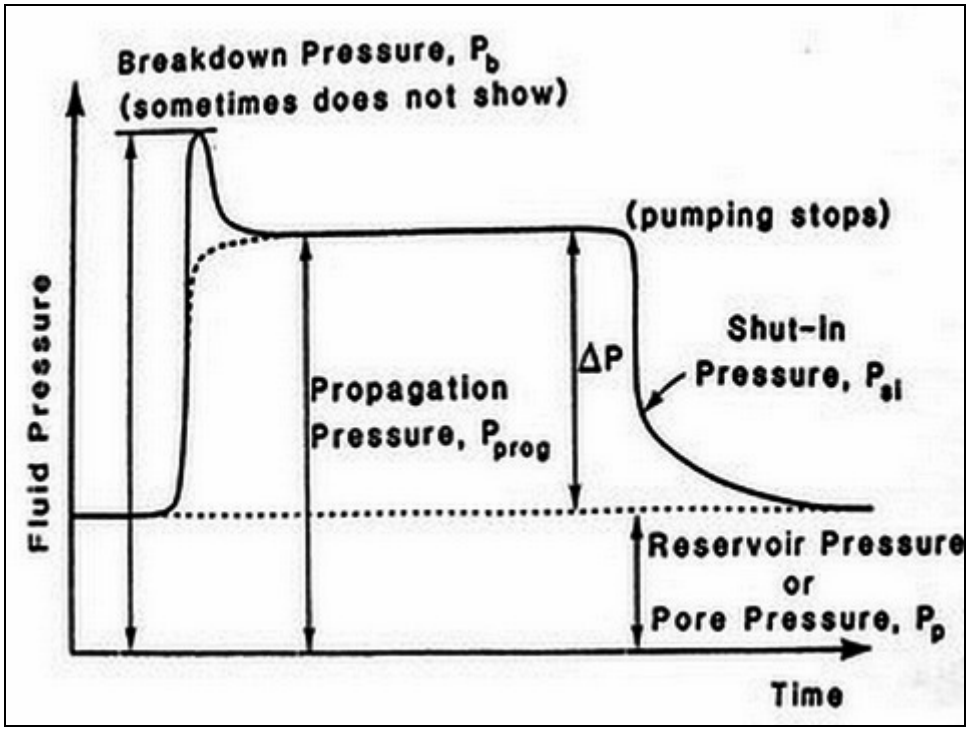

Figure 4.6 Bottom-hole pressure graph (Yew, 1997)

Hydraulic fracture treatment of an oil or gas well is usually conducted at a depth greater than 1000 m, and the minimum *in situ* stress is usually in the horizontal plane, so the induced fracture is a vertical fracture whose plane is perpendicular to the minimum *in situ* stress. Therefore, the growth of fracture height is in part controlled by the vertical distribution of the horizontal minimum *in situ* stress. When the contrast of horizontal stress distribution between vertically adjacent stress zones is large, the growth of fracture height is constrained and horizontal propagation takes place in the lower stress zone.

Early models for the propagation of a fracture make use of this limited vertical height fracture configuration in order to simplify a complex 3-D problem into a 2-D problem in which the fracture has constant height. The Khristianovic and Zheltov (KZ) model (Khristianovic and Zheltov 1955) as well as the Perkins and Kern (PK) model (Perkins and Kern 1961), are the most widely used models. These two models assume that the fracture has a constant height and propagates in a plane in two opposite directions; these assumptions allow plane-strain boundary conditions to be assumed as well. It is assumed that the strain of fracture only occurs in the horizontal direction in the KZ model. A vertical plane-strain condition is also assumed in the PK model in which the fracture has only strain normal to a vertical plane and has relatively larger length than height. Nordgren (1972) studied this model further and gave an analytical solution for the width, length, and pressure of the PK-type fracture. The further developed model is often referred to as the PKN (Perkins-Kern-Nordgern) model.

Figure 4.7 is a sketch of the PKN-type fracture model (half fracture or one side of the fracture). The geometry of the PKN fracture is in an elliptical cross-section shape at the vertical mid-point plane and

at the horizontal mid-point plane as well and it is assumed that fracture toughness has no effect on the geometry, i.e., the K_{IC} is assumed to be zero (Yew 1997).

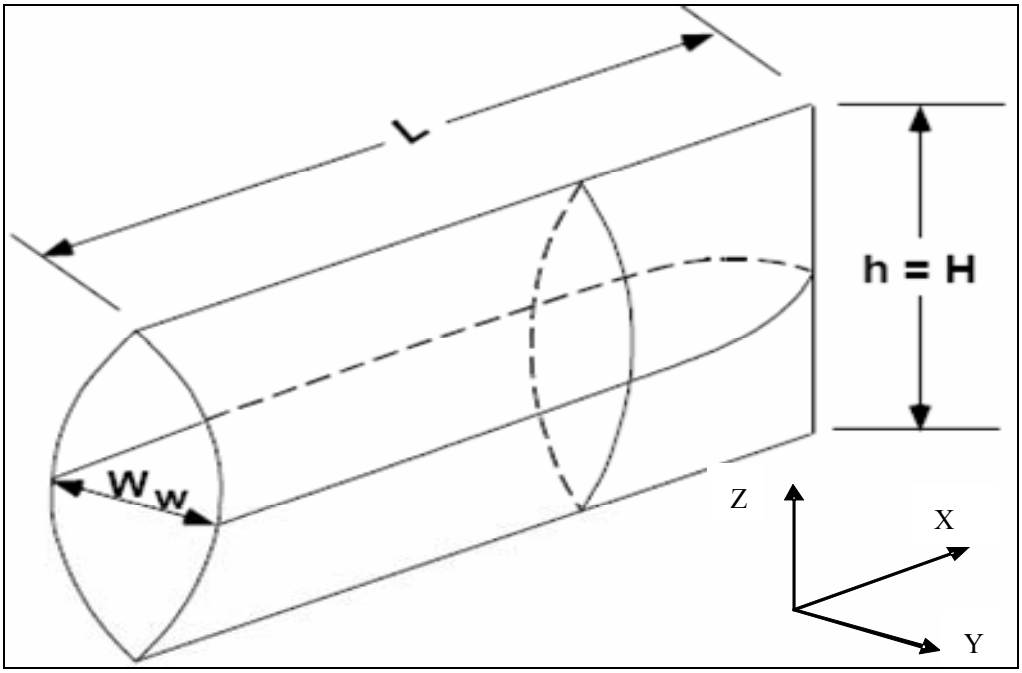

Figure 4.7 PKN fracture model geometry (US EPA 2004)

In Nordgren's study, the mass balance equation, derived from the continuity equation, for flow inside the fracture is written as:

$$\frac{\partial q}{\partial x} - q_{leak} + \frac{\partial A}{\partial t} = 0 \tag{4.5}$$

where q(x,t) = volume rate of flow through a cross-section of the fracture

$q_{leak}(x,t)$ = volume rate of fluid leak-off per unit fracture length

A(x,t) = cross-sectional area of the fracture

The fracture is of elliptical shape with the width given by:

$$w = \frac{P_w(1-\nu)}{G}\sqrt{(h^2 - 4z^2)} \tag{4.6}$$

where P_w = bore hole net pressure, = $P_{frac} - \sigma_3$

G = Shear modulus

ν = Poisson's ratio

P_{frac} = absolute pressure in the fracture

The area of an ellipse can be written as:

$$A = \int_{-h/2}^{h/2} w dz = \frac{\pi}{4} Wh \tag{4.7}$$

where W = maximum width of the fracture. The averaged width is introduced into the description of the geometry of fracture, using *W* for the width at the midpoint (maximum width).

$\overline{w} = (\frac{\pi}{4})^2 W$ for elliptical cross-section area.

In an elliptical tube, the flow rate q for laminar flow of a Newtonian fluid is a function of the pressure gradient and is written as:

$$q = -\frac{\pi W^3 h}{64\mu} \frac{\partial p}{\partial x} \tag{4.8}$$

The liquid leak-off rate from the fracture, q_l, developed in an approximate form by Carter (1957), is expressed as:

$$q_l = \frac{2c_l h}{\sqrt{t - \tau(x)}} \tag{4.9}$$

where c_l = leak-off coefficient, ($m/s^{1/2}$)

$\tau(x)$ = time at which fluid leak-off begins at position x, (s)

Upon the substitution of Equation (4.6), Equation (4.7), Equation (4.8) and Equation (4.9) into Equation (4.5), the governing equation for the propagation of a hydraulically fracture is developed as:

$$\frac{G}{64(1-\nu)\mu h} \frac{\partial^2 W^4}{\partial x^2} = \frac{8c_l}{\pi\sqrt{t - \tau(x)}} + \frac{\partial W}{\partial t} \tag{3.10}$$

The initial condition is: W(x,0) = 0

The boundary conditions are:

$$W(x,t) = 0 \text{ at } x \geq L(t) \tag{4.11}$$

$$\frac{\partial^2 W^4}{\partial x^2} = -\frac{256(1-\nu)\mu}{\pi G} Q \tag{4.12}$$

where Q is the injection rate.

Nordgren solved the above equation for two cases, a large leak-off condition and no leak-off. The former is equivalent to high formation permeability and no filter-cake damage effect on the fracture wall; the latter is equivalent to an impermeable formation or to the case where a filter-cake of low permeability is reducing the transmissivity of the facture wall to a small value.

The large leak-off condition

Fracture length is given as:

$$L = \frac{Q}{\pi c_l h} t^{1/2} \tag{4.13}$$

Maximum fracture width is:

$$W = 4[\frac{2(1-\nu)\mu Q^2}{\pi^3 G c_l h}]^{1/4} t^{1/8} \tag{4.14}$$

Net well bore pressure is

$$P_w = 4[\frac{2G^3\mu Q^2}{\pi^3(1-\nu)c_l h^5}]^{1/4} t^{1/8} \tag{4.15}$$

The zero leak-off condition

Fracture length is given as:

$$L = 0.68[\frac{GQ^3}{\mu(1-\nu)h^4}]^{1/5} t^{4/5} \tag{4.16}$$

Maximum fracture opening width:

$$W = 2.5[\frac{2(1-\nu)\mu Q^2}{Gh}]^{1/5} t^{1/5} \tag{4.17}$$

Net well bore pressure:

$$P_w = 2.5[\frac{G^4\mu Q^2}{(1-\nu)^4 h^6}]^{1/5} t^{1/5} \tag{4.18}$$

As in the development of the PKN model, Geertsma and de Klerk (Geertsma and de Klerk 1969) further developed the KZ case, and the result is often referred to as the KGD model. The horizontal plane strain condition of the KGD geometry would result in a fracture with a rectangular profile. The height is also confined to a constant value. The rectangular shape of a cross section further from the well has a smaller width, decreasing to zero at the tip of the fracture. The geometry of KGD fracture is shown in Figure 4.8 (half fracture or one side of the fracture). Geertsam and de Klerk obtain the approximate solutions of the fracture geometry for the no fluid leak-off condition.

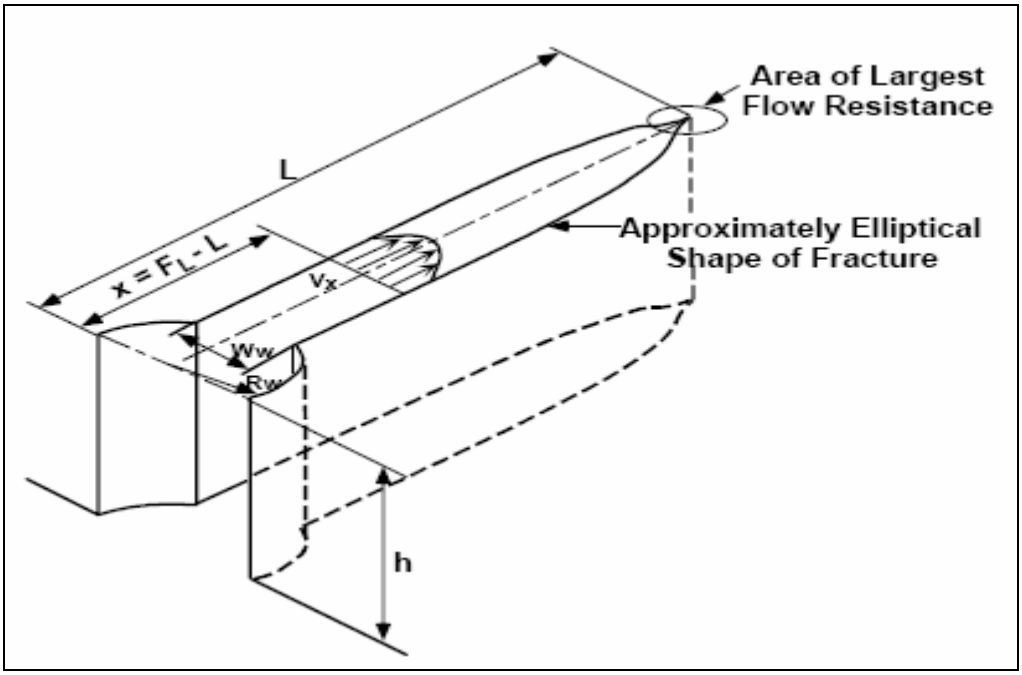

Figure 4.8 KGD geometry (US EPA, 2004)

Fracture length:

$$L = 0.48[\frac{8GQ^3}{(1-\nu)\mu}]^{1/6} t^{2/3} \tag{4.19}$$

Maximum fracture opening width:

$$W = 1.32[\frac{8(1-\nu)Q^3\mu}{G}]^{1/6} t^{1/3} \tag{4.20}$$

Wellbore pressure:

$$P_{bore} = \sigma_{\min} + 0.96[\frac{2G^3Q\mu}{(1-\nu)^3 L^2}]^{1/4} \tag{4.21}$$

For the derivation of the solution for the KGD model, it is assumed that the dry zone in front of the fracture tip is small and the effect on overall geometry of the local tip stress singularity is small.

Comparing the pressure equations from both models, it can be found that the net pressure is increasing with the developing of the fracture in PKN model, but in contrast the KGD model shows that the pressure decreases with fracture extension. Hence, the two models cannot be applied interchangeably. Fractures in formations that are clearly bounded at the top and bottom by lithologies or stress contrasts that are likely to restrict the fracture height can best be approximated with the PKN model. Relatively uncontrolled fracture height cases or small fracture treatments where the length-to-

height ratio is not too large can best be approximated with the KGD model. In general, KGD-type fractures are not interesting from a production point of view (Valko and Economides 1995).

4.3 Conception of Filtration and Models

With the slurry injected into the porous medium continuously, a pressure higher than the formation stress is induced. Hence, the high fluid pressure gradient between the fracture and the far-field ($P_f - P_p$) leads to flux across the fracture wall into the porous medium; this results in the deposition of the solids component in the slurry onto the fracture wall. During fracturing, therefore, part of the biosolids form filter cakes as the water filters into the formation, and the rest of the biosolids and slurry propagate down the fracture to cause fracture extension. The mechanisms of deposition of solids components onto the fracture wall are analogous to a liquid/solids separation process. Therefore, the theory of filtration for highly compactable biosolids is of considerable interest for biosolids injection. Also, the solid part of the injected slurry is mainly composed of biosolids which are highly compactable, so the filter cake itself is susceptible to further compaction and consolidation under the effect of seepage stresses and overburden stresses.

The conventional theory of filtration was developed based on Darcy's law for liquid phase flux in the porous solids cake as well as a static force balance, giving a governing equation in which the flow rate is a function of porosity and liquid pressure. An assumption for the theory of filtration is that particles are in point-contact and that the solids phase is non-deformable (Figure 4.9).

The conventional model for filtration is one-dimensional. The continuity equation is employed to depict the flow through the filter media. The rate of flow into the filter media at location x ($q_L(x,t)$) minus the rate of flow out of the filter media at x=0 ($q_L(t)$) equals the rate of change of liquid content in the filter media. The equation for constituent conservation is written as:

$$q_L(x,t) - q_L(t) = \frac{\partial}{\partial t}\int_0^x \phi(x,t)dx \tag{4.22}$$

Hence, the equation for the solids phase is given as Equation 4.23

$$q_S(x,t) = \frac{\partial}{\partial t}\int_0^x (1-\varepsilon_L(x,t))dx \tag{3.23}$$

where ϕ = porosity

$q_s(x,t)$ is solids flow rate at location x

Differentiating Equations 4.22 and 4.23 with an assumption of a linear changing of ϕ yields Equations 4.24 and 4.25

$$\left(\frac{\partial q_L}{\partial x}\right)_t = \left(\frac{\partial \phi}{\partial t}\right)_x \tag{4.24}$$

$$\left(\frac{\partial q_S}{\partial x}\right)_t = \left(\frac{\partial \varepsilon_s}{\partial t}\right)_x \tag{4.25}$$

where ε_s = volume fraction of solids (defined as solidity equal to 1 - ϕ by definition).

Hence, Equations 4.24 and 4.25 can be combined together as:

$$\left(\frac{\partial q_L}{\partial x}\right)_t + \left(\frac{\partial q_S}{\partial x}\right)_t = 0 \tag{4.26}$$

The static force balance depicts the stresses exerted on the filter cake; the total applied pressure (P) is equal to the pressure on liquid phase (P_L) plus the solid pressure (P_S) that describes the contact force between the solids in filtration theory. This force is also referred to as the effective stress on solids (σ') in geomechanics. In this section, P_S is used as a contact force between solids or a solid pressure for filtration theory as it is widely accepted, while it represents the same concept as an effective stress (σ') in geomechanics. The equation is written as:

$$P = P_L + P_S \tag{4.27}$$

The gravity force and the inertial force are assumed to be negligible and the solid particles are non-deformable. There are only point contacts among particles, without creep of particles. Then, at a fixed time, the force balance can be expressed as Equation 3.28. The liquid pressure and effective stress are exerted on the overall cross-section area of the medium.

$$\left(\frac{\partial P_L}{\partial x}\right)_t + \left(\frac{\partial P_S}{\partial x}\right)_t = 0 \tag{4.28}$$

For the volume of solids in filtration, the differential volume of solids d ω in dx and the total volume of solids in a cake of thickness Y are given by $d\omega = \varepsilon_s dy$, so the integration form is as $\omega = \int_0^Y \varepsilon_s dy = \varepsilon_{sav} Y$. And the resistance of filter cake is as $\alpha = 1/k\varepsilon_s$.

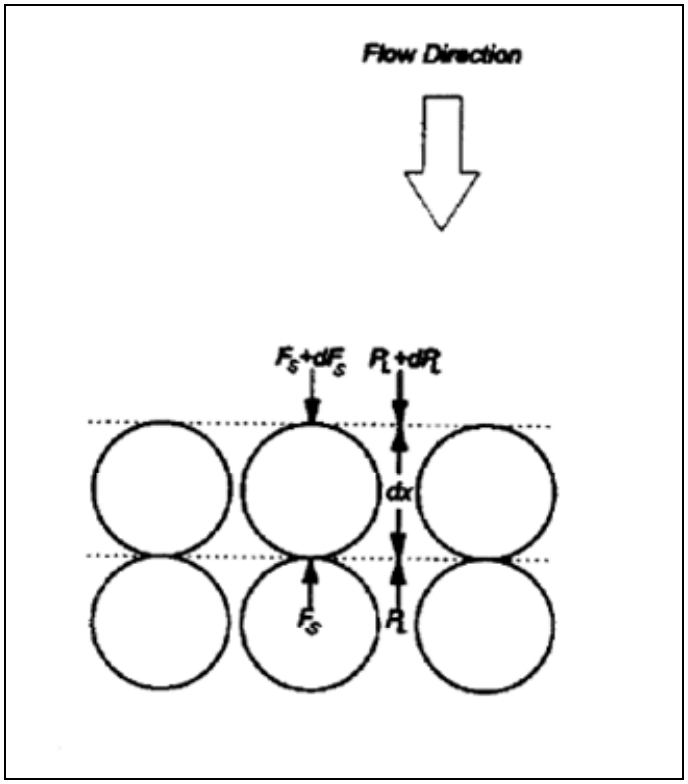

Figure 4.9 Depiction of one dimensional filtration (Lee and Wang 2000)

Darcy's law is the fundamental theory for flow in permeable media driven by the pressure drop across the medium. The conventional Darcy equation for flow through incompressible media is expressed as:

$$q_L = \frac{k}{\mu}\frac{dP_L}{dx} = \frac{1}{\alpha\mu}\frac{dP_L}{d\omega} \tag{4.29}$$

where P_L = liquid pressure, Pa

x = distance measured from the medium supporting the cake m

ω = volume of inert solids per unit area in distance x m

k = permeability m^2

α = 1/k specific resistance with units m^{-2}

μ = viscosity Pa · s

The solids phase in the filtration process is in motion, so a variable flow rate through the filter cake is introduced into the Darcy equation. The Darcy-Shirato model is first developed (Shirato *et al.* 1969) by combining the variable velocity of flow with the Darcy equation. The Darcy-Shirato model is written in the form:

$$\frac{dP_L}{dx} = -\frac{\mu\phi}{k}(u_L - u_s) \tag{4.30}$$

where $u_L - u_S$ = velocity of the liquid relative to the solids.

The equation can be written in both spatial and material coordinate systems in one dimension. The relationship between effective stresses on the solids and the porosity for a material is obtained from empirical tests. Substituting such an empirical equation for the relation of effective stress to porosity into the governing equation of filtration, the differential equation is reduced to one variable, which usually is effective stress. The governing equations can be solved under appropriate initial and boundary conditions.

Finally, the governing equation can be developed from the substitution of $q_L = \phi \times u_L$, $q_S = (1-\phi) \times u_S$ into Equation 4.30, giving:

$$q_L = -\frac{(1-\phi)k}{\mu}\left(\frac{\partial P_S}{\partial x}\right) + \phi q_l \tag{4.31}$$

where q_l is liquid flow rate at medium m/s^{-1}

Assuming that ϕ is only a function of solid pressure (P_S) or effective stress (σ'), Equation 4.31 can be transformed into (Lee and Wang 2000):

$$\frac{1}{\mu\rho_s}\left(\frac{\partial^2 P_s}{\partial x^2}\right) - \frac{1}{\mu\rho_s\alpha}\frac{d\alpha}{dP_s}\left(\frac{\partial P_s}{\partial x}\right)^2 - q_l\alpha\frac{d\varepsilon}{dP_s}\left(\frac{\partial P_s}{\partial x}\right) + \alpha\frac{d\varepsilon}{dP_s}\left(\frac{\partial P_s}{\partial x}\right) = 0 \tag{4.32}$$

A power-law equation can be employed to describe filter cake characteristics of highly compressible sludge or biosolids in the filtration process. The power-law type equations are in the forms (Koenders and Wakeman 1995):

$$\alpha = \alpha_0(a_1 + b_1 P_S)^{n1} \tag{4.33}$$

$$1 - \phi = (1 - \phi_0)(a_2 + b_2 P_S)^{n2} \tag{4.34}$$

where a_1 and a_2 are assumed to be 0 or 1; $b_1 = b_2 = P^{-1}{}_i$. The P_i is a reference pressure that is the threshold pressure for the compression of the filter cake, and n_1 and n_2 are solid material characteristics which specify the degree of compressibility. α and α_0 are specific resistance and reference specific resistance for the condition where solids are in contact and $P_S = P_0$.

Another form of resistance of filter cake in filtration processes is written as Equation 4.35 (Wakeman *et al.* 1991).

$$\alpha = \alpha_i\left(\frac{P_S}{P_i}\right)^n \tag{4.35}$$

where α_i = the reference resistance

P_i = the reference pressure

The pseudo-steady state of filtration is the most common assumption in conventional analysis. This assumption leads more easily to an answer because of easier transformation of partial differentials into an ordinary differential equation. In this case, two boundary conditions can be used to solve the problem even without the initial condition.

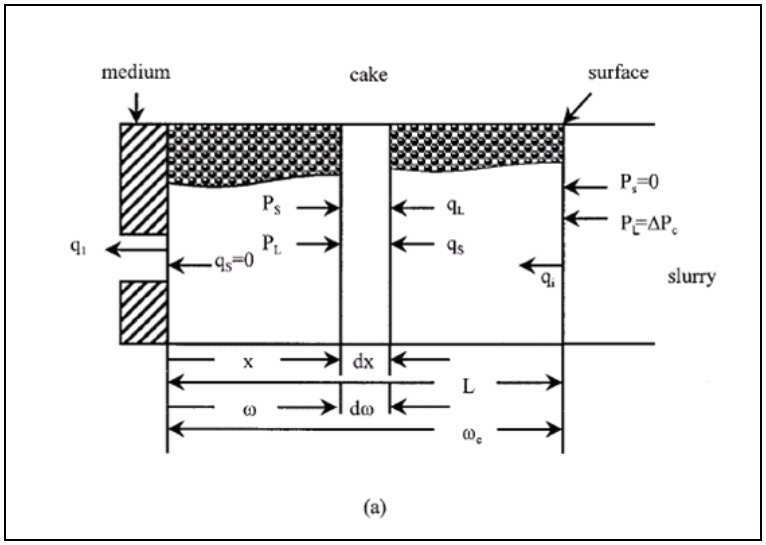

Figure 4.10 One dimensional filtration process

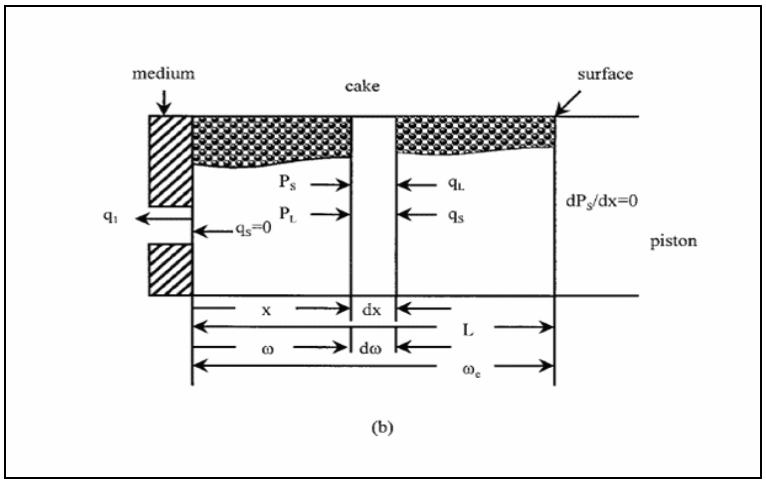

Figure 4.11 One dimensional consolidation (Lee and Wang, 2000)

4.4 Consolidation Theory

Compression of a porous permeable material is achieved through rearranging the soil solids or extruding the pore air or water. A decrease of water content in a saturated soil without the

replacement of water by air is defined as consolidation. When saturated soft soils that have a low permeability are subjected to a loading, the pore pressure immediately increases. Because of the low permeability of soils, there is a considerable time lag between the application of a load and the full extrusion of the excess pore water.

In standard one-dimensional consolidation tests, the consolidation can be divided into three phases: the initial compression phase, a primary consolidation phase, and a secondary consolidation phase. The initial compression is small and can be neglected. The two main phases in consolidation processes, primary consolidation and secondary consolidation, are discussed here.

In primary consolidation, when a load is first applied to a saturated compressible soil mass, the water in the pores usually carry the load initially because the water is relatively more incompressible than the soil. The incremental load results in excess pore pressure, which is called excess hydrostatic pressure. The high gradient of pore pressure dispels water out of the system, and the effective stresses in the solid matrix increase as the pore pressure dissipates, causing compaction. In other words, the transfer of a load is accompanied by a change in volume of the soil mass equal to the volume of water drained. A theory relating loading, time, and volume change has been proposed and has become known as the Terzaghi theory of consolidation. One of the major assumptions in the theory is the volume change and the outflow of pore water occurs in one dimension only. For this reason it is sometimes referred to as the Terzaghi one-dimensional consolidation theory (Fang 1997). The assumptions in the theory of consolidation are listed as:

1. Material is homogeneous;
2. Material is fully saturated;
3. Compression of material is the change in void space only, which in turn squeezes out water from the void spaces;
4. Darcy's law is valid;
5. Deformation of material occurs only in the direction of load application;
6. The coefficient of consolidation C_v is constant during consolidation

During the consolidation, the rate of change of unit soil volume is equal to the rate of change of the void volume. So

$$\frac{\partial V}{\partial t} = \frac{\partial V_v}{\partial t} = dV_s \frac{\partial e}{\partial t} = \frac{dxdydz}{1+e}\frac{\partial e}{\partial t} \tag{4.36}$$

where V_v is void volume

V_s is solid volume

e is void ratio

An assumption that the change in void ratio is linearly dependent on the increase of effective stress is made during the derivation of Terzaghi consolidation equation. Again, the increase of effective stress is equal to the decrease of excess pore water pressure. Hence,

$$\partial e = -a_v \partial(\Delta\sigma') = a_v \partial p_0 \tag{4.37}$$

The flow of water out of a unit volume of saturated soil is given as $\frac{K}{\gamma}\frac{\partial^2 p_0}{\partial z^2} dxdydz$

The basic differential equation for Terzaghi consolidation is derived as:

$$\frac{K}{\gamma}\frac{\partial^2 p_0}{\partial z^2} = \frac{1}{1+e}\frac{\partial e}{\partial t} = \frac{a_v}{1+e}\frac{\partial p_0}{\partial t} = m_v \frac{\partial p_0}{\partial t} \tag{4.38}$$

$$\frac{\partial p_0}{\partial t} = \frac{K}{\gamma m_v}\frac{\partial^2 p_0}{\partial z^2} = C_v \frac{\partial^2 p_0}{\partial z^2} \tag{4.39}$$

where p_0 is the pore water pressure

C_v is coefficient of consolidation = $\frac{K}{\gamma m_v}$

m_v is coefficient of volume compressibility = $\frac{a_v}{1+e}$

γ is unit weight of water

a_v is coefficient of compressibility

The Terzaghi equation implies both a settlement degree and a time rate (Braja 1997). The coefficient of compressibility (a_v) is the slope of the relationship between void ratio and effective stress in arithmetic space. The coefficient of consolidation (C_v) is a measure of the rate of change of volume during primary consolidation.

From a standard one-dimensional consolidation test, the coefficient of permeability, K, can be obtained from the following equation:

$$K = C_v\, m_v\, \gamma_w \tag{4.40}$$

where C_v can be obtained from a routine consolidation test and m_v is the coefficient of volume compressibility that is the change in volumetric strain per unit volume per unit change in effective stress in one-dimensional compression (unit: m/MN).

Shirato *et al.* (1965) assumed a Terzaghi-type relationship for porosity ($\phi = \phi(\sigma')$), and took $n_2 = -1$, $a_2 = 1$ and $b_2 = -\alpha_E (1 - \phi_{LO})$ in Equation 3.34. Consequently, the equation for consolidation of highly compactable material was developed and was written as a Terzaghi spring analogy equation:

$$e = e_0 - a_E P_S \tag{4.41}$$

where e = void ratio ($e = \phi / 1 - \phi$), and a_E is the spring constant.

In addition, from a compression plot of void ratio vs. σ', a typical e vs. log (σ) plot, the compression index C_c can be obtained:

$$C_c = \frac{e_1 - e_2}{\log \sigma_2' - \log \sigma_1'} = \frac{\Delta e}{\log(\frac{\sigma_2'}{\sigma_1'})} \tag{4.42}$$

If compression index C_c is known, we can do a back calculation of any value of e_2 at the corresponding effective stress σ_2', taking e_1 and σ_1' as reference values.

When material like soft soil or biosolids continues to compact under constant effective stress at the end of primary consolidation, the deformation is referred to secondary consolidation. The magnitude of secondary consolidation is often defined by:

$$C_s = \frac{\Delta H / H}{\log t_2 - \log t_1} \tag{4.43}$$

However, this is a purely empirical equation based on long-term testing on materials. As in the case of biosolids, for example, the secondary consolidation is mainly the result of the creep effects and biodegradation, but Equation (4.43) does not take any biodegradation into account. Therefore, some other models have been specifically developed to consider creep effects on sludge or biosolids under consolidation conditions.

Because the consolidation properties of biosolids must be determined by empirical testing at the relevant stresses and temperatures, and must include the effects of decomposition, the necessary parameters are not yet available (no tests have been done yet). Some implications are obtained from the study done by O'Kelly (2005).

- Consolidation properties of biosolids are attributed to both the dewatering properties of biosolids and the biodegradation properties.
- Highly stabilized (decomposed) biosolids respond with a larger degree of deformation to primary consolidation (in short term).
- Moderately degraded biosolids respond with a larger secondary deformation, because of degradation.
- A highly degraded sludge is more permeable than moderately degraded biosolids because of less organic material, so the biodegradation of the moderately degraded biosolids causes more creep deformation (long term deformation), and the higher content of organic material should also slow down the rate of primary consolidation because of a lower permeability.

Chapter 5

Physical Model for Deep Underground Injection of Biosolids

5.1 Hydraulic Fracturing Model for the Injection Phase

Hydraulic fracturing processes have been applied for many decades in low permeability reservoirs to increase production. During hydraulic fracturing in a permeable formation, the fluids partially filtrate into the formation to displace the formation fluid under the pressure gradient between the fracture and formation. This flow rate of filtration is called the leak-off rate in hydraulic fracture treatments.

The leak-off rate has a significant impact on the geometry of induced fractures and hydraulic fracture design. The prediction of leak-off rate is also critical to interpret net pressure response at bottom-hole during the fracturing operation.

Carter (1957) initially developed a solution for fracturing fluid leak-off under assumptions of constant fracture width and pressure. In the Carter model, a leak-off coefficient was used that is inversely proportional with the square root of time. It is the fundamental original leak-off model for further studies of the leak-off rate.

Many studies have been conducted experimentally of the leak-off behavior (McDaniel *et al.* 1985; Gulbis 1982, 1983; Roodhart 1985; Mayerhofer *et al.* 1991). Theoretical models (Settari 1985, 1988) were developed to simulate this important process in hydraulic fracturing treatment. These models have generally confirmed the linear relation between leak-off volume and square root of time which is obtained from Carter's theory.

Yi & Peden (1993) and Fan (1995) introduced models to describe leak-off mechanisms in three individual cases. The models were mainly based on the fundamental equations for fluid flow through porous media but looked at other than linear relations of leak-off volume and square root of time. The models developed by Yi and Fan also incorporated non-Newtonian fluid invasion into the porous medium, rather than the traditional Newtonian fluid leak-off models. In Fan's studies, a new leak-off model incorporating a solution for the moving interface problem was given in terms of the pressure gradient between the fracture and the formation. Mayerhofer (1991) studied filter cake properties and their relations with the leak-off rate. The concept of the filter cake resistance is introduced into the interpretation of the leak-off behavior and the theory of viscoelasticity is applied to describe the incompressible filter cake behavior in his study.

In the frac&pack treatment, the fracturing fluid conveys solid propping agents into the fracture; this process shares physical similarities with solids injection. The frac&pack treatment normally is operated in one stage, although it has two distinct stages during the process (Wong *et al*. 1993, Roodhart *et al*. 1993). When the frac&pack treatment is applied in the case of a high permeability reservoir, a large fracture width is required but this also leads to short fracture lengths. In order to obtain high fracture conductivity, a tip screen-out during the aggressive frac&pack treatment is achieved in part by fracturing fluids that do not build a particularly large filtration cake. The other

aspects of frac&pack treatment are that very high injection pressures are achieved with high concentrations of proppant toward the end of the process to force a large width fracture packed full of proppant.

The frac&pack models focus on the fracturing process under regular conditions in which the injection liquid is assumed to bleed off at a constant rate. However, biosolids injection is different from the frac&pack treatment because the latter does not generate a thick filter cake during active pumping.

As discussed in Section 4.2, most 2-D models developed are based on one of two assumed fracture geometries (PKN and GDK). For engineering purposes, the PKN type geometry is selected for the development of the research model.

The fracture models result from the combination of a fundamental law (material balance) and constitutive equations which describe elasticity and fluid rheology. The model is intended to be a representation of certain physical processes having major influences on the final geometry of the created fracture. The model developed for biosolids injection couples the solids filtration and consolidation processes into the fracture propagation model.

5.1.1 Formation of filter cake on fracture face

Biosolids sludge and other fine-grained solid wastes in slurry form can be injected down hole above the formation fracture pressure into appropriate sandstone formations. During injection, the injected fluid filters into the surrounding rock because of the high fluid pressure difference between the fracture and formation. During the filtration process, biosolids are deposited on the fracture walls; thus, a biosolids filter cake is formed along the fracture faces and it largely blocks the formation permeability near the wall, resulting in a massive change of leak-off rate. Also, the fracture must become wider to accommodate both the deposited biosolids and the requirement for fluid flow. Hence, the fracture geometry is altered through the build-up of the filter cake, yet the fracture must remain open to transfer slurry further down the fracture. Thus, the distinct properties of injected municipal solid wastes predominated by biosolids could impact the geometry of the fracture profoundly.

Most studies of hydraulic fracturing with leak-off are conducted mainly with an assumption of a constant leak-off rate. Although the frac&pack treatment process shares a physical similarity with biosolids injection, the proppant placed in the fracture during the process does not dramatically impair the permeability of the fracture wall. Fine-grained biosolids can invade somewhat into the pores of the formation as well as deposit on the fracture face. The leak-off rate during a biosolids hydraulic fracturing process is therefore altered dramatically with time as the fracture wall rapidly becomes almost impreperable. Because the leak-off rate has a marked effect on the final geometry of the fracture during the period of dynamic fracture extension and growth, the change in the dynamic leak-off rate is a key factor for the biosolids injection process.

5.1.2 Impacts of dynamic leak-off or filtration on hydraulic fracture propagation

During the injection process, the biosolids deposited on the formation face are under a high fluid pressure difference between the fracture and formation. For example, at a depth of 1000 m in a permeable sandstone, the fracture pressure may be as high as 22-24 MPa, but the formation pore pressure just inside the formation is only about 10 MPa, and does not increase because the filtration rate across the biosolids cake is small compared to the transmissivity of the sandstone. The filter cake in this case would be subject to an effective stress as high as 12-14 MPa on the formation face, and the biosolids are therefore compacted and the resistance to flow across the filter cake would increase correspondingly. Therefore, the compacted filter cake decreases the leak-off rate, so less injected fluid would filter into the formation. This means that, according to the principles of general mass balance, the fracture would propagate forward, and a new fracture face created. The leak-off rate through the old faces would be less than through the new fracture faces under the same condition, as a consequence of the low permeability of the filter cake.

A dynamic leak-off coefficient, decreasing with time or injection volume, is introduced as a descriptor for the deposition and plugging effect of biosolids, which dominantly impacts the fracture geometry. Based on filtration theory for highly compactable biosolids (Cleveland *et al*. 1996), the flow resistance is a function of the pressure drop across the filter cake, which results in the high effective stress that consolidates the deposited biosolids that in turn generates reduced permeability. The deposition of fresh biosolids on to the old filter cake also increases the cake thickness, and partially contributes to the increased flow resistance. Hence, a filter cake with varied thickness, exposed to different ΔP for different time, leads to different leak-off behaviors.

5.2 Model Description

A Perkins-Kern-Nordgren (PKN) leak-off model is selected to describe biosolids injection. A dynamic leak-off coefficient, decreasing with time (or injection volume), is incorporated into the model to represent the deposition (filtration) and plugging effect of biosolids, which in turn affects the fracture geometry.

A finite difference fracture propagation model based on mass balance is developed under the conditions of constant injection rate and constant time step discretization. Both fracture area and average width can vary with time. Each fracture surface element at a time step is assigned a leak-off coefficient according to the pressure profile on the filter cake and its thickness. Each element is assumed to share the same leak-off evolution history, which means that the process is self-similar as the fracture propagates outward.

Because of the distinct properties of biosolids which can alter formation face permeability dramatically, the induced fracture geometry should be different from the results from conventional fracturing models for proppant injection or other typical hydraulic fracturing models. The newly developed semi-numerical model for biosolids injection couples the distinct properties of biosolids into the hydraulic fracturing process and tries to overcome shortcomings of previous models.

5.2.1 General mass balance equations for the fracture

With large volumes of fluid injected down the well under pressure, a hydraulic fracture is created. The mass balance gives the fundamental description of the relation between injected fluid volume and fracture volume. The overall material balance for a hydraulic fracture can be written as:

$$V_i = V + V_l \tag{5. 1}$$

where V_i = injected fluid volume

V = volume of fracture

V_l = leak-off volume

The partial differential equation form of the mass balance for a fracture is written as:

$$\frac{dV}{dt} = Q - Q_l - S_p \frac{dA}{dt} \tag{5. 2}$$

where Q = injection rate

Q_l = leak-off rate or filtration loss rate

S_P = spurt loss coefficient

A = fracture face area.

$$V = \frac{\pi}{2} hL\overline{w} \tag{5. 3}$$

$$A = 4Lh \tag{5. 4}$$

where L is the half fracture length, one side of fracture

h is the fracture height

$\overline{w}$ is the averaged width of fracture

The rate of filtration loss per unit of exposed surface of the fracture is indicated by u; thus leak-off volume is:

$$Q_l = \int_0^A q_l dA = \int_0^t q_l \frac{dA}{d\tau} d\tau \tag{5. 5}$$

where q_l is the leak-off rate (fluid flow rate) per unit area.

5.2.2 Finite difference equations in the model

The one-side fracture can be discretized with time into a set of fracture segments, and is composed of a set of segments. As a result, numerical equations for a set of fracture segments propagating with time are developed.

A single elementary volume between location x and x+Δx is applied to describe the initiation of fracture during the time changing from t to t + Δt. The continuity equation for flow in the fracture and the mass balance equation controlling the fracture volume are coupled to give the fracture propagation volume. Incompressible fluid behaviors and Darcy flow are assumed in the simulation.

The equations for this element flow are:

Volume increase

= Volume flowing into the element - Volume flowing out of the element - Volume leaking off from the element

$$q(x)\Delta t - q(x+\Delta x)\Delta t - V_l = [A_c(t+\Delta t) - A_c(t)]\Delta x \quad (4.\ 6)$$

$$V_l = 2\Delta t\Delta x\int_0^{h_f} \frac{C_l h}{\sqrt{t-\tau}}dh + 2\Delta x\left[h(t+\Delta t) - h(t)\right]S_p \quad (5.\ 7)$$

When a constant height of fracture is assumed, substituting Equation 5.7 into Equation 5.6, difference equations which are used to calculate the initial fracture element geometry length can be written as (Valko and Economides 1995):

$$q(x)\Delta t - q(x+\Delta x)\Delta t - 2\Delta t\Delta x\frac{C_l h}{\sqrt{t-\tau}} + 2\Delta x h S_p = [A_c(t+\Delta t) - A_c(t)]\Delta x \quad (5.\ 8)$$

$$\frac{q(x) - q(x+\Delta x)}{\Delta x} - 2\frac{C_l h}{\sqrt{t-\tau}} + \frac{2hS_p}{\Delta t} = \frac{[A_c(t+\Delta t) - A_c(t)]}{\Delta t} \quad (5.\ 9)$$

$$A_c = h \times \bar{w} \quad (5.\ 10)$$

where A_c = fracture cross-section area

h = height of fracture

$\bar{w}$ = averaged width of fracture

C_l = leak-off coefficient

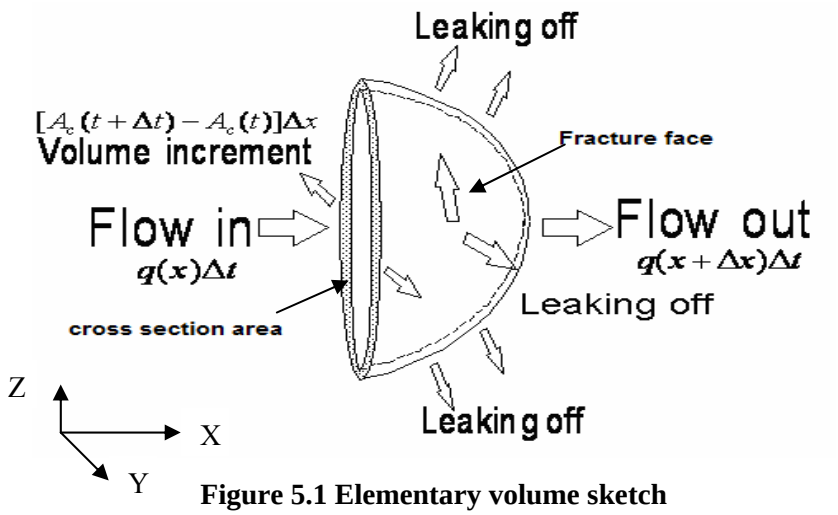

Figure 5.1 Elementary volume sketch

The created fracture at the first time step is subject to the original *in situ* condition and the boundary conditions (Valko and Economides 1995) used for the equation are written as:

$$X = 0 \ : \ q(x,t) \ = \ Q(t) \tag{5. 11}$$

$$X = l \ : \ q(x,t) \ = \ \mu_f(t) \times A_c(x,t) + 2 \times \mu_f(t) \times h_f(x,t) \times S_p \tag{5. 12}$$

where μ_f = dL/dt, μ_f is defined as the growth-rate of the fracture length

$A_c(x,t)$ = fracture cross-section area

A numerical program is developed to solve Equation 5.9 subject to stipulated boundary conditions.

Furthermore, spurt loss (S_p) equal to zero is assumed for the computation of fracture length at the first time step in the program code.

During fracture generation in the first step, the filter cake build-up on the fracture face associated with the leak-off processes contributes to a dynamic leak-off process. From the second time step on, the dynamic leak-off process is accounted for the fracture propagation. This numerical material balance solution allows the surface area and average width to vary with time under a constant injection rate and the same time step condition. The discretized material balance equation is written as:

$$Q\Delta t = 2\sqrt{\Delta t}\sum_{j=1}^{n}\frac{C_{n-j+1}(A_j - A_{j-1})}{\sqrt{n-j+0.25}} + 2S_p(A_n - A_{n-1}) + A_n w_n - A_{n-1}w_{n-1} \tag{5. 13}$$

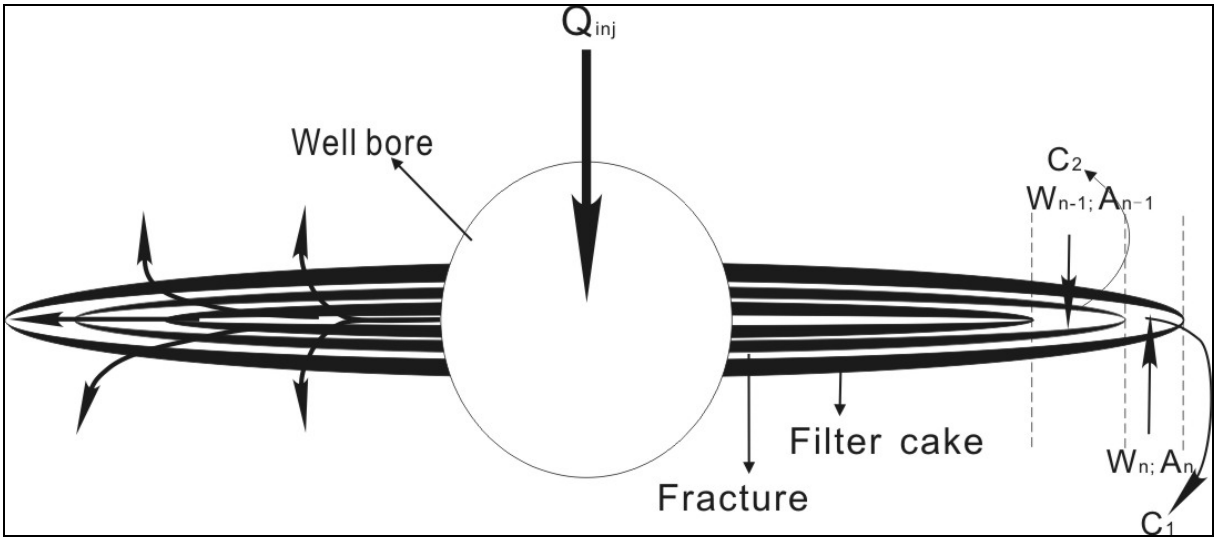

Figure 5.2 Sketch for the induced fracture

The subscript (n) denotes the time step number. Each element of the fracture is assumed to share the same leak-off evolution history as the previous time step. Hence, for each time step, each fracture element has a corresponding fluid flow resistance that increases from the tip of the fracture to the end of fracture near the well bore. The number of 0.25 in the equation is the constant for the description of the starting point of leak-off rate in the time interval. The optimal choice is 0.25, e.g. 0.5 represents leak-off rate starting at the middle of the time interval, and 1 represents leak-off at the end of the time interval (Valko and Economides 1995).

Since the fracture has been created, the initial condition for Equation 5.13 is written as:

$$t = t_1 = \Delta t \ : \ A_1 = X_1 \ \times \ h \ , \ C_1 = C_0 \tag{5. 14}$$

Because of an open system for fracture propagation, only the mass balance controls the fracture propagation. There is no boundary condition needed for Equation 5.13.

5.2.3 Equations of the dynamic leak-off coefficient in the model

Mayerhofer *et al*. (1991b) first developed a relationship between filter cake and pressure given by:

$$\Delta P_{face} = \frac{\pi \mu R_0}{A} R_D q \tag{5. 15}$$

where R_0 is the reference resistance for the formation (m^{-1}) and R_D is the characteristic resistance of the filter-cake reached in the time t_c.

Rewriting Equation 5.15, the leak-off rate equation is given below. The average filter cake resistance of the fracture area is involved in this equation (Mayerhofer *et al.* 1991b, Mayerhofer *et al.* 1993).

$$q = (\frac{\Delta P_{face}\sqrt{t_c}}{\pi\mu R_0})A\frac{1}{\sqrt{t}} \tag{5. 16}$$

where t_c is the characteristic time.

So, comparing with the leak-off model by Carter, the pseudo leak-off coefficient is written as:

$$C_l = (\frac{\Delta P_{face}\sqrt{t_c}}{\pi\mu R_0}) \tag{5. 17}$$

In the filtration process, as described in Section 4.3, Darcy flow is assumed and Darcy's Law is used to represent the flow of liquid through the compactable, porous media with the filtration effect. It relates the flow rate to the liquid pressure gradient. For one-dimensional planar filtration, the total applied stress is as Equation 4.23. The differential form of Equation 4.23 is written as:

$$dP_L + dP_S = 0 \ ; \ dP_L = -dP_S \tag{5. 18}$$

A modified Darcy's Law relates the effective stress gradient and flow rate in material coordinate systems, when the contact force between solids P_S (or effective stress σ') is substituted for liquid pressure in Equation 4.29. The equation is given by:

$$\frac{dv}{dt} = q_l = -\frac{k}{\mu}\frac{dP_s}{dx} = -\frac{1}{\mu\alpha}\frac{dP_s}{d\omega} \tag{5. 19}$$

where v = the filtrate volume per unit filter area

α = specific resistance

q_L= the liquid flow rate per unit filter area

x = the distance from the supporting medium to an arbitrary point in the cake

ω = the volume of solids per unit filter area in the distance x.

The differential volume of solids $d\omega$ in dy and the total volume of solids in a cake of thickness Y are given by:

$$d\omega = \varepsilon_s dy,$$

$$\omega = \int_0^Y \varepsilon_s dy = \varepsilon_{sav} Y \tag{5. 20}$$

where ε_s = volume fraction of solids (defined in Equation 4.25)

ε_{sav} = averaged volume fraction of solids

Integrating the material coordinate formula in Equation 5.19 and introducing the concept of average specific resistance expressed by α_{av}, one may obtain:

$$\mu q_l \omega = \int_0^{\Delta Ps} \frac{dP_s}{\alpha} = \frac{\Delta P_s}{\alpha_{av}} = \mu\frac{dv}{dt}\omega \tag{5. 21}$$

where α_{av} = average specific resistance defined as:

$$\alpha_{av} = \frac{1}{\varepsilon_s k} \tag{5. 22}$$

According to the definition of R, the form of R is written as $R = \frac{\Delta P_c}{q_l} = \mu \alpha_{av} \omega$

Now substituting R into Equation 5.17, the result is:

$$C_l = \frac{\Delta P \sqrt{t}}{\pi \mu^2 \alpha_{av} \omega} \tag{5. 23}$$

The empirical relations for the solidity, specific flow resistance and permeability as functions of effective pressure are given in power law approximation (Cleveland *et al.* 1996). The equation form is written as:

$$\left(\frac{\varepsilon_s}{\varepsilon_{so}}\right)^{\frac{1}{\beta}} = \left(\frac{\alpha}{\alpha_o}\right)^{\frac{1}{n}} = \left(\frac{k}{k_o}\right)^{\frac{-1}{\delta}} = 1 + \frac{P_s}{P_a} \tag{5. 24}$$

Subscript o refers to the null stress value of ε_s, k, and α, while β, n, δ are parameters of compactibility. The P_a is an arbitrary reference pressure. The permeability, specific resistance, and solidity, along with their corresponding exponents in the empirical models, are related by (Tiller *et al*. 1999):

$$\varepsilon_s \times \ k \times \alpha = 1, \delta = n + \beta \tag{5. 25}$$

The parameters used in the model are from experimental data. For highly compactable biosolids, the parameter n is typically larger than 1. (Tiller *et al.* 1999, Tiller and Kwon 1998)

$$\alpha_{av} = \alpha_0 (1 + \frac{P_s}{P_a})^n \tag{5. 26}$$

$$\omega = \frac{q \times t \times SC}{L} \tag{5. 27}$$

where SC is the solids content, L is the fracture half length.

Hence, a dynamic leak-off coefficient can be written in a form by combining the parameter of compactibility of biosolids.

$$C_l = \frac{\Delta P \sqrt{t}}{\pi \mu^2 \alpha_{av} (1 + \frac{P_s}{P_a})^n \times \frac{q \times t \times SC\%}{L}} \tag{5. 28}$$

5.3 The Numerical Code Development

The numerical code is developed based on the difference equations listed above, using Matlab software. The controlling PDE is reduced to a non-linear equation, which can be solved numerically. An appropriate root-finding algorithm is applied to solve the non-linear equation.

Because of the physical nature of the biosolids filter-cake and the impact of deposited biosolids filter-cake on leak-off rate, each segment is assigned a corresponding leak-off rate. Figure 4.3 describes this physical process with an assumption of each segment bearing the same evolution of leak-off process (the assumption of self-similarity).

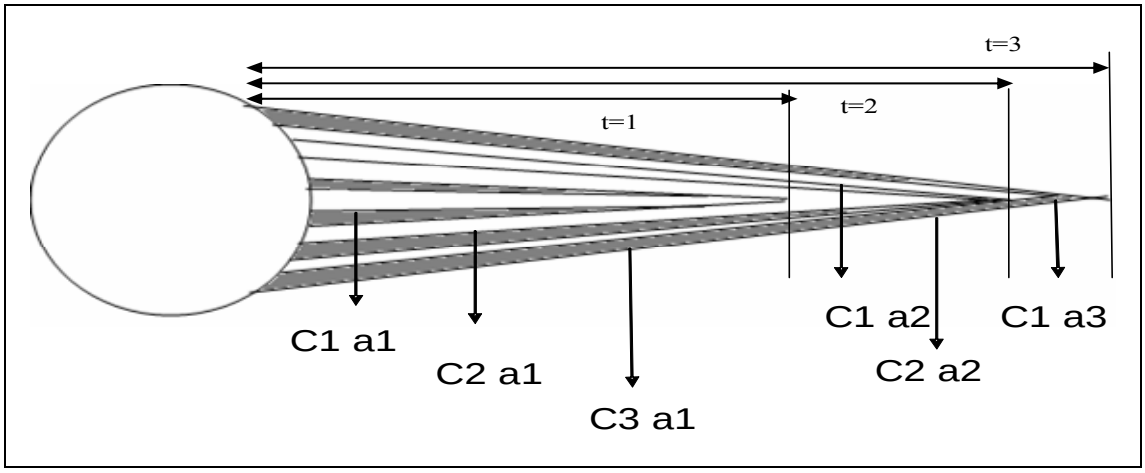

Figure 5.3 D**ynamic leak-off rate for each segment in every time step (one side of fracture)**

The PKN-type fracture geometry is used to compute the fracture width (Valko and Economides 1995):

$$\overline{w} = 2.05(\frac{\mu(1-\nu)QL}{G})^{1/4} = a_1 L^{1/4} \tag{5. 29}$$

The net pressure is:

$$p_w = 4[\frac{2G^3\mu Q}{\pi^2(1-\nu)^3 h^4}]^{1/4} L^{1/4} \tag{5. 30}$$

The controlling equations for the first time step are given by:

$$a_1 = 2.05(\frac{\mu(1-\nu)Q}{G})^{1/4} \tag{5. 31}$$

$$a_2 = 4C_l\sqrt{\Delta t} \tag{5. 32}$$

$$a_3 = q \times \frac{\mathrm{t}}{\mathrm{h}} \tag{5. 33}$$

$$a_3 - a_2 \times L - a_1 \times L^{\frac{5}{4}} = 0 \tag{5. 34}$$

This non-linear equation for the initial fracture propagation in the first time step can be solved by the appropriate root-finding method. It is a one-time-step calculation.

The mass balance of a fracture in terms of a differential equation is transformed into a finite difference equation for the numerical scheme at the second time step, and is given by:

$$dV = Q \times dt - Q_l \times dt - S_p dA \tag{5. 35}$$

$$dV = A_n w_n - A_{n-1} w_{n-1} \tag{5. 36}$$

$$Q_l = 2 \times \int_0^t C \frac{dA}{d\tau} \frac{d\tau}{\sqrt{t-\tau}} \tag{5. 37}$$

$$Q \times \Delta t = 2 \times \sqrt{\Delta t} \times \sum_{\mathrm{j=1}}^{\mathrm{n}} \frac{\mathrm{C_{n\text{-}j+1}(A_j - A_{j\text{-}1})}}{\sqrt{n - j + 0.25}} + Sp(A_n - A_{n-1}) + A_n w_n - A_{n-1} w_{n-1} \tag{5. 38}$$

The area of a fracture face is:

$$A_n = 2 L_n h \tag{5. 39}$$

The leak-off coefficient is:

$$C_n = \frac{\Delta P_n \sqrt{t_n}}{\pi \alpha_0 (1 + \frac{\Delta P_n}{P_a})^{nn} \omega_n} \tag{5. 40}$$

where ‘nn’ is used in the model instead of power law coefficient ‘n’ in Equation 5.24

$$\omega_n = \frac{q_s \times \Delta t}{L_n} + \omega_{n-1} \tag{5. 41}$$

Substituting equations (5. 38) to (5. 40) into Equation (5. 37), we can get the nonlinear equation for a fracture at time t_n:

$$\begin{aligned} & a_1 L_n^{5/4} + (4 C_1 \sqrt{\Delta t} + 2 S_p) L_n \\ & = \frac{Q \Delta t}{h_f} - 2 \sqrt{\Delta t} \sum_{i=1}^{n-1} C_{n-i+1} \frac{L_i - L_{i-1}}{\sqrt{n - j + 0.25}} \\ & + 4 C_1 \sqrt{\Delta t} L_{n-1} + 2 S_p L_{n-1} + L_{n-1} w_{n-1} \end{aligned} \tag{5. 42}$$

$$a_2 = (4C_1\sqrt{\Delta t} + 2S_p) \tag{5. 43}$$

$$a_4 = \frac{Q\Delta t}{h_f} - 2\sqrt{\Delta t}\sum_{i=1}^{n-1} C_{n-i+1}\frac{L_i - L_{i-1}}{\sqrt{n-j+0.25}} + 4C_1\sqrt{\Delta t}L_{n-1} + 2S_pL_{n-1} + L_{n-1}w_{n-1} \tag{5. 44}$$

For fracture propagation with dynamic leak-off, the controlling equation is given by:

$$a_1 L_n^{5/4} + a_2 L_n - a_4 = 0 \tag{5. 45}$$

The fracture length at time step n can be obtained by an iterative calculation associated with the method of approximating locations of roots for Equation (5. 45) and (5. 34) (Mathews 2003).

In order to determine the fracture length at time step n, we have to use the results known from the previous step (n-1).

In Equation 5.42, the leak-off volume is given as the sum of the leak-off through the fracture face along the whole length created. Therefore, there is a second iterative calculation of leak-off volume inside the first iterative loop for the fracture length. The number of iteration is the number of the current time step minus 1 since the first time step is already calculated.

When the fracture length is obtained at a particular time step, this value is then used to calculate the fracture width, net pressure and leak-off coefficient of the element near the borehole at this time step, which are used for the next time step repetition to calculate the propagation of fracture in length. The assumption in the code is that each new element of fracture near the tip shares the same leak-off evolution history as the previous element at the previous time step and the current element of fracture shares the same leak-off coefficient as the previous element at the previous time step (see Figure 5.3).

See Appendix A for the computer code.

5.4 Model Stability

5.4.1 Limits of calculation procedures

In order to define the limits of calculation procedures, different calculation step sizes are applied in the model. The results for the constant leak-off condition from the model do not change out to three significant digits, even after the number of time steps increased from 300 to 600.

The leak-off coefficient for the dynamic leak-off condition is calculated depending on the time from which the filter cake is exposed to the fracture net pressure. The smaller the time interval, the more sensitive the solution is to the changing of the leak-off coefficient; therefore, the change of results from a constant leak-off condition is employed to define the limits of the calculation procedures.

The computational model is divided into two components to simulate the fracture propagation. The first part provides the initial condition for the second part. While the first time step calculation is just the initiation of a fracture, the second part of the model with the dynamic leak-off process starting from the second time step describes the fracture propagation. Since the first part of the model has a dominant impact on the final result when fewer calculation steps are used, a number of calculation step less than 50 is not reasonable. The differential part (first part) of the model only considers the constant leak-off circumstance of the fracture propagation, a one time leak-off process in which the leak-off only happens once over the whole face of fracture. Hence, it is an instantaneous development of the fracture. In fact, the fracture propagates continuously, and the leak-off process occurs through the open fracture face elements continuously until the injection is ceased.

Plots of model stability are shown in the following graphs, where the results from the constant leak-off condition are used to confine the number of calculation steps. The input parameters are given in Table 5.1

Table 5.1 Input parameters

$Q = 0.042\ m^3/s$	$E = 0.1\times10^{11}$ Pa	$n = 1.83$
$H = 30$ m	$\mu = 0.01$ Pa*s	$P_0 = 1000$ Pa
$C = 59.4\times10^{-6}\ m/s^{1/2}$	$\upsilon = 0.25$	$\alpha_0 = 4.02\times10^{11}\ m^{-1}$
$T = 600$ seconds	$\Delta t = 1$ to 600 seconds	$q_s = 0.0084\ m^3/s$

5.4.2 Plots of model stability

From Figures 5.4 to Figure 5.8, it is found out that the smaller time interval in the calculation, the smaller the variation in results. This trend complies with the principles of numerical computation. Once the number of steps is over 300, the variation in results becomes insignificant. The results of the model reach a constant value, which indicates the appropriate calculation limit. As shown in Figures 5.7 and 5.8, the smaller the size of time step applied in the model; the smaller the variation in results. When the time step is smaller than 1 second, the variation of result output is no bigger than 0.02 in length. Hence, the model performs in a stable manner with an appropriate time step size.

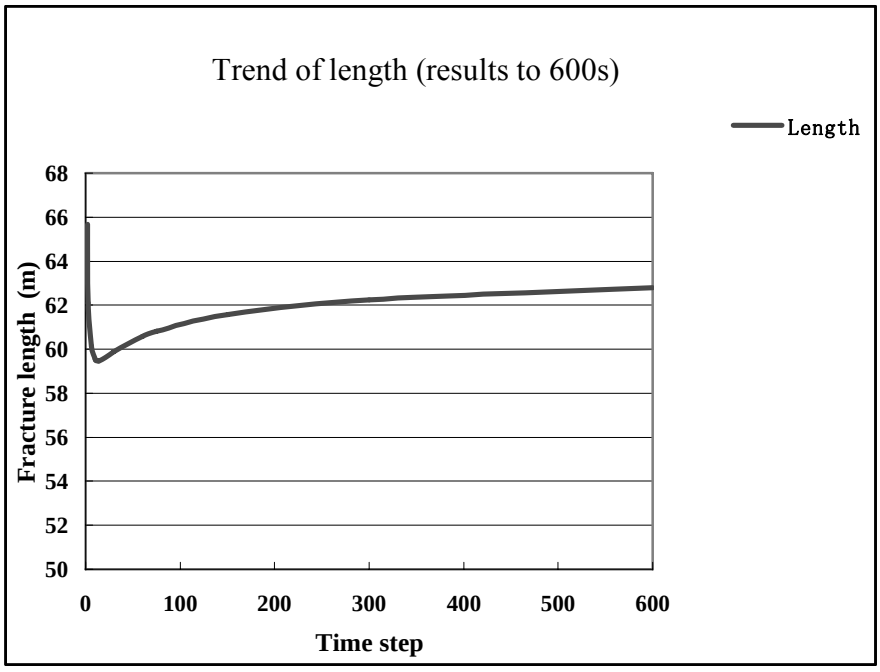

Figure 5.4 Lengths of fracture from different time step calculations to 600 s

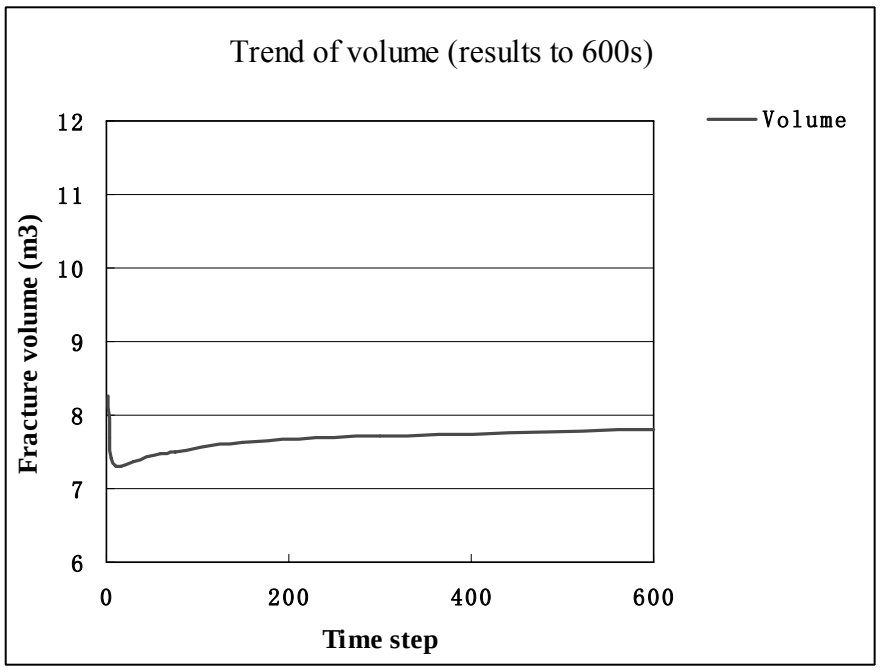

Figure 5.5 Fracture volumes from different time step calculations to 600 s

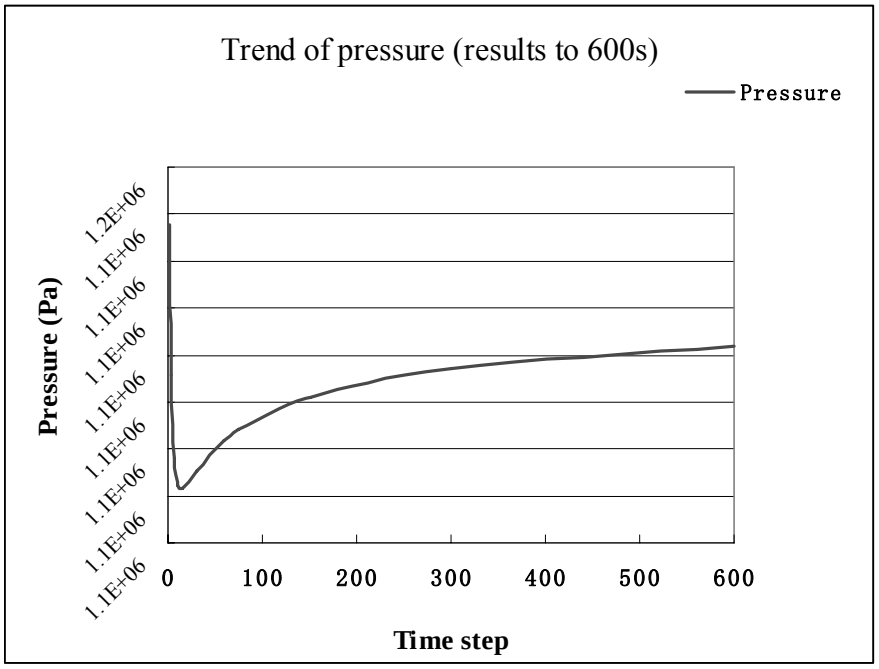

Figure 5.6 The net fracture pressures from different time step calculations to 600 s

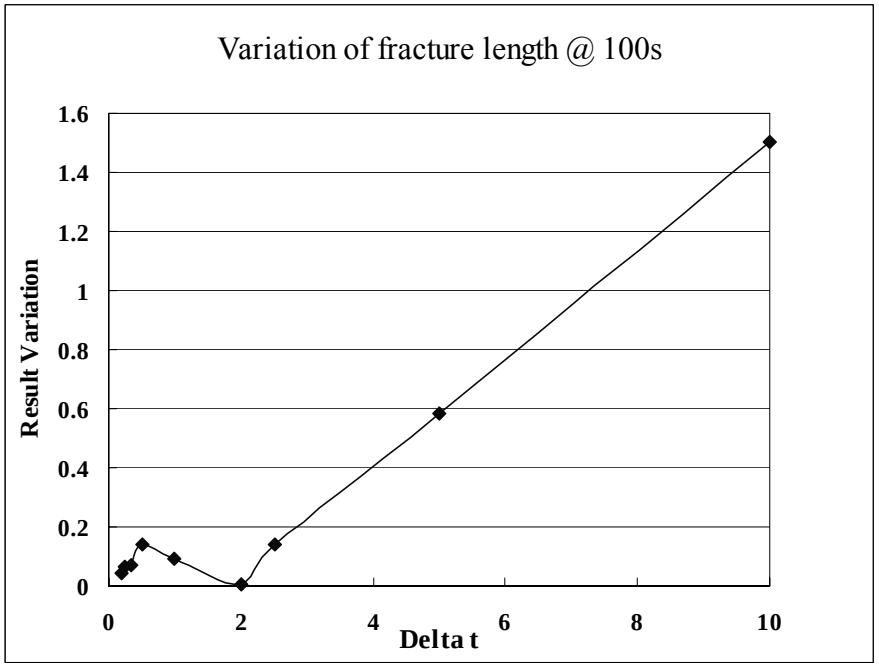

Figure 5.7 Variation of fracture length at different time step calculations to time = 100 s

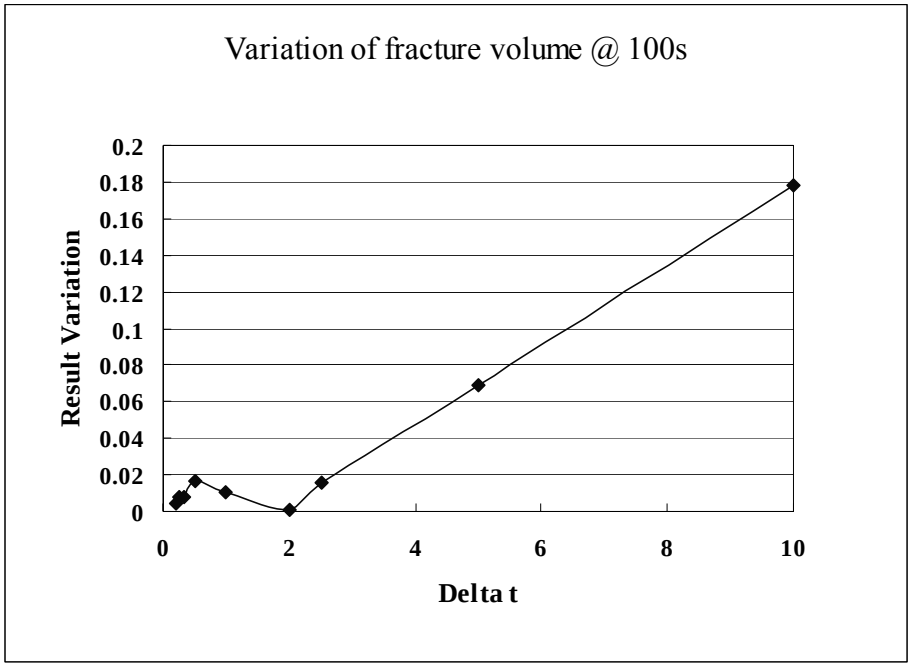

Figure 5.8 Variation of fracture volume at different time step calculations to time = 100 s

5.5 Consolidation of Biosolids in the Closure Phase

Biosolids or sludge injected into the reservoir will undergo substantial dewatering and compaction, achieving a high density because of the high effective stresses during the filtration process. Once the injection is stopped, the excess pore pressure in the biosolids dissipates according to consolidation processes.

Knowledge of consolidation properties of both sludge and biosolids is limited. In practice, at the surface of the earth under the small stresses in filter belts or sludge ponds, it is difficult to dewater the sludge to a low water content. Normally, the water content can be reduced only to 230% to 570% by a belt filter press; a recessed plate filter press can achieve a somewhat lower water content of 100% to 400% (Drost 1996). The water content (w_i) here is defined as the ratio of the mass of water in the void space to the mass of solids in the slurry as a percentage.

The consolidation properties may be quite different as sewage can come from different sources, leading to different constituents in the sludge. For example, the organic content of sludge can vary from 70% to 45% of the dry mass for moderately and fully biodegraded sewage sludge, respectively (Imhoff *et al.* 1971). The value of the specific gravity of sludge solids ranges from 1.4 to 2.1 for sewage sludge (Campbell *et al*. 1978). Dry powdered test specimens ignited at 440˚C over a period of 18 hours give the loss on ignition (LOI) value of 70% dry mass for moderately digested sludge and this is a convenient way to measure the organic content (Skempton and Petley 1970). Fully digested sludge would typically yield a LOI value in the range of 45%-55%.

The solids content (SC) value is defined as the ratio of the dry mass of the solid particles to the bulk sludge mass given as a percentage.

$$SC = \frac{100}{1+(\frac{w_i}{100})} \times 100\% \quad (4.46)$$

5.5.1 Data for consolidation of sewage sludge

Consolidation tests were conducted by O'Kelly on slurry specimens and air-dried compacted sludge using oedometer, hydraulic consolidation cell and traxial apparatus methods (O'Kelly 2005). He studied the compressibility index, consolidation and compaction properties of sewage sludge from Tullamore municipal wastewater treatment plant in Ireland.

The sludge he studied had a water content of about 725%, and a specific gravity of solids (G_s) of 1.55. He conducted several parallel consolidation tests with different sludges and the cumulative strain of moderately degraded specimens, which were consolidated by oedometers under two-way vertical drainage conditions, was obtained.

Two moderately degraded specimens C and D in his study were tested under different procedures. Specimen D, which underwent stabilization prior to consolidation, achieved a higher degree of consolidation than specimen C, which did not undergo stabilization. The water content was reduced from 725% to 170% for specimen D. The water content of specimen C was reduced from 725% to 225%. A volumetric strain of 52% for specimen D was achieved, because of the much stronger degradation that had occurred. In contrast, specimen C undergoing a consolidation process along with biodegradation achieved a volumetric strain of only 17.5%.

Specimens E1 to E3 from the consolidated specimen C, which is a moderately degraded material, underwent further isotropic triaxial testing. Triaxial specimen F of strongly degraded material was formed from specimen D for comparison purposes.

Figure 5.9 shows the sludge material's void ratio – log σ' behavior. The compression index (C_c), which is defined as the gradient of the void ratio – log σ' curve, can be calculated from the plot.

The coefficient of secondary compression (C_s) is defined as the specimen strain that occurs over one log cycle of time after primary consolidation is completed. These values are listed in Table 5.1 and Table 5.2

Table 5.2 Coefficient of secondary compression (C_s) values for bioactive moderately degraded sludge (O'Kelly, 2005)

Multiple increment	Single increment	
Specimen A	Specimen B	Specimen C

Applied Stress (kPa)	3	6	12	25	50	100	25	50	100	200	400	100	100
C_s	0.02	0.03	0.07	0.08	0.07	0.05	—	0.0	0.03	0.04	0.05	0.07	0.32*a*

Both creep deformation and biodegradation of the organic particles take place in the bioactive material, while creep deformation alone occurred in the stabilized material. O'Kelly (2005) also reported that the contribution of biodegradation to the long-term deformation of bioactive material would have been even larger at lower applied stress, because the creep rate is dependant on stress-level. Consequently, the coefficient of secondary compression is larger during bioactive sludge consolidation than for stabilized material. However, the highly degraded material was much more permeable during primary consolidation, so the rate of primary consolidation is faster for highly degraded material.

Table 5.3 Coefficient of secondary compression (C_s) values for stabilized sludge from single-increment consolidation tests (O'Kelly, 2005)

State of biodegradation	moderate			strong	
Specimen	E3	E2	E1	D	F
Effective confining stress	35	80	150	300	300
C_s	0.10	0.18	0.24	0.08	0.10

The void ratio is calculated through the equations listed below.

$$\frac{1}{Sg_{slurry}} = \frac{1-SC}{\rho_w} + \frac{SC}{Sg_{Sludge} \times \rho_w} \tag{4. 47}$$

where Sg_{slurry} = specific gravity of slurry

Sg_{sludge} = specific gravity of sludge

SC = solids content

ρ_w = density of water

$$e = \frac{1}{SC} \times \frac{Sg_{sludge}}{Sg_{slurry}} - 1 \tag{4. 48}$$

where e = void ratio

Based on the data from O'Kelly (2005), Terzaghi-type relationships for specimens are plotted in Figure 4.9. The power law approximations of primary consolidation properties under different effective stresses are also given in the Figure 4.9. Using the power law approximations, we can estimate the void ratio of filter cake corresponding to its effective stress.

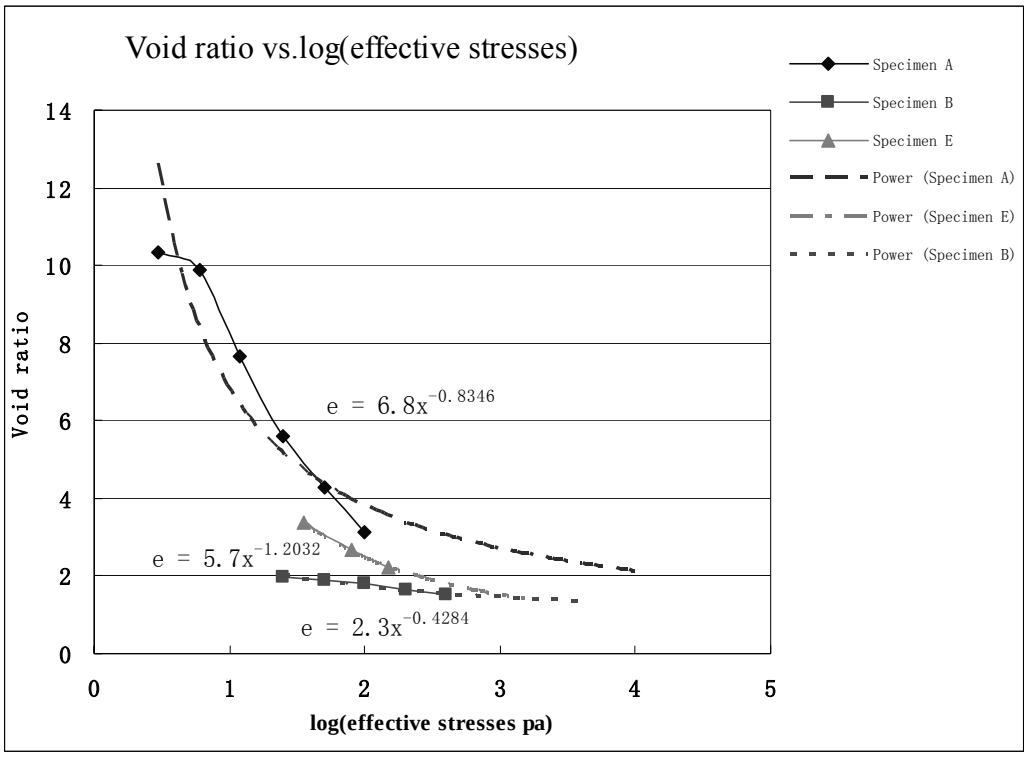

Figure 5.9 Void ratio vs. effective stress

Because the porosity of the filter cake is a function of effective stress, it varies with different effective stresses. The porosity of filter cake subject to the *in situ* effective stress finally decreases to a specific value when the excess pore pressure decays to the formation pore pressure. The integration of the porosity of the filter cake gives the volume change after the injection process. The relation of void ratio and porosity is given by:

$$e = \frac{\phi}{\phi - 1} \tag{4. 49}$$

$$V_{space} = 2 \times L \times 2 \times \int_0^x \phi(x) dx \tag{4. 50}$$

$$\phi(x) = F(\sigma', x) \tag{4. 51}$$

where x is the thickness of the filter cake.

Chapter 6

Summary of Model Results and Discussion

6.1 Comparison of Results from Hydraulic Fracture Model

To test the validity of the proposed injection model, it is first applied to both a high leak-off condition and an impermeable condition. Then, the model designed for biosolids injection, in which the leak-off behavior is changing with time, is used with a dynamic leak-off condition. The simulation results are discussed here. The resistance of the filter cake on the fracture face is related to the solids content of the slurry. Different solids content values are used in the simulation to estimate the impact of solids content. At different depths, the induced fractures could response differently because of different *in situ* stress profiles. In addition, different values for biosolids compressibility are incorporated into the simulations.

6.1.1 Volume of injected biosolids in a hydraulic fracture

For verification and comparison purposes, three different leak-off conditions are investigated including no-leak-off, constant leak-off and dynamic leak-off.

No-leak-off condition:

For the no-leak-off condition, the magnitude of the leak-off coefficient is set to be on the order of 10^{-9} to initiate the computation. This value is a good approximation to zero in the computational calculation. In this case, the fracture geometry is mainly dominated by rock elasticity and fluid properties as a leak-off process does not occur. The fracture volume should converge to the total injection volume.

Constant leak-off condition:

For the constant leak-off condition, the leak-off coefficient is assigned as 5.9×10^{-5} m/s$^{1/2}$ which is a constant value with time and length. The effect of injected solids on the leak-off is ignored, which means the solids content is 0. The model in this situation should finally regress to a traditional PKN leak-off model.

Dynamic leak-off condition:

The fracture is first created at the initial *in situ* condition. With fracture propagation, the injected solids begin to deposit on the fracture face. Only the fresh fracture face of the new fracture element is assigned an initial leak-off coefficient. The dynamic leak-off coefficients for each old fracture face are applied; the value depends on how much time has elapsed, associated with the filter cake thickness, the pressure exerted on the filter cake and the formation resistance.

The model is executed for injection at a depth of 800 m. The minimum horizontal stress is assumed to be 18 MPa and the pore pressure is 8 MPa. The input parameters are listed in Table 6.1. The plots of results are shown in Figure 6.1, which illustrate the fracture volume, fracture half-length, and changing of leak-off coefficient and net pressure at the borehole.

Figure 6.1 represents the basic simulation from this work, depicting the different results under no-leak-off, dynamic leak-off and constant leak-off conditions, respectively.

In the no-leak-off condition, the formation is assumed to be impermeable. Hence, the leak-off coefficient is set to 0. Consequently, based on the mass balance, the fracture volume converges to the total injection volume. In Figure 6.1a, results show that the curve for the fracture volume under a no-leak-off condition overlaps with the curve for the total injection volume.

In the constant leak-off condition, the injection is conducted with clean injection fluid, which means the solids content is set to 0. Correspondingly, the model regresses to a typical PKN leak-off model. It gives results identical to other typical PKN leak-off models. In Figure 6.1a, the curve for constant leak-off shows the results under a constant leak-off condition.

Comparing simulation results under dynamic leak-off conditions with a typical PKN leak-off model, the fracture volume is larger because of impaired leak-off caused by filtration and cake build-up. The fracture length is greater for the dynamic (impaired) leak-off condition than for the constant leak-off condition (Figures 6.1a and b). The fracture length and fracture volume with time have a trend similar to the trend of leak-off coefficient, as fracture length and fracture volume increase with the decrease of dynamic leak-off coefficient in Figure 6.1c, The net pressures for three different leak-off cases are also given in Figure 6.1c. A decreasing leak-off coefficient promotes an increase of bottom-hole net pressure; consequently, a larger fracture volume and a longer fracture length are predicted

As mentioned above, simulation results provide certain model validations based on mass balance when leak-off coefficients are set to be 0 and of constant value. The curve of fracture volume and the curve of fracture length are identical to the results from a no-leak-off model and a typical PKN leak-off model, respectively.

The results provide a reasonable validation for the model because results are identical to other well-known cases.

Table 6.1 Input parameters

$Q = 0.042\ m^3/s$	$E = 0.1\times10^{11}$ Pa	$n = 1.83$
$H = 30$ m	$\mu = 0.01$ Pa*s	$P_0 = 1000$ Pa
$C = 59.4\times10^{-6}\ m/s^{1/2}$	$\upsilon = 0.25$	$\alpha_0 = 4.02\times10^{11}\ m^{-1}$
$T = 600$ seconds	$\Delta t = 1$ second	$q_s = 0.0084\ m^3/s$

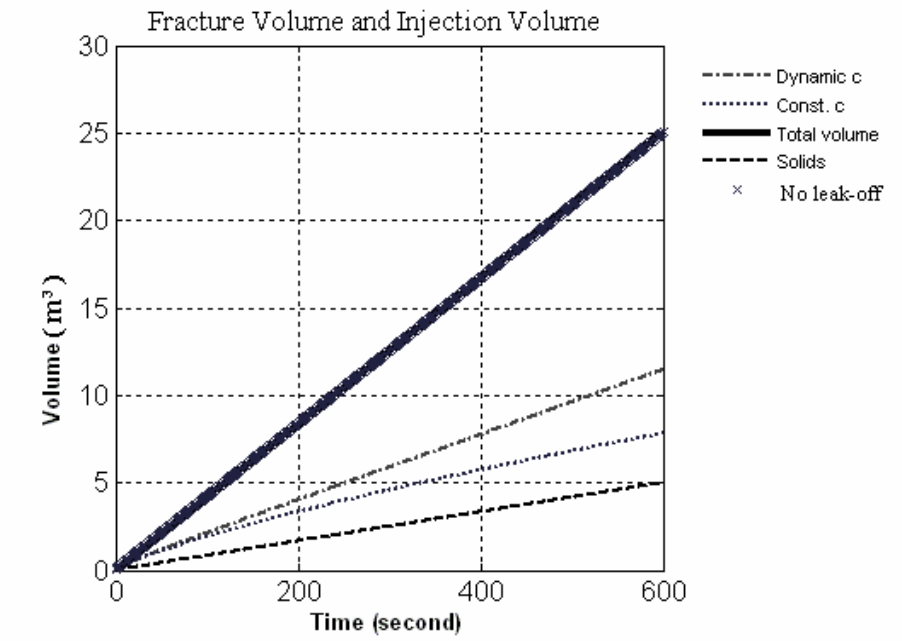

Figure 6.1 a) Fracture volumes under different leak-off conditions

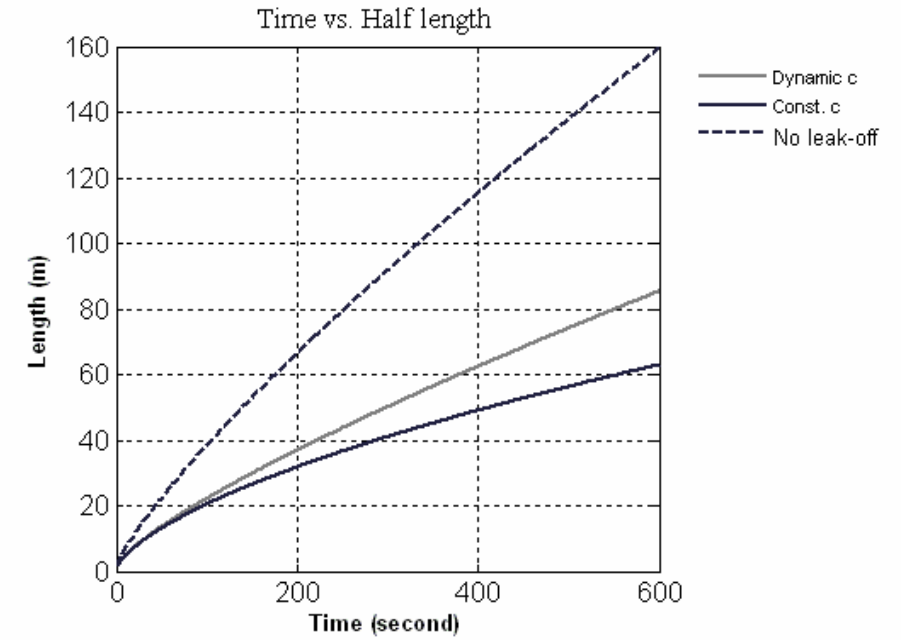

Figure 6.1 b) Fractures half-lengths under different leak-off conditions

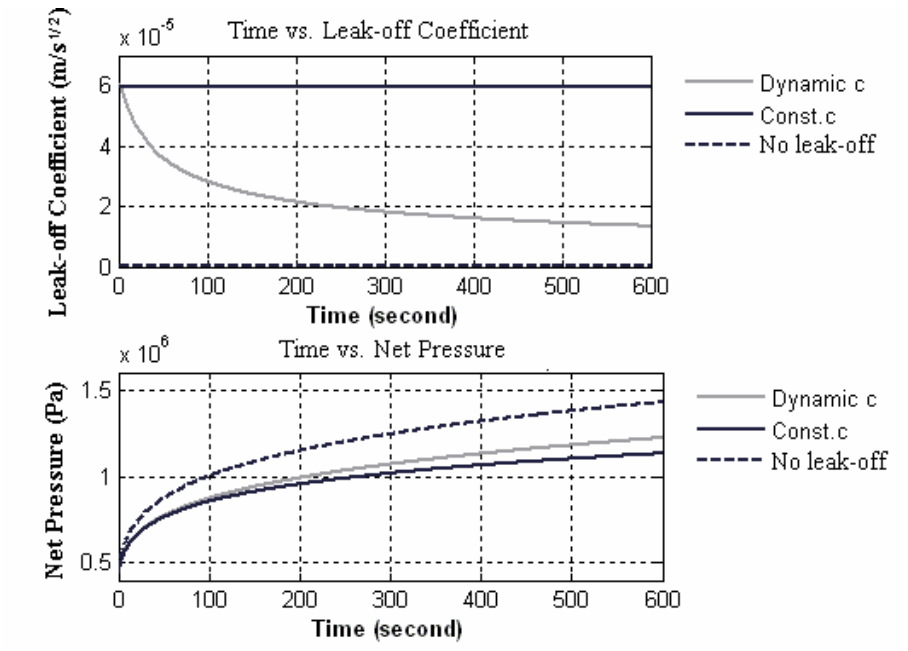

Figure 6.1 c) Variation of leak-off coefficients and net pressures with time under different leak-off conditions

To test the performance of the proposed injection model, it is also applied under different sets of simulation parameters. The following paragraphs describe simulations using different solids contents and injection depths.

Injection at different solids contents

Four solids contents, 5%, 10%, 15%, 20%, are used for the simulations in all cases, while keeping other parameters as in Table 6.1. The effects of injection at different solids contents are analyzed and the plots for four scenarios are given in Figure 6.2

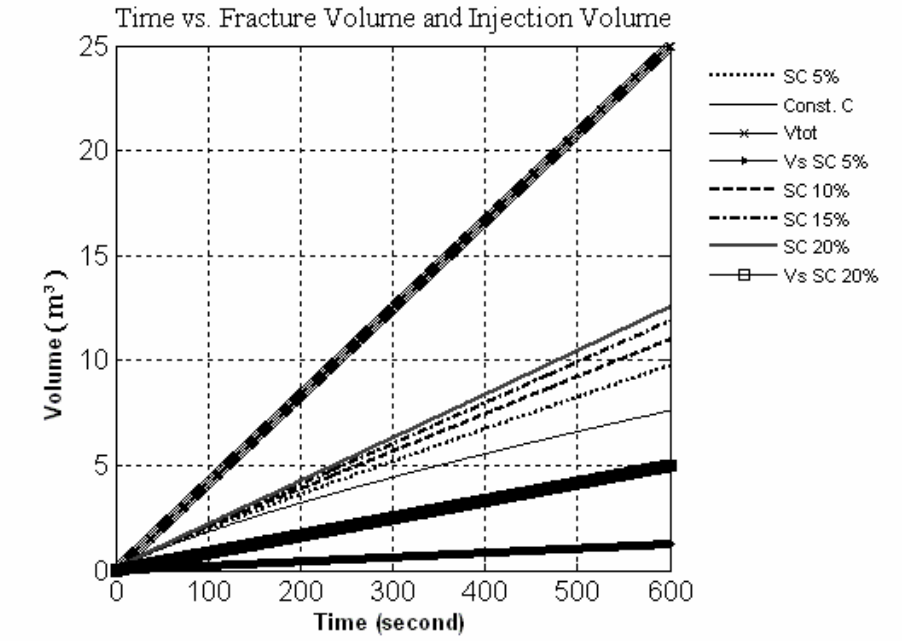

Figure 6.2 a) Fracture volumes under different solids contents in slurry

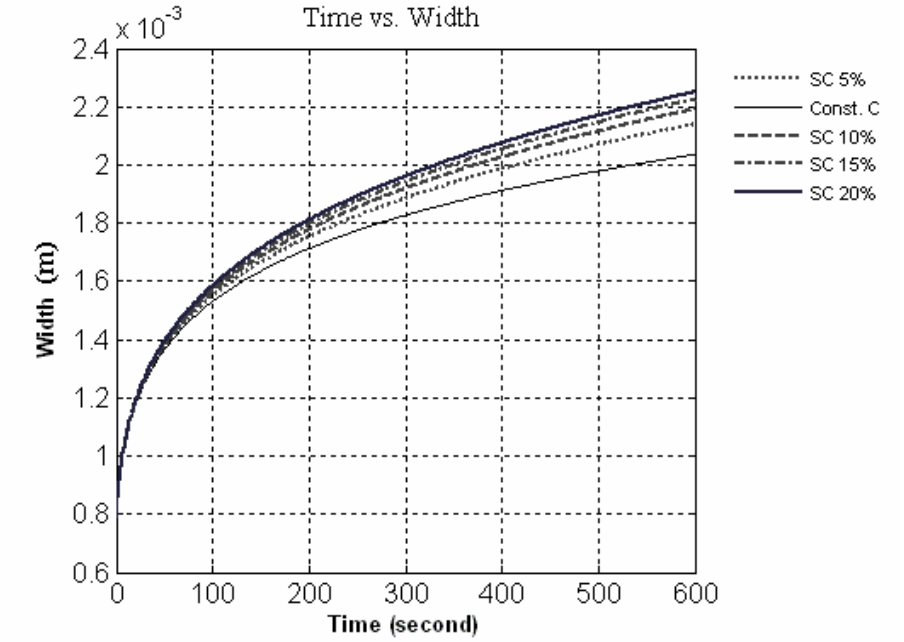

Figure 6.2 b) Fracture lengths at different solids contents

Injections at different depths

The simulations are conducted at different depths, 300 m, 600 m, 1000 m, and 1500 m, in which different Young's modulus values are used to reflect the effect of depth on formation stiffness. The

corresponding Young's moduli are 3 GPa, 8 GPa, 15 GPa, and 30 GPa, respectively. Other parameters are as in Table 6.1 (see above)

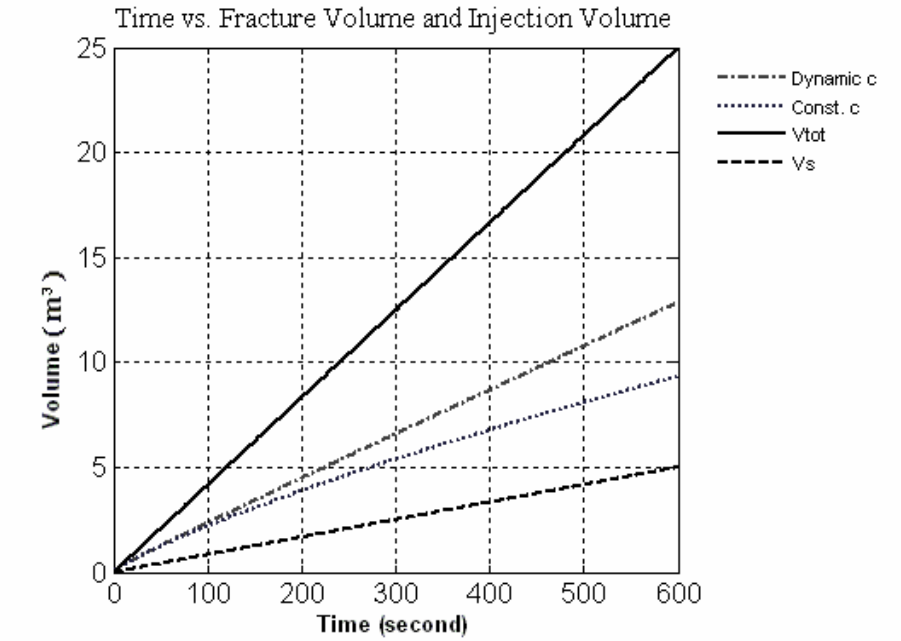

Figure 6.3 a) Fracture volumes at a depth of 300 m

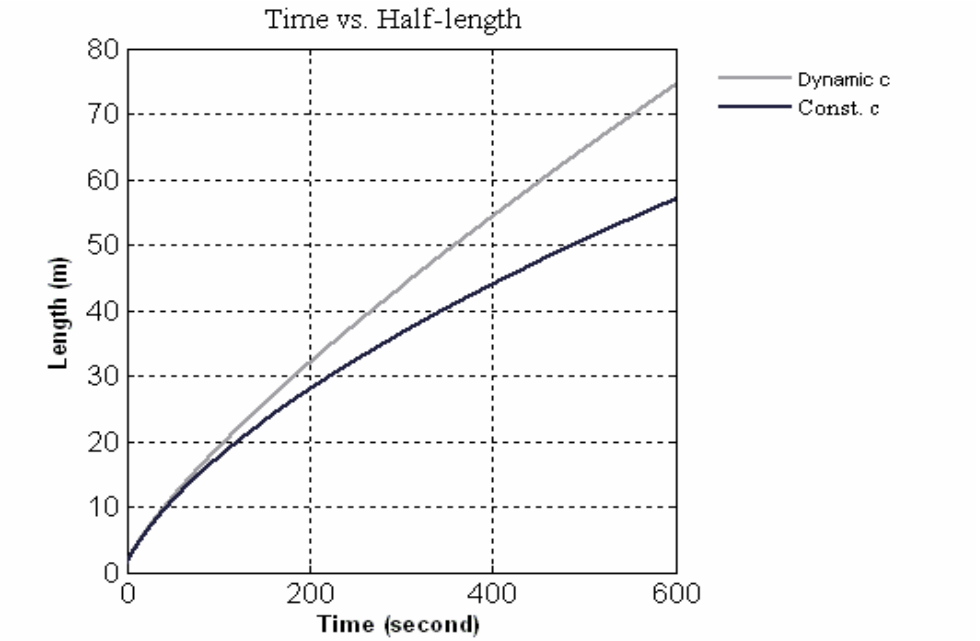

Figure 6.3 b) Fracture half-lengths at a depth of 300 m

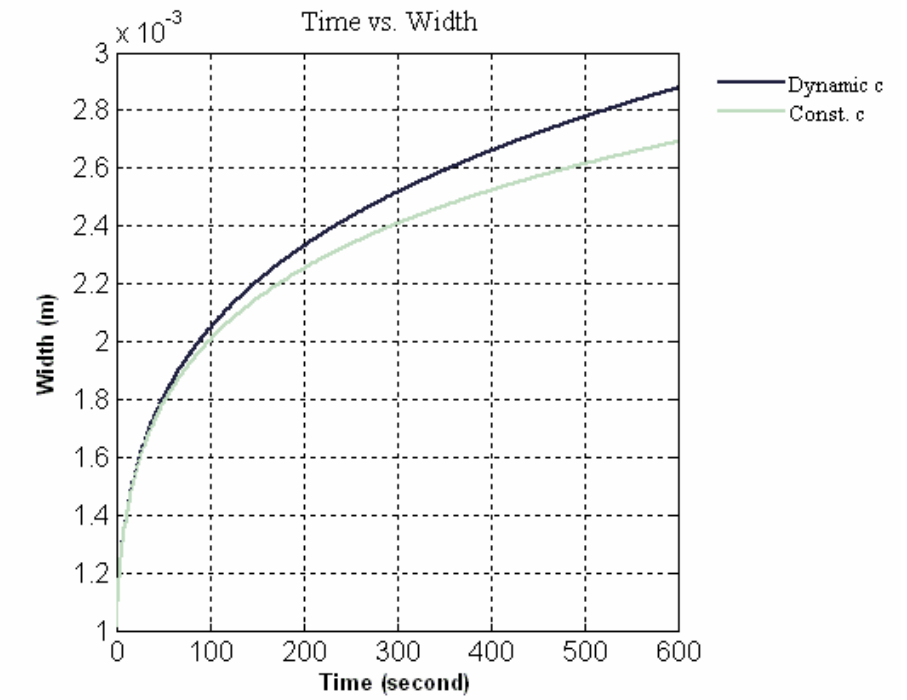

Figure 6.3 c) Fracture widths at a depth of 300 m

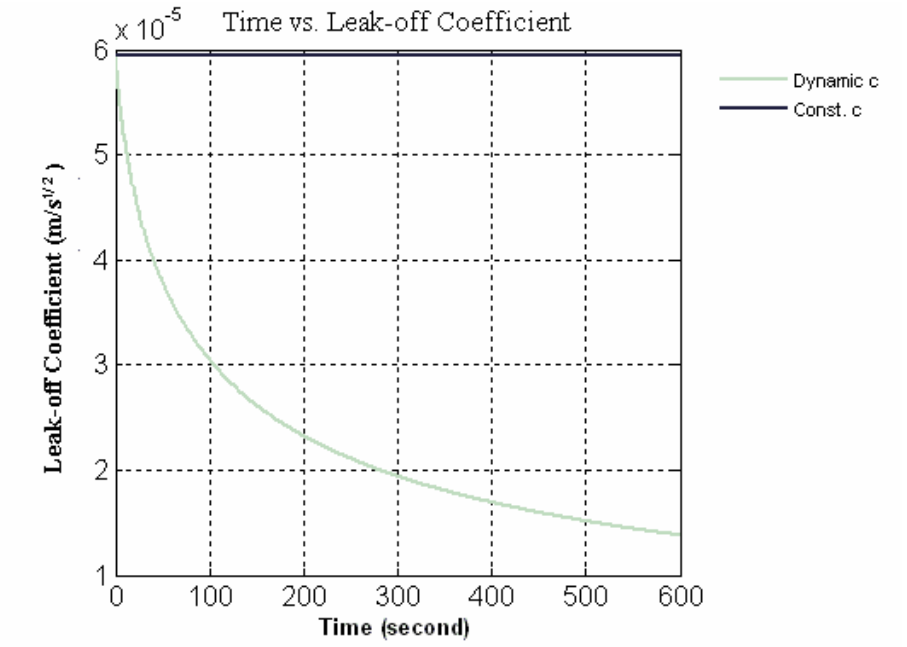

Figure 6.3 d) Leak-off coefficients at a depth of 300 m

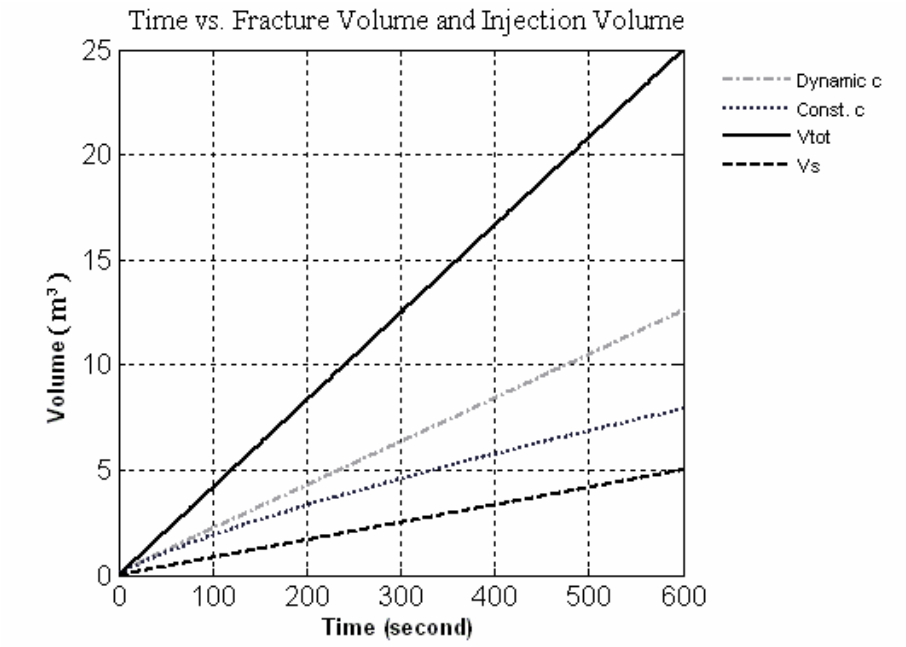

Figure 6.4 a) Fracture volumes at a depth of 600 m

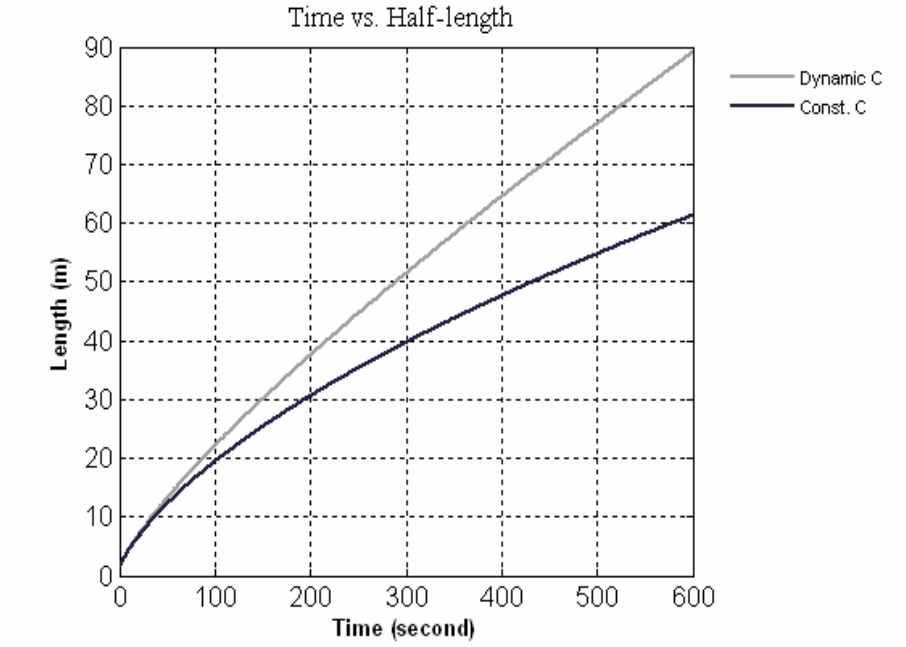

Figure 6.4 b) Fracture half-lengths at a depth of 600 m

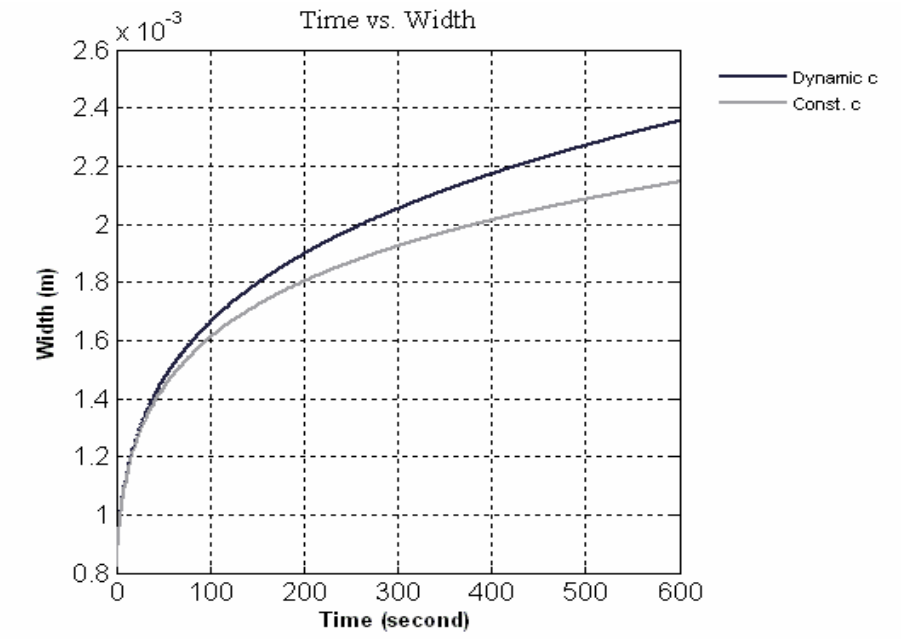

Figure 6.4 c) Fracture widths at a depth of 600 m

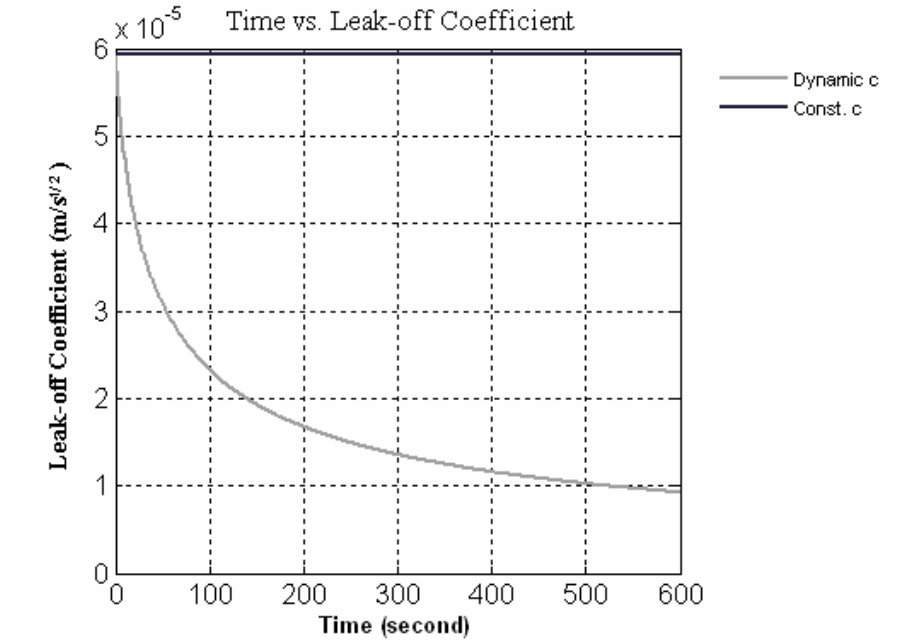

Figure 6.4 d) Leak-off coefficients at a depth of 600 m

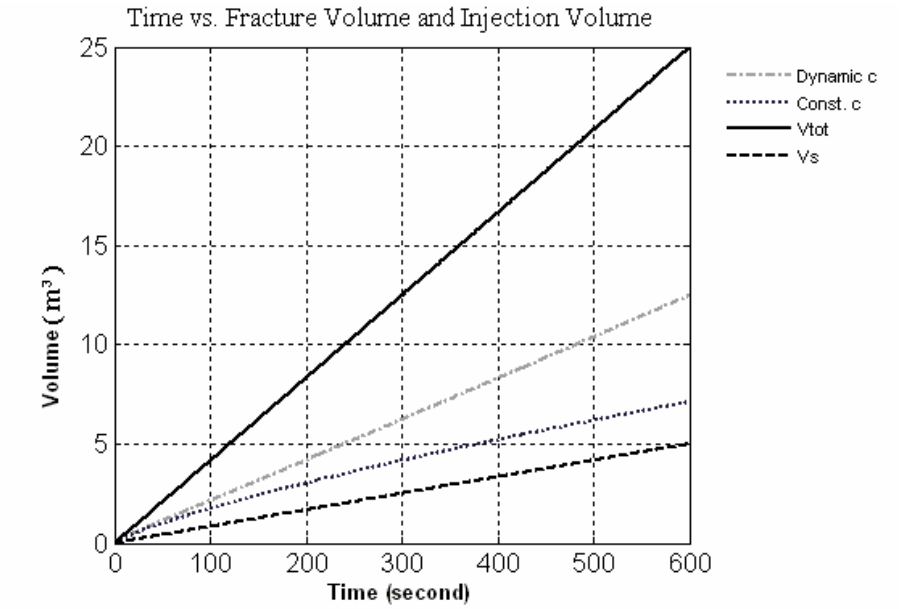

Figure 6.5 a) Fracture volumes at a depth of 1000 m

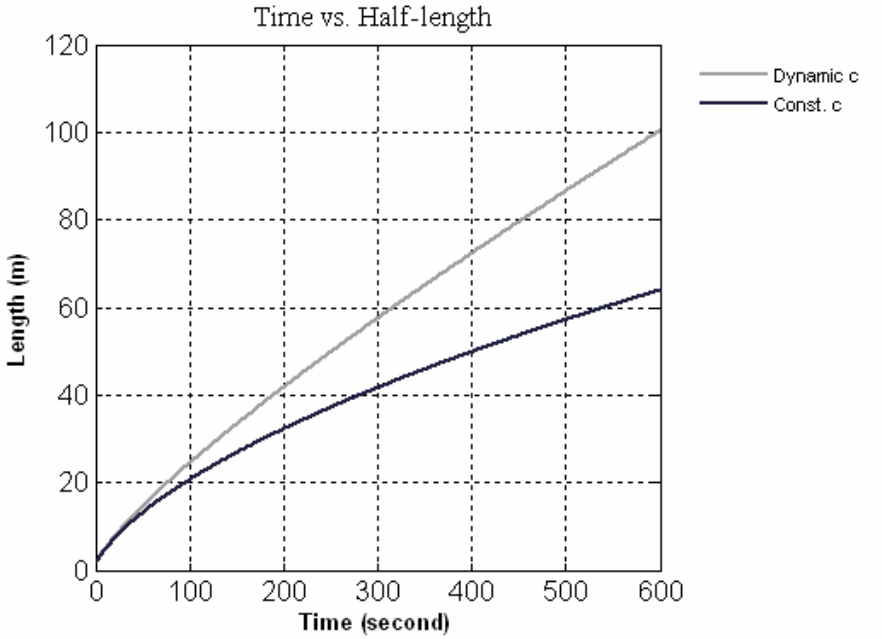

Figure 6.5 b) Fracture half-lengths at a depth of 1000 m

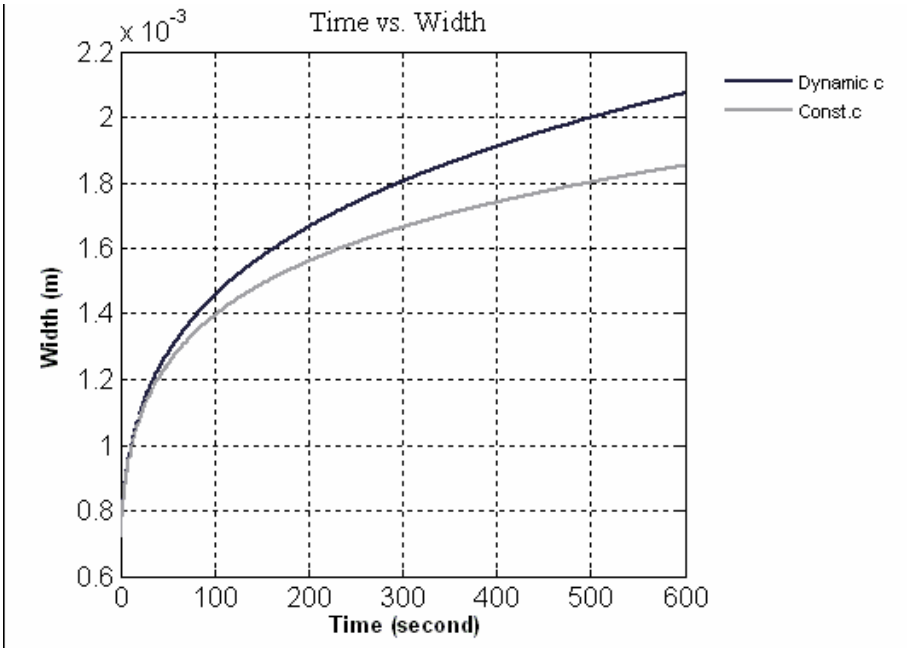

Figure 6.5 c) Fracture widths at a depth of 1000 m

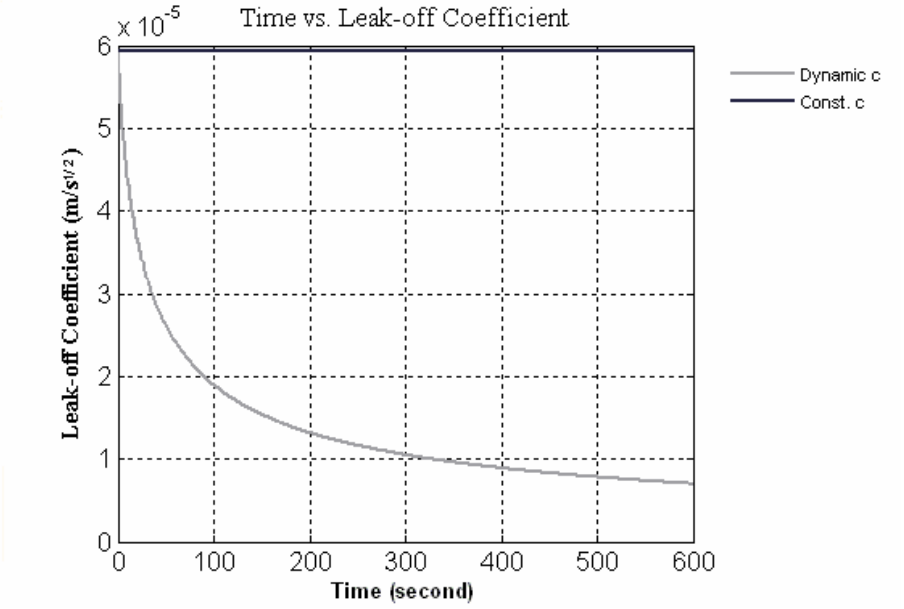

Figure 6.5 d) Leak-off coefficients at a depth of 1000 m

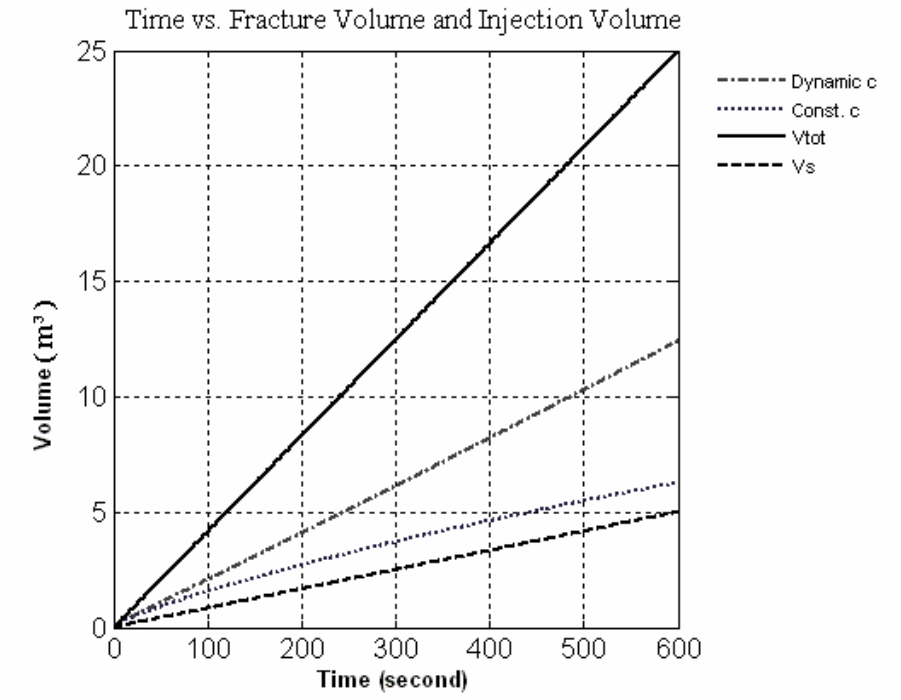

Figure 6.6 a) Fracture volumes at a depth of 1500 m

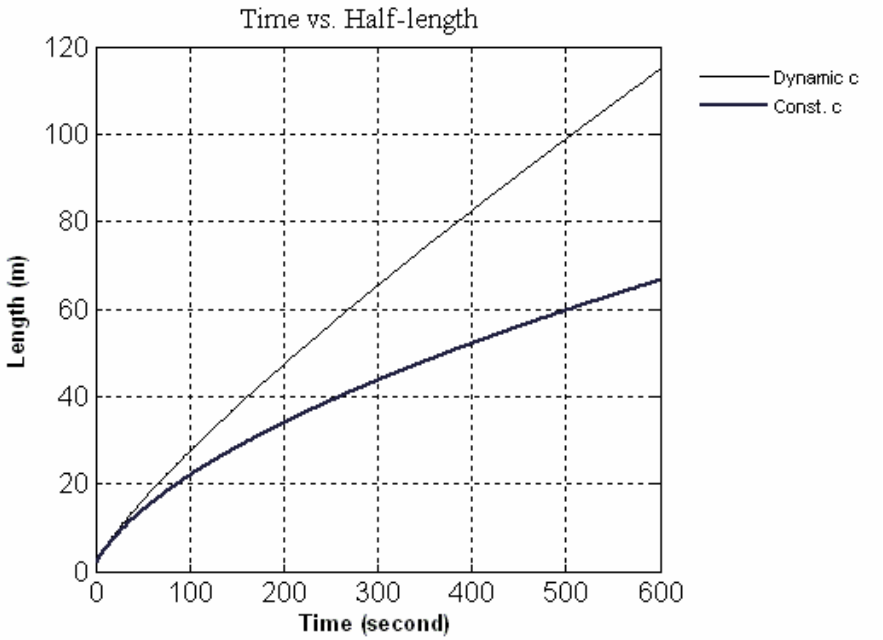

Figure 6.6 b) Fracture half-lengths at a depth of 1500 m

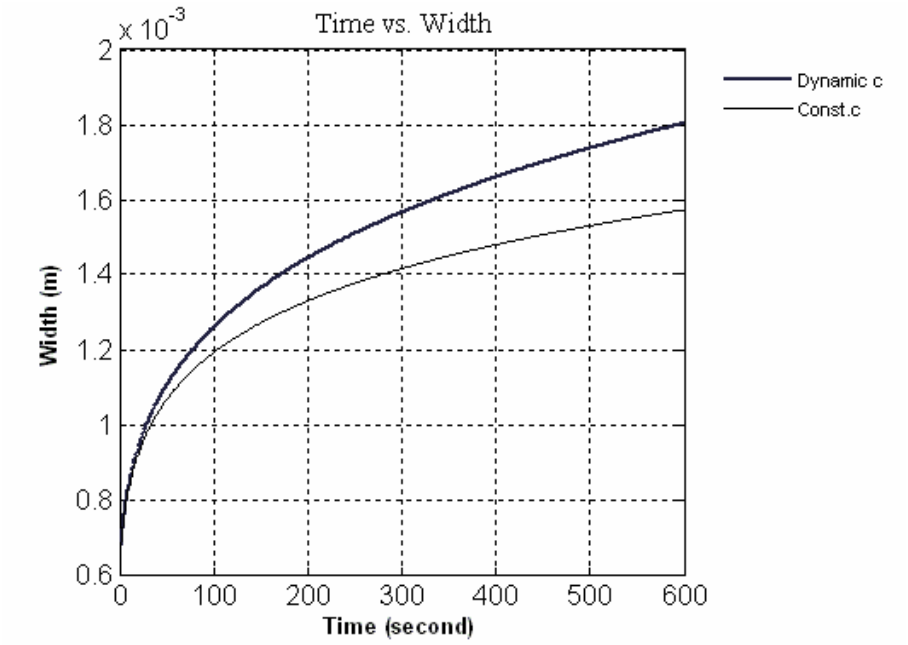

Figure 6.6 c) Fracture widths at a depth of 1500 m

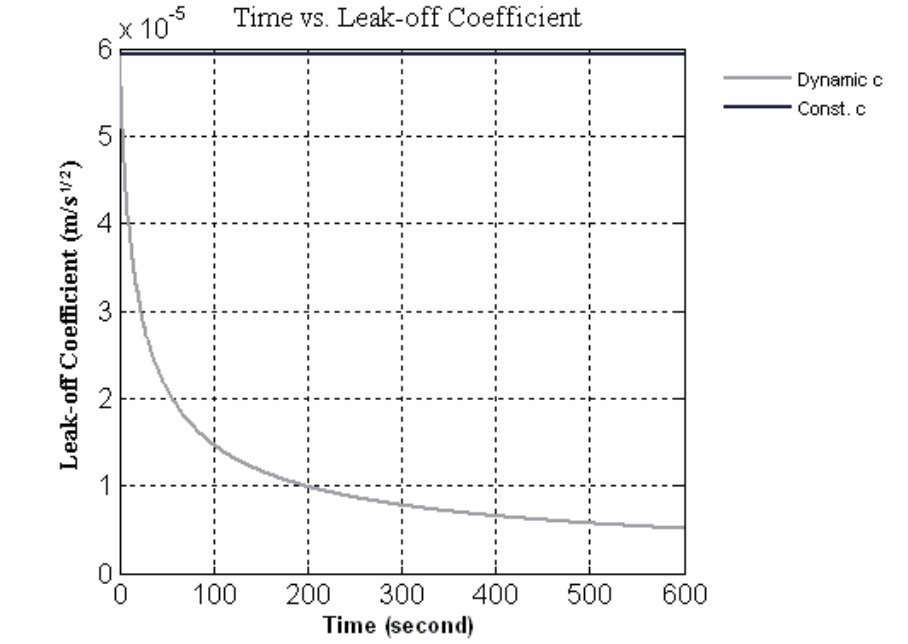

Figure 6.6 d) Leak-off coefficients at a depth of 1500 m

Since the rock is stiffer with depth, the original leak-off rate is smaller for a lower porosity formation in hydraulic fracture processes. Hence, the model is executed at a deeper depth with a bigger Young's modulus and a lower leak-off rate, and in a shallower formation with a smaller Young's modulus and a higher leak-off rate. The shallow depth is 300 m and the deepest depth is 1500 m. The Young's

moduli for 300 m and 1500 m are 3 GPa and 30 GPa, respectively. The leak-off coefficients are 9.94×10^{-5} m/s$^{1/2}$ and 5.94×10^{-6} m/s$^{1/2}$, respectively, in all cases, keeping other parameters the same as in Table 6.1. The results are plotted in Figure 6.7 and Figure 6.8.

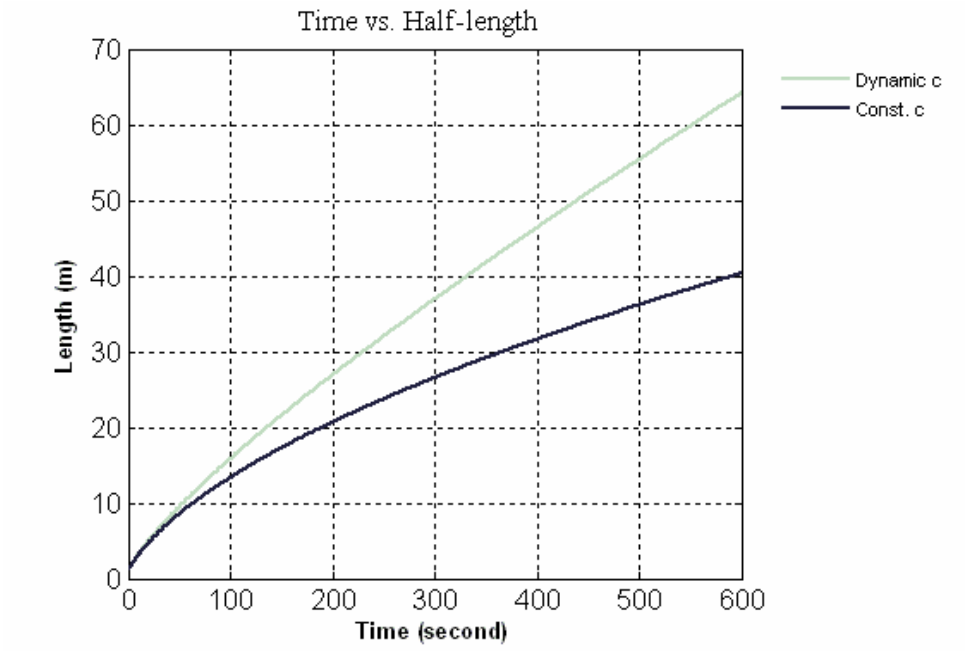

Figure 6.7 a) Time vs. fracture half-lengths

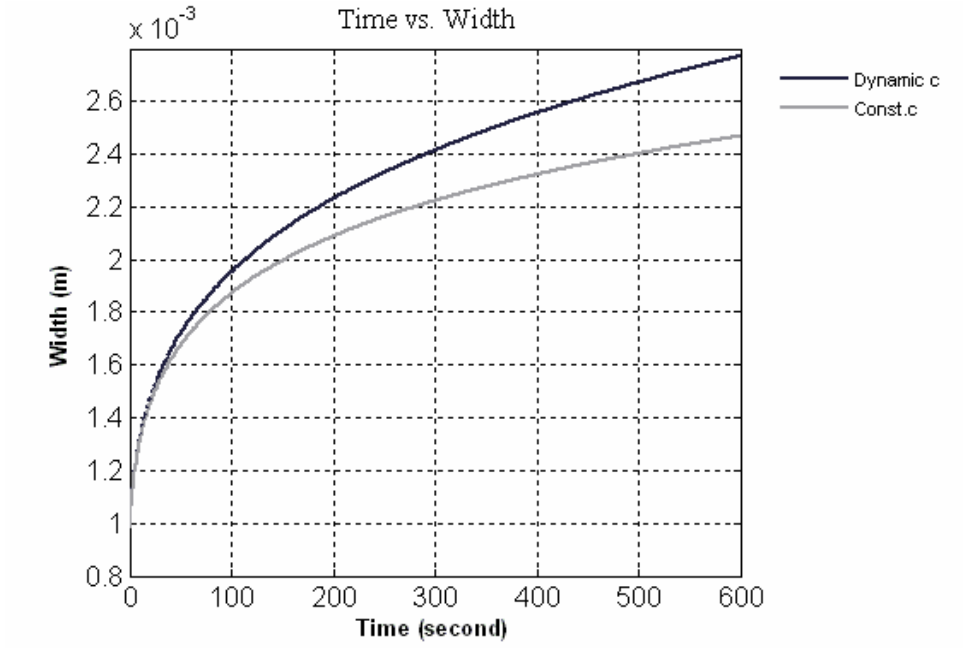

Figure 6.7 b) Time vs. fracture widths

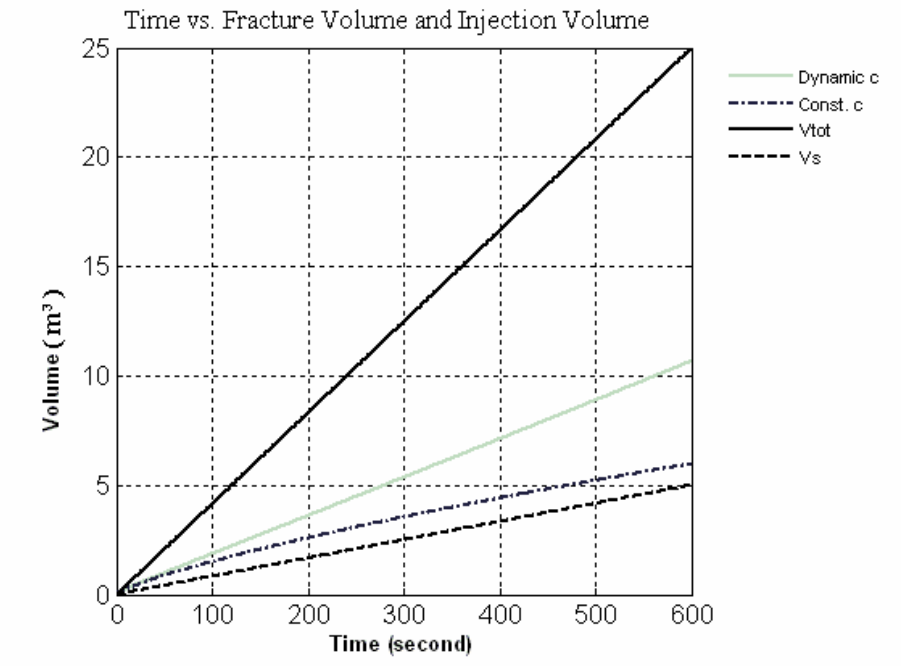

Figure 6.7 c) Time vs. fracture volumes

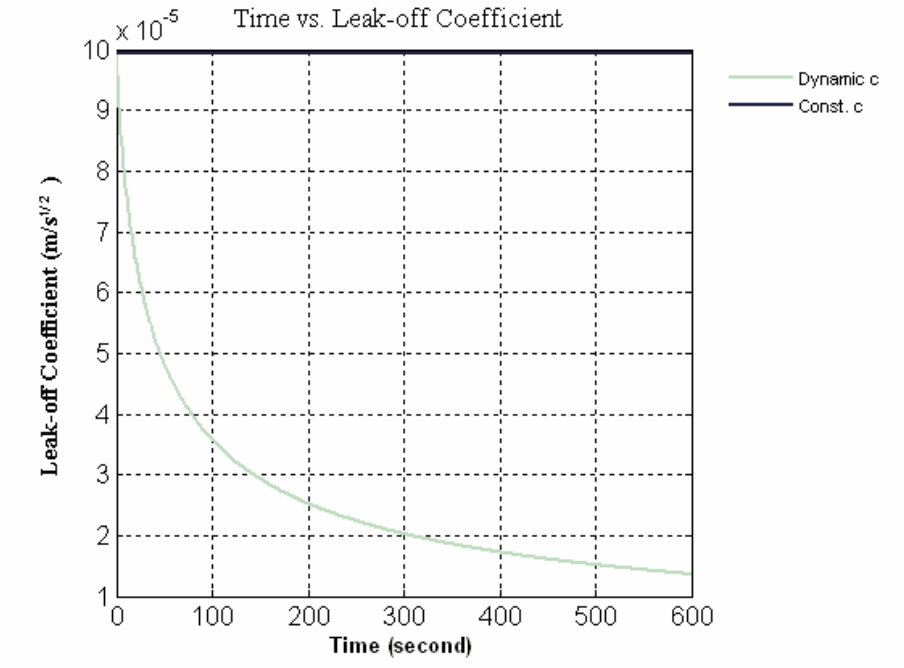

Figure 6.7 d) Time vs. leak-off coefficients

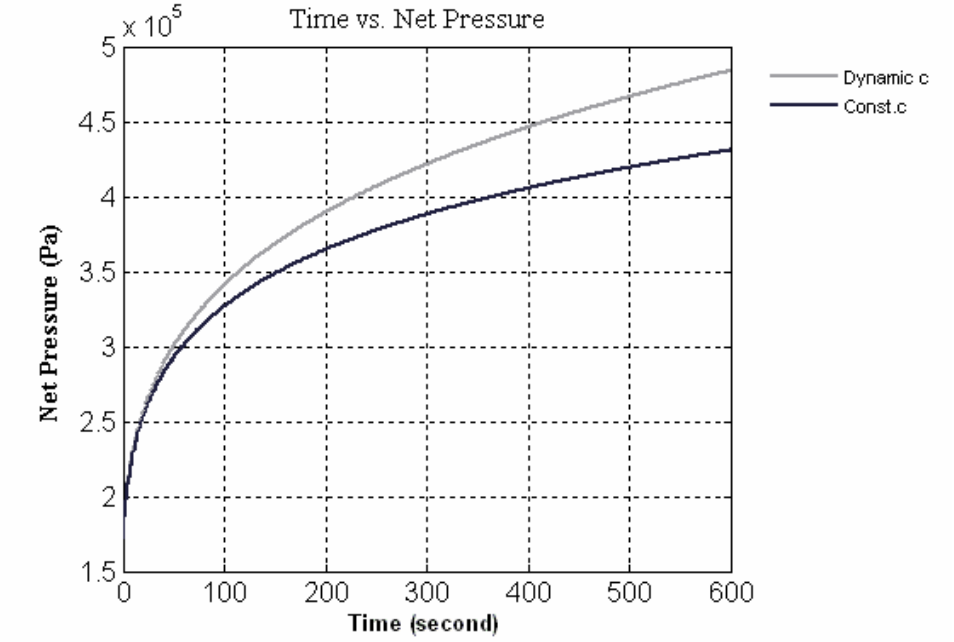

Figure 6.7 e) Time vs. net pressures

Figure 6.7 Injection operated at 300 m with a high leak-off coefficient gives the plots a) Time vs. fracture half-lengths; b) Time vs. fracture widths; c) Time vs. fracture volumes; d) Time vs. leak-off coefficients and e) Time vs. net pressures

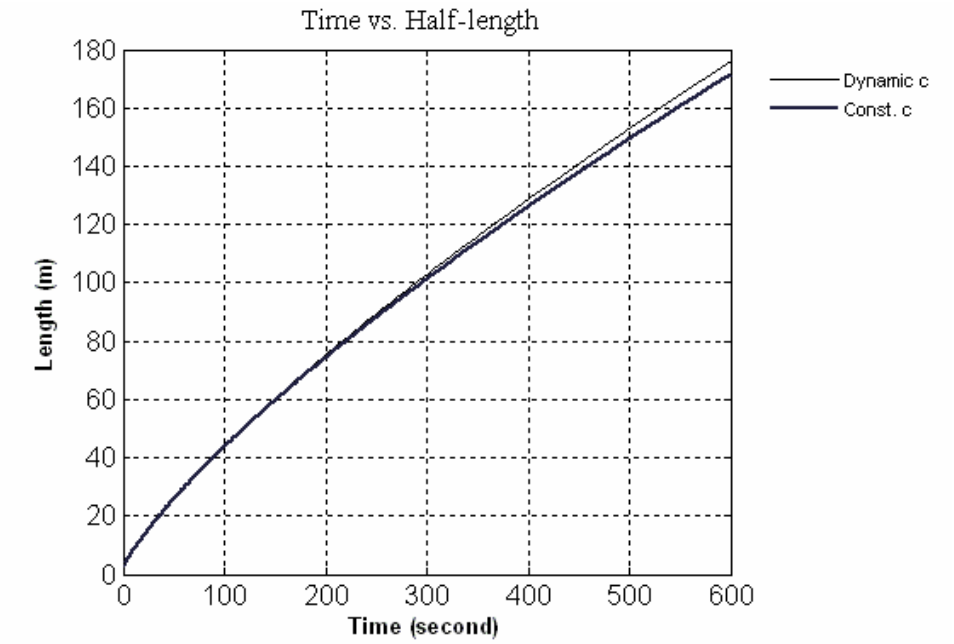

Figure 6.8 a) Time vs. fracture half-lengths

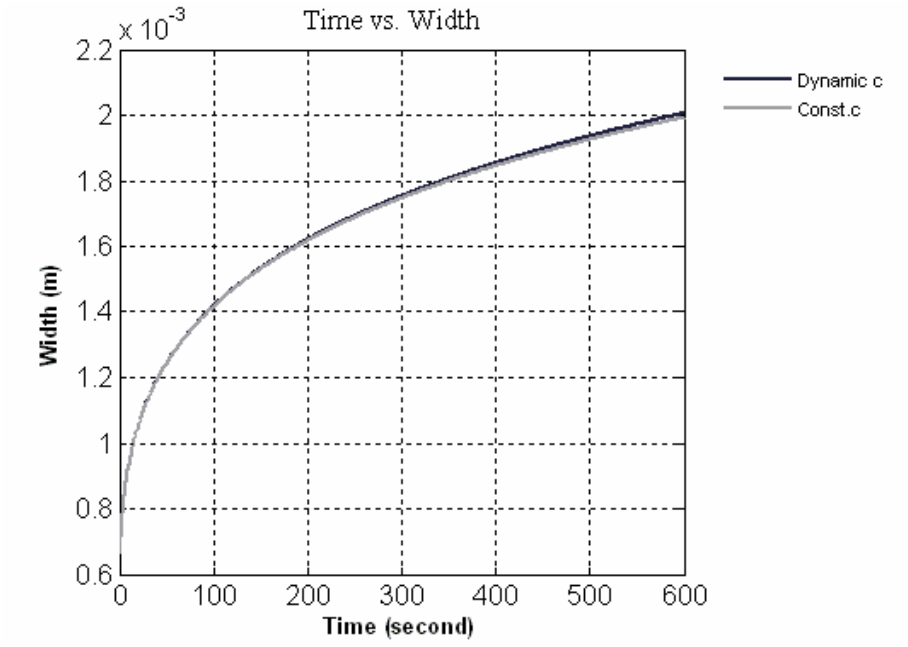

Figure 6.8 b) Time vs. fracture widths

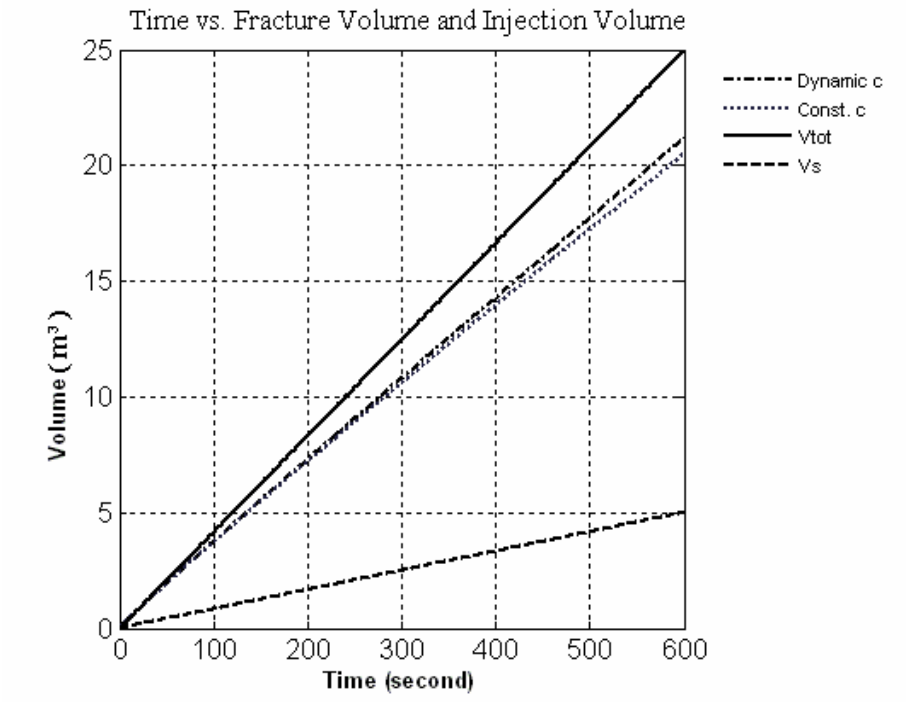

Figure 6.8 c) Time vs. fracture volumes

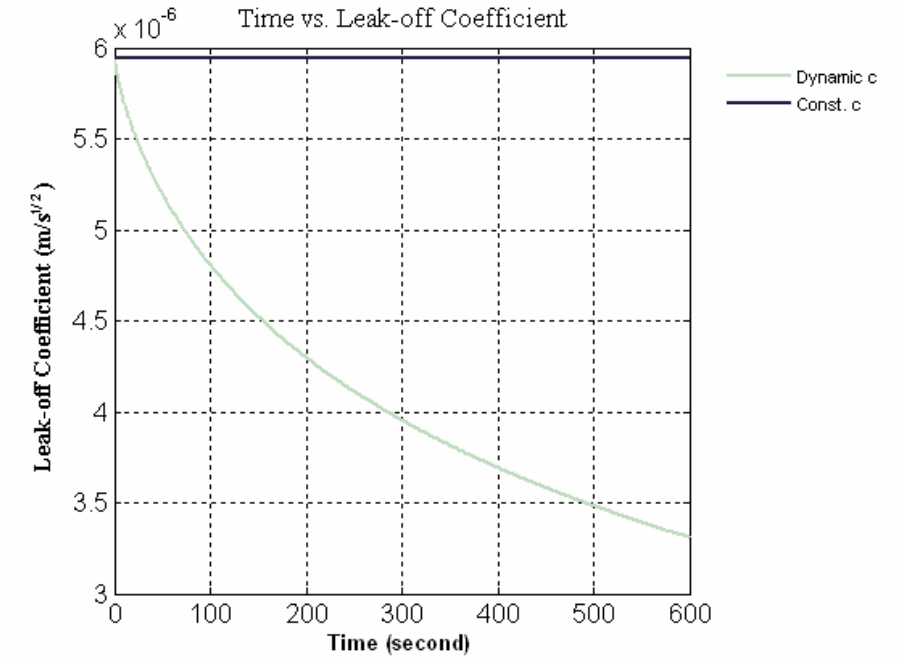

Figure 6.8 d) Time vs. leak-off coefficients

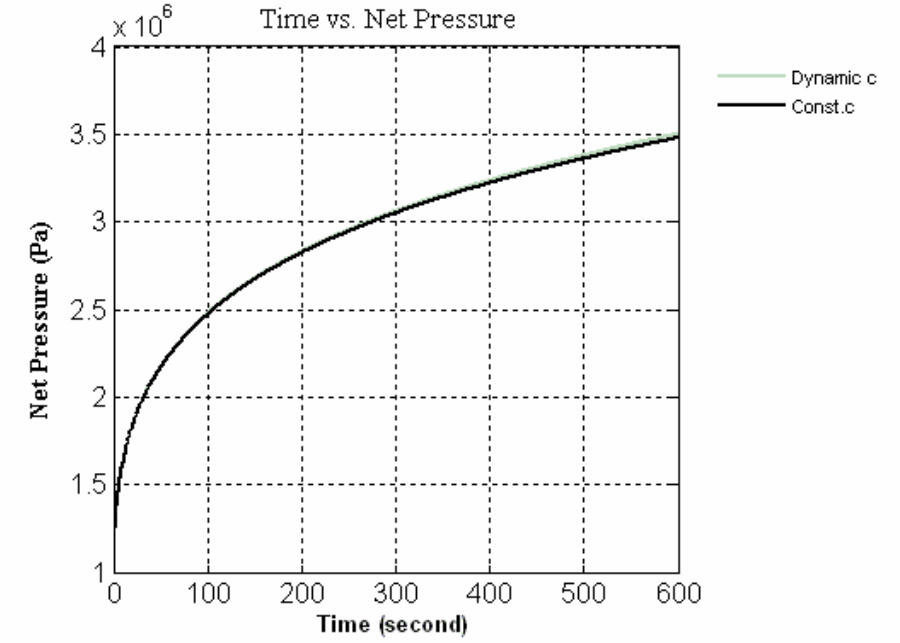

Figure 6.8 e) Time vs. net pressures

In Figure 6.8 injection at 1500 m with a low leak-off coefficient was used, giving the following plots: a) Time vs. fracture half-lengths; b) Time vs. fracture widths; c) Time vs. fracture volumes; d) Time vs. leak-off coefficients, and, e) Time vs. net pressures

Different biosolids characteristics

The biosolids material in the slurry has a distinctively compressible property that is different from the solids content in the regular frac&pack treatment.

The parameter for biosolids compressibility is reduced to 1.5 for highly compressible material from 1.83 for very highly compressible material. The simulation results are plotted in Figure 6.9. The simulation is conducted at a depth of 600 m, keeping all other parameters as in Table 6.2.

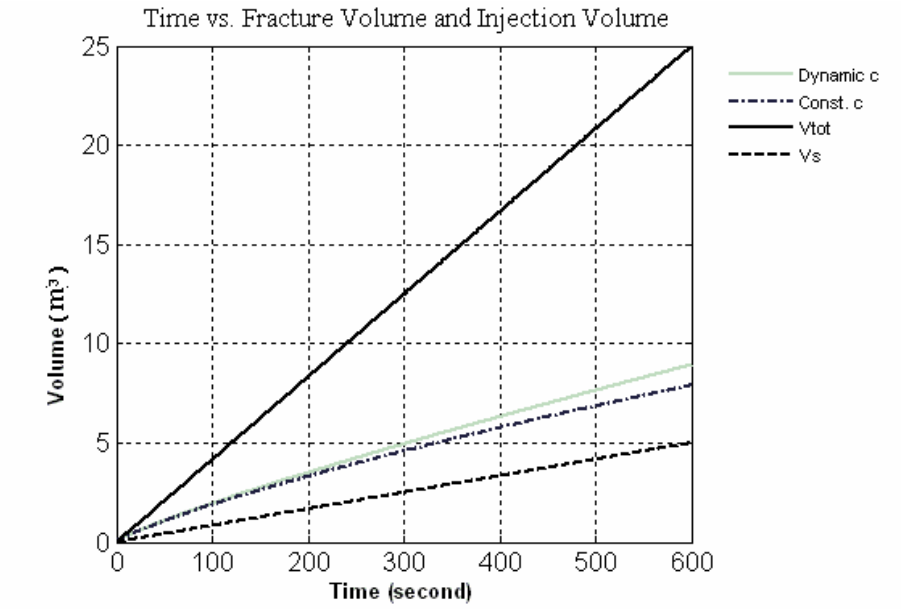

Figure 6.9 a) Time vs. fracture volumes and injection volumes

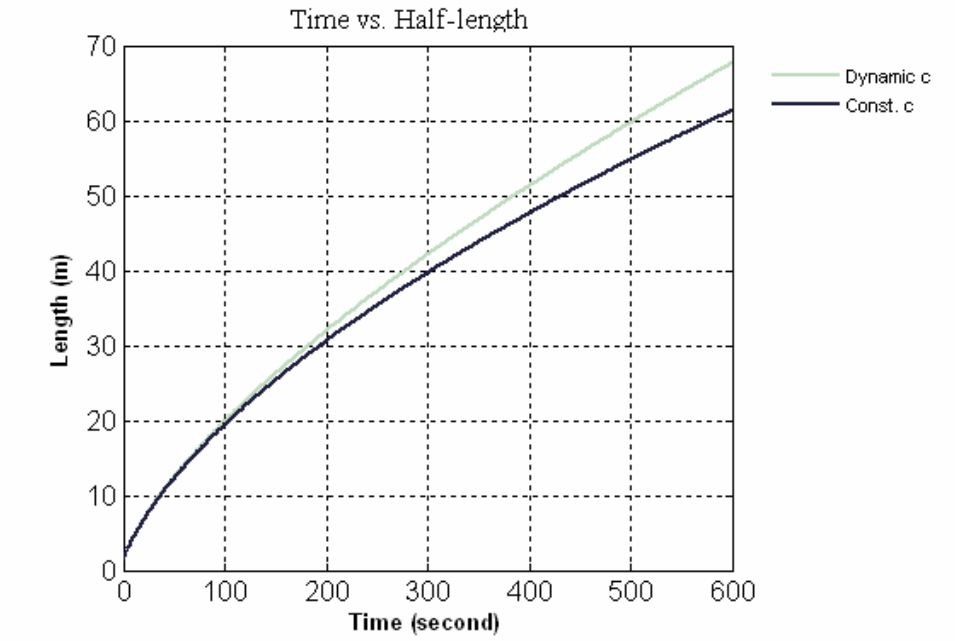

Figure 6.9 b) Time vs. fracture half-lengths

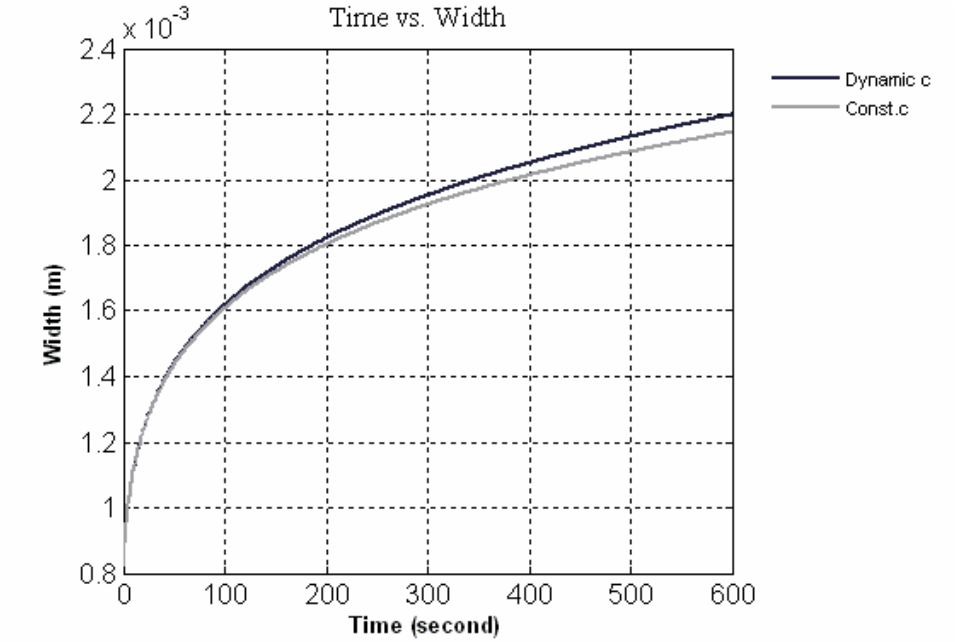

Figure 6.9 c) Time vs. fracture widths

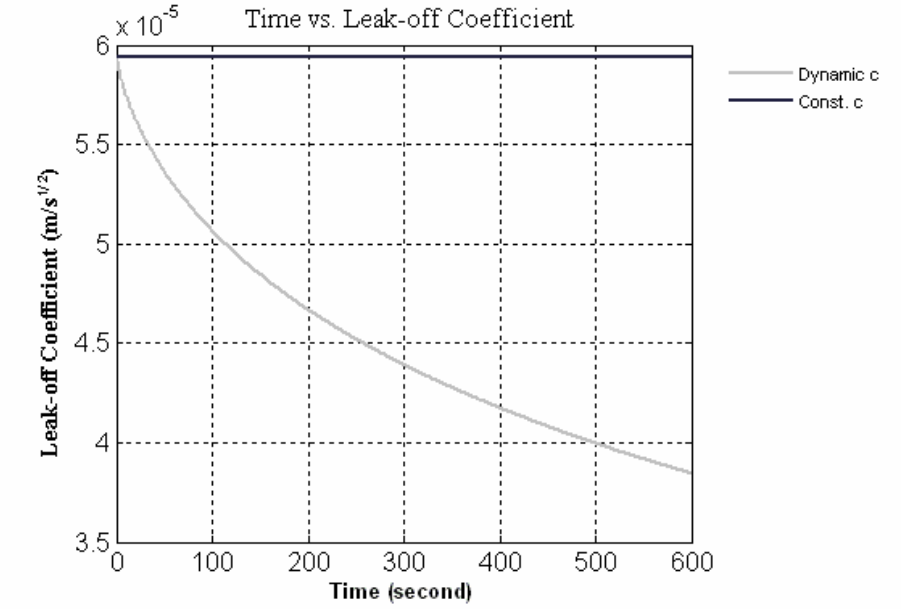

Figure 6.9 d) Time vs. leak-off coefficients

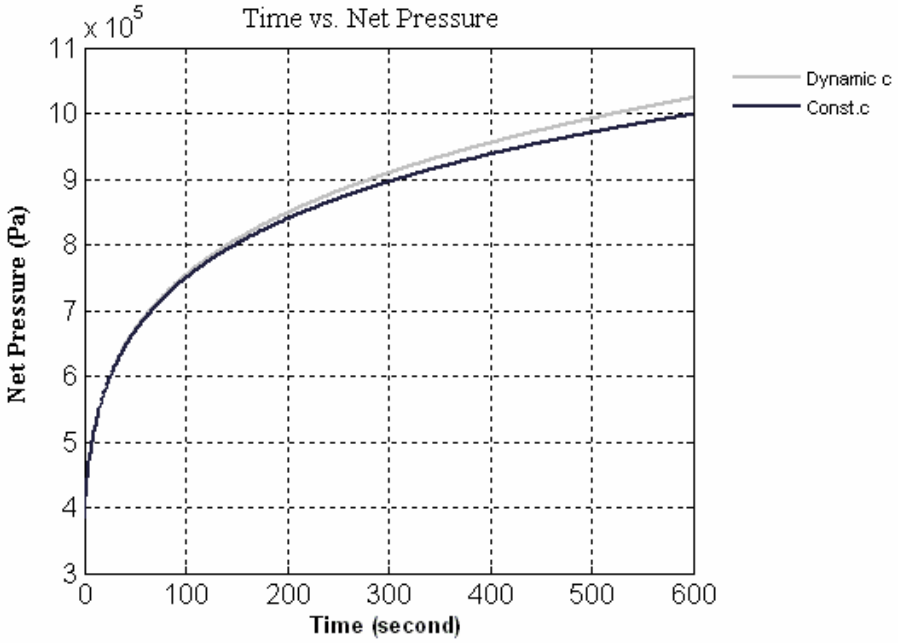

Figure 6.9 e) Time vs. net pressures

In the parametric investigation, four solids contents and different biosolids compressibility parameters are used. The higher solids content of slurry results in thicker filter cake deposited on the fracture face which reduces leak-off rate dramatically, giving a bigger fracture volume. Meanwhile, the result in Figure 6.2 shows that a big volume differential is produced once biosolids is coupled into

the model. With the increase of solids content in the slurry, the impact of solids content declines gradually.

As shown in Figure 6.3 to Figure 6.5, a narrower fracture is generated in deeper formations, because of the bigger Young's modulus. Furthermore, the net pressure is higher when injection is conducted in a deeper formation than in a shallow formation. The filter cake under higher net pressure results in lower leak-off rate. Consequently, a long and narrow fracture is generated as expected at greater depths. Furthermore, a bigger difference in geometry between the dynamic leak-off case and the constant leak-off case is recorded when the process of hydraulic fracture is implemented at a depth of 1500 m than at a shallow depth of 300 m.

Comparing the results in Figure 6.7 with Figure 6.8, one distinct conclusion is that the initial leak-off rate has a significant impact on the geometry of a hydraulic fracture. The impact of depth on the geometry of the fracture at a small leak-off rate is not as much as in a high leak-off rate condition. The fracture volume from the simulation with dynamic leak-off conditions does not deviate too much from the result at constant leak-off conditions.

A smaller value for biosolids compressibility is incorporated into the simulation for 600 m depth. The coefficient is reduced from 1.83 to 1.5, thus the less compressible biosolids have a smaller impact on the leak-off rate. The fracture volume at dynamic leak-off conditions does not deviate much from the fracture volume at constant leak-off conditions. The higher compressibility parameter increases the geometry difference between the dynamic leak-off conditions and the constant leak-off conditions.

6.1.2 Volume of biosolids after compaction

Simple calculations are completed to compute the water content of biosolids after injection, based on the mass balance $V_{total} = V_{solids} + V_{water}$. Because of the high effective stress on the biosolids from the elevated *in situ* loads, a high degree of primary compaction of biosolids is achieved. Hence, the final volume of injected biosolids is dependent on the final effective stress on the biosolids when the fluid pressure is equalized with formation pore pressure. One dimensional consolidation of biosolids is assumed because of the shape of the fracture (long and narrow).

For the injected slurry, which contains 20% of solids by volume, the water content is 280%. The value is calculated using $G_s = 1.55$ for sludge, which is a similar value to specimen E in the work of O'Kelly (see above). The void ratio of slurry can be calculated based on the equation for specimen E in Figure 5.9.

As in the case of an open fracture, the effective stress on the filter cake can range from 0.1 MPa to 8 MPa across the filter cake, and assumed to be linearly increasing across the thickness. The void space of the filter cake across the thickness is plotted in Figure 6.10.

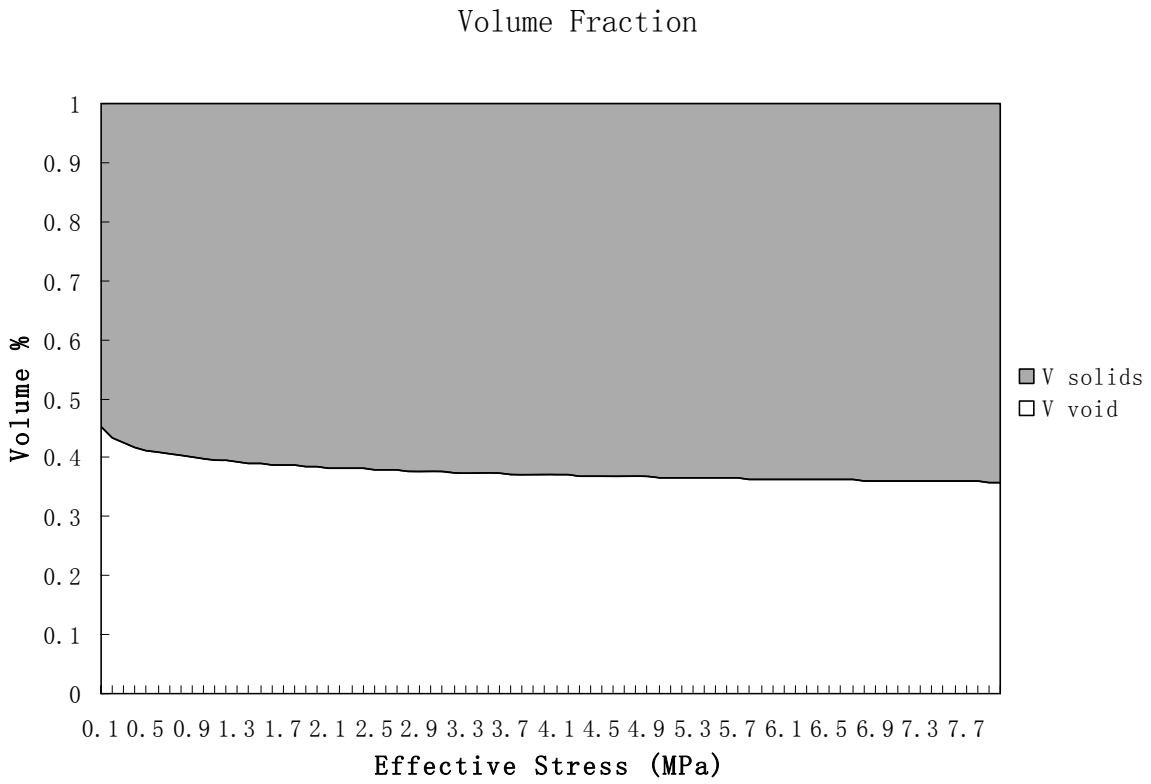

Figure 6.10 Volume fraction of solid to the effective stress

6.2 Discussion and Conclusions

The hydraulic fracture model considers elastic rock behavior, fluid flow, biosolids filtration and consolidation, and massive changes in rock face permeability. This numerical model is used to estimate the fracture volume, length, and biosolids volume in one injection cycle. Comparing simulation results by the proposed model with a typical PKN leak-off model, the fracture volume is larger because of the impaired leak-off, and the compacted biosolids in the fracture generate a remnant volume change in the formation as well. Figure 6.1 shows the basic simulation work. The fracture volume and fracture length correspond to the decrease of leak-off coefficient with injection because of the filtration and cake compaction process.

The calculation of volume change of biosolids during active injection at a depth of 600 m

The results from the simulation of injection at 600 m to 600 s are used to compute the volume change of biosolids in a fracture. The closure stress is 14 MPa, and pore pressure is 6 MPa. The input parameters are listed in Table 6.2. The dimension of the hydraulic fracture is listed in Table 6.3

Table 6.2 Input parameters for injection at 600 m

$Q = 0.042\ m^3/s$	$E = 8\times10^9$ Pa	n = 1.83
H = 30m	$\mu = 0.01$ Pa*s	$P_0 = 1000$ Pa
$C = 5.94\times10^{-5}\ m/s^{1/2}$	$\upsilon = 0.25$	$A_0 = 2.02\times10^{11}$
T = 600 seconds	$\Delta t = 1$ second	q_s=20% of Q

Table 6.3 Dimension of the hydraulic fracture

Half-length of fracture	85 m
Width of fracture	2.33 mm
Volume of fracture	12 m^3

The total volume of slurry injected is 25 m^3. The volume of solids is 5 m^3. Based on the simple calculation, the residual volume of water is 7 m^3. At the point of instantaneous shut-in, the volume of slurry in the fracture is about 48% of the initial volume of slurry. The porosity of slurry at this point is about 60%.

The calculation of volume change of biosolids during closure phase at a depth of 600 m

When the fracture is closed, effective stresses compact the filter cake as the fluid pressure in the filter cake declines back to the formation pore pressure, and then a stable void ratio of biosolids is achieved. The void ratio of filter cake at the effective stress of 8 MPa at a depth of 600 m is 0.55. The porosity of consolidated biosolids in the fracture is about 36%. The final volume of injected slurry is 31% of the initial volume. The volume reduction is resulting from consolidation is given by.

$$Vt = Vs \times (1 + e) = 5\ m^3 \times (1 + 0.55) = 7.75\ m^3 \ : (7.75/25 = 31\%)$$

This volume is computed using only the primary consolidation behavior. Similar calculation can be done once the secondary consolidation and biodegradation behaviors are known.

The consolidation process of biosolids is analyzed in a highly empirical manner and is mainly based on practical laboratory measurements. Because the composition impacts sludge consolidation properties significantly, volumes of different biosolids in a fracture could vary markedly under the same consolidation condition. Hence, the volume change of biosolids in the closure phase should be calculated with the appropriate experimental data.

The entire processes of volume change over time can provide guidelines for the design of biosolids treatment through deep injection. The model cannot give exact predictions of the geometry of fracture and volume change of biosolids by consolidation, but additional effects could be incorporated to address this issue. However, the model can serve as an assessment method for practical purposes.

Chapter 7
Implication and Future Work

The goal of this thesis was to propose a physical model for the deep injection of biosolids in terms of assessment of volume change. This chapter lists the contributions. Furthermore, limitations of the model developed are pointed out as an impetus for further work.

7.1 Implications of the Research Results

7.1.1 Contributions of the research

The primary goal of this thesis is to estimate volume of biosolids in the deep formation through one cycle of injection. The goal has been met with the following contributions:

A new semi-numerical model for the fracture injection of biosolids is proposed for the process of *in situ* placement of biosolids. During the injection process, the filtration of biosolids is an important part of the hydraulic fracture process. The biosolids filter cake formed during the injection affects the geometry of the induced fractures. Therefore, a dynamic leak-off coefficient that changes with injection time is introduced into the model to represent the filtration process. In Chapter 4, the model is coupled with a descriptor that represents a dynamic leak-off coefficient to modify the simulation results from the traditional PKN leak-off model.

The resistance of the filter cake is calculated based on filtration theory for highly compactable biosolids as stated in Chapter 3. The equation developed for the flow resistance of filter cake is substituted into the pseudo-leak-off coefficient equation. Therefore, the leak-off coefficient is a function of the net pressure on the filter cake, the amount of biosolids injected, and the time since the opening of the fracture.

Based on the data published in the literature about the consolidation properties of biosolids, approximate equations used to represent the properties are developed for the calculation of volume change. Hence, the volume change of biosolids occurring in the closure phase can be estimated.

7.1.2 Limitations

The developed method is divided into two parts including the injection phase and the closure phase. The computational model for the hydraulic fracture injection has its limitations, just as other computational hydraulic fracture models.

In the hydraulic fracture model, an important assumption is the constant height fracture that confines the propagating fracture to a constant height. The second one is the plane strain condition of the hydraulic fracture, which could make the problem solvable, while it is not strictly true. The assumptions confine the growth of the fracture to two dimensions defined by width and length. Although proper geological sites should have strict barriers above and below the injecting zone, the fracture could propagate in height over time.

In the estimation of the propagation of a fracture, it is divided into a series of elements. The assumption of self-similar propagation for each element is made, and this results in errors to some extent because absolute self-similarity is violated with time.

In the implementation of the dynamic leak-off coefficient, the amount of biosolids injected controls the resistance of the filter cake to flow, and is closely related to the leak-off coefficient. However, its thickness has a strong relation to the propagation of the fracture; the biosolids filter cake is treated as having an even disposition on the fracture face of each element in terms of equal deposition at each step on each element face. It is a simplified assumption for the leak-off coefficient. The computational model has good performance when a proper resistance of the formation and the proper time step size for the calculation are introduced into the model, but the algorithm can experience instability or errors. A long time period of injection also can induce a big error because of very thick filter cake build up. This thick filter cake influences the stress profile underground, in turn controlling the geometry of fracture. This can cause a change in fracture orientation, or the re-injection of a new fracture. This is beyond the scope of this work, and must be addressed with more complex numerical models.

For the consolidation phase, 1-D consolidation is assumed to occur in the closure phase and this makes the problem solvable. However, the results need to be carefully calibrated. The method could provide guidance for a long term change of volume but not for precise prediction.

7.2 Future Work Requirements

In this thesis, a review of the literature on the mechanisms of hydraulic fracture, filtration of highly compactable sludge and consolidation properties of biosolids is conducted. Most hydraulic fracture models are developed based on one of the two major 2-D models coupled with various geological properties. The injection of a high content of solids has not been investigated. The distinct properties of solids injected impacts the fluid filtration through the fracture face over the whole process. Hence, the fluid flow properties could affect biosolids injection. Furthermore, the large amount of solids placed inside the fracture underground alters the stress profile, correspondingly changing the orientation and geometry of the fracture. In order to make a precise estimation of volume change, the *in situ* stress profile should be investigated simultaneously and introduced into the models.

After the placement of biosolids underground, a series of volume change processes occur. Biosolids undergo a shrinkage process, mostly caused by consolidation and degradation. Consolidation is highly dependent on the components in the biosolids. More studies on consolidation properties of biosolids are required to collect data for further analysis. During degradation, organic

components in biosolids are consumed by microbes; hence, the volume of the biosolids will decrease substantially. Meanwhile, methane is produced along with the degradation. If large amounts of methane can be produced by biosolids placed underground, profit will offset some cost of this operation. Also, carbon left behind after biodegradation may have a value as sequestered carbon when a carbon-tax regime is implemented, giving an extra economical incentive. Therefore, research on the methane production and accumulated from underground injection of biosolids should draw more interest, as well as carbon sequestration.

Appendix A

Computational Code for Hydraulic Fracture in Matlab

Master code*:*

```
function [pw,pww,X,XX,V,VV,C,W,WW] = PKNt(T)
clc
global q h c g u v c01 m n
[m,n]=size(T);
q=2.5/60;
h=30;
c=5.9386e-5;
g=1.5e10;
u=0.01;
v=0.25;
c01=2.05*(u*q/(2*g/(1-v)))^(1/4);
[X,W,V,C,pw,WM]=PKNCTest(T);
[XX,CC,VV,WW,pww]=PKNCcon(T);
WW=c01*XX.^(1/4);
AA=XX.*h;
Vtotal=T.*q;
Vs=T.*q*0.2;
figure,plot(T,V,'g-',T,VV,'b-',T,Vtotal,'k-',T,Vs,'k--','LineWidth',2),grid on
title('Time VS Frac Volume and Inj Volume')
xlabel('Time (second)')
ylabel('Volume (cubic meter)')
legend('Dynamic c','Const. c','Vtot','Vs')
figure,plot(T,X,'g-',T,XX,'b-','LineWidth',2),grid on
title('Time VS Half-length')
xlabel('Time (second)')
ylabel('Length (m)')
legend('Dynamic c','Const. c')
figure,plot(T,C,'g-',T,CC,'b-','LineWidth',2),grid on
title('Time VS Leak off coefficient')
xlabel('Time (second)')
ylabel('Leak off coefficient (m/s1/2)')
legend('Dynamic c','Const. c')
```

```
figure,plot(T,pw,'g-',T,pww,'b-','LineWidth',2),grid on
title('Time VS Net pressure')
xlabel('Time (second)')
ylabel('Net pressure (pa)')
legend('Dynamic c','Const.c')
figure,plot(T,WM,'r-',T,W,'b-',T,WW,'g-','LineWidth',2),grid on
title('Time VS Width')
xlabel('Time (second)')
ylabel('Width (m)')
legend('Waste Material','Dynamic c','Const.c')
return
```

***Dynamic leak off code**:*

```
function [X,W,V,C,pw,WM]=PKNCTest(T)
clc
global q h c g u v t a1 a2 a4 m n
%assign matrix
A=zeros(m,n);
X=zeros(m,n);
W=zeros(m,n);
K=zeros(m,n);
V=zeros(m,n);
C=zeros(m,n);
C(1)=c;
c01=2.05*(u*q/(2*g/(1-v)))^(1/4);
t=T(n)/(n-1);
a1=2.05*(u*q/(2*g/(1-v)))^(1/4);
a2=4*c*sqrt(t);
%initial state of fracutre @ time =1
X(1)=feval(@findRoot,t);
A(1)=X(1)*h;
W(1)=c01*X(1)^(1/4);
V(1)=A(1)*W(1);
pw(1)=4*(2*g^3*u*(q/2)*X(1)/(h^4*pi^2*(1-v)^3))^(1/4);
K(1)=c*X(1)/sqrt(n-1+.25);
```

```
Rf=pw(1)*sqrt(t)/(pi*u*c);          %resistance of formation
%coeff for leak off rate
nn=1.83;
p0=1000;
coeff=1;
%coeff=5;
a0=2.02e11;
ww=0;
%Iterate to calculate each step from time =2 to the end
epsilon=1e-10;
for j=2:n
   w=W(j-1);
   a=X(j-1);
   r=K(j-1);
   a4=q*t/(2*h)+(4*c*sqrt(t)+w)*a-2*sqrt(t)*r;
   %a4=q*t+(4*c*sqrt(t)+w)*a
   x1=X(j-1);
   x3=X(j-1)+j*1;
   x=[x1:0.001:x3];
   R=feval(@approot,x,epsilon);
   %R=approot(x,epsilon);
   X(j)=R;
   A(j)=X(j)*h;
   W(j)=c01*X(j)^(1/4);
   pw(j)=4*(2*g^3*u*(q/2)*X(j)/(h^4*pi^2*(1-v)^3))^(1/4);
   tt=t*j;
%add C function HERE to control the leak off rate.
   cc=a0*(1+pw(j)/p0)^nn;
   ww1=(q/2)*t*0.2/(2*X(j-1)*h);
   ww=ww1+ww;
   WM(j)=ww;
   %ww2=(q/2)*t*j*0.2/(2*X(j-1)*h);
   %WM2(j)=ww2;
   %RR(j)=(q/2)*tt*0.2/(2*X(j-1));
   %RR(j)=u*cc*((q/2)*tt*0.2/(2*X(j-1)));
```

```
   %Rf=pw(j)*sqrt(t)/(pi*u*c);
   C(j)=(pw(1)*t^(1/2))/(pi*u*(Rf+u*cc*ww));
   %C2(j)=coeff*(pw(j)*tt^(1/2))/(u^2*cc*ww);
   lk=K(1);
      for l=2:j
         aa=X(l-1);
        if l-2==0;
            ab=0;
         else
            ab=X(l-2);
         end
         cr=C(j-l+2);
         lk1=cr*(aa-ab)/sqrt(j-l+0.25);
         lk=lk1+lk;
      end

% assign leak off rate values for next step
   K(j)=lk;
%calculate the volume for this step
   V(j)=A(j)*W(j)*2;
End
```

Roots finding code:

```
function R= approot (x,epsilon)
Y=f(x);
yrange=max(Y)-min(Y);
epsilon2=yrange*epsilon;
n=length(x);
m=0;
x(n+1)=x(n);
Y(n+1)=Y(n);
for k=2:n,
   if Y(k-1)*Y(k)<=0,
      m=m+1;
      R(m)=(x(k-1)+x(k))/2;
```

```
    end
    s=(Y(k)-Y(k-1))*(Y(k+1)-Y(k));
    if (abs(Y(k))<epsilon2)&(s<=0),
        m=m+1;
        R(m)=x(k);
    end

end
```

References

Arfie, M., Marika, E., Purbodiningrat, E.S. and Woodard, H.A. 2005. Implementation of Slurry Fracture Injection Technology for E&P Wastes at Duri Oilfield. Paper SPE 96543 presented at the SPE Asia Pacific Health, Safety and Environment Conference and Exhibition held in Kuala Lumpur , Malaysia , 19–20 September.

Bastian, R. 1997. The Biosolids (Sludge) Treatment, Beneficial Use, and Disposal Situation in the USA. European Water Pollution Control Journal. Vol. 7, No. 2, pp. 62-79. March.

Braja M. D. 1997. Advanced Soil Mechanics Second Edition. 2nd ed. Washington: Taylor & Francis Ltd.

Bruno, M.S. 2000. Converting Biosolids to Energy by Deep Well Injection and Biodegradation. Paper Presented at the Canadian National Residuals and Biosolids Management Conference, Toronto, Ontario, September 24-26.

Bruno, M.S., Young, J.T., Moghaddam, O., Wong, H., and Apps, J.A. 2005. Chapter 46: Thermal Treatment, Carbon Sequestration, and Methane Generation Through Deep-Well Injection of Biosolids. In Underground Injection Science and Technology, C.F. Tang and J. Apps, ed., Elsevier, Amsterdam, 2005.

Campbell, H.W., Rush, R.J. and Tew, R. 1978. Sludge Dewatering Design Manual. Research Report No. 72, Ontario Ministry of the Environment. Toronto, Ont.

Carter, R.D. 1957. Derivation of the General Equation for Estimating the Extent of the Fractured Area, Appendix to "Optimum Fluid Characteristics for Fracture Extension", by Howard, G.C. and Fast, C.R., Drilling and Production Practices, API, pp. 261-270.

Cleveland, T.G., Tiller, F.M and Lee, J.B. 1996. Theory of Filtration of Highly Compactable Biosolids. Water Science. and Technology. Vol. 34, No. 3-4., pp. 299-306.

Council of Economic Advisors. 1999. Economic Report of the President, US Government Printing Office, Washington, DC.

Drost, R.L. 1996. Theory and Practice of Water and Wastewater Treatment. New York: John Wiely& Son

Dusseault, M.B. 1993. Slurry Injection Disposal of Granular Solid Waste. Proceeding International Symposium on Geology and Confinement of Toxic Wastes, France, Balkema (Rotterdam), pp. 511-518

Dusseault M. B., Bilak, R.A., and Rodwell, G. L. 1997. Disposal of Dirty Liquids Using Slurry Fracture Injection. Paper SPE 37907 presented at the SPE/EPA Exploration and Production Conference, Dallas, TX, 3-5, Mar.

Dusseault, M.B. 2003. Report of Municipal Waste Treatment Using Deep Biosolids Injection. Unpublished.

Eberhardt, E. 2004. In Situ Stress & Stress Measurement. Course power point for Geotechnical Engineering Practice & Design, university of British Columbia, Vancouver, Canada.

Epstein, E. 2002. Land Application of Sewage Sludge and Biosolids. CRC Press. LLC.

Fan, Y. and Economides, M.J. 1995. Fracturing Fluid Leak-off and Net Pressure Behavior in Frac&Pack Stimulation. Paper SPE 29988. International Meeting on Petroleum Engineering. Beijing, 14-17 November.

Fang, H.Y. 1997. Introduction to Environmental Geotechnology. CRC Press. LLC.

Geertsma, J. and de Klerk, F. 1969. A Rapid Method of Predicting Width and Extent of Hydraulically Induced Fractures. Journal of Petroleum Technology, Vol. 21, No. 12, pp. 1571-1581.

Gidley, J.L., Holditch, S.A., Nierode, D.E. and Veatch, R.W. 1989. Recent Advances in Hydraulic Fracturing, Monograph No. 12, Society of Petroleum Engineers, Dallas, Texas.

Gulbis, J. 1982. Dynamic Fluid Loss Study of Fracturing Fluids. Paper CIM 82-33-18 presented at the 1982 Annual Technical Meeting of the Petroleum SW. of CIM, Calgary, 6-9 June.

Gulbis, J. 1983. Dynamic Fluid Loss of Fracturing Fluids. Paper SPE 12154 presented at the 1983 SPE Annual Technical Conference and Exhibition, San Francisco, Oct 5-8

Hainey, B.W., Keck, R.G., Smith, M.B., Lynch, K.W. and Barth, J.W. 1997. On-site Fracturing Disposal of Oilfield Waste Solids in Wilmington Field, Long Beach Unit, CA. Paper SPE 38255 presented at the 1997 Western Regional Mtg. of SPE, Long Beach, California, 23-27 June.

Harkness, G.E, Reed, C.C., Voss, C.J. and Kunihiro, C.I. 1994. Composting in the Magic Kingdom. Water Environment and Technology, Vol. 6, No. 8, pp. 64-67

Imhoff, K., Muller, W.J. and Thistlethwayte, D.K.B. 1971. Disposal of Sewage and Other Water-borne Wastes. Butterworths, London, UK.

Lee, D.J. and Wang, C.H. 2000. Theories of Cake Filtration and Consolidation and Implications to Sludge Dewatering. Water Resources Vol. 34, pp. 1-20.

Khristianovic, S.A and Zheltov, Y.P. 1955. Formation of Vertical Fracture by Means of Highly Viscous Fluids, Proceeding World Petroleum Congress, Rome, Vol. 2, pp. 579-586,

Koenders M. A. and Wakeman R. J. 1995. Radial Flow Dependence in Filtration Experiments. Chemical Engineering Science. Vol. 50, pp. 3777-3782.

Kvenvolden, K. 1995. Natural Gas Hydrate Occurrence and Issues. Sea Technology. Vol. 36, pp. 69-74.

Malachosky, E., Shannon, B.E. and Jackson, J.E. 1991. Offshore Disposal of Oil Based Drilling Fluid waste. SPE 23373; presented at the International Conference on Health, Safety and Environment, The Hague, Netherlands.

Mathews, J.H., Fink, K.D. 2003. Numerical Methods Using Matlab 4th ed. New York: Prentice Hall.

Mayerhofer, M.J., Economides, M.J. and Nolte, K.G. 1991a. Experimental Study of Fracturing Fluid Loss. Paper CIM/AOSTRA 91-92, Annual Technical Conference of the Pet. Soc. of CIM and AOSTRA, Banff, 21-24 April.

Mayerhofer, M.J., Economides, M.J. and Nolte, K.G. 1991b. An Experimental and Fundamental Interpretation of Fracturing Filter-Cake Fluid Loss. 66th Annual Technical Conference and Exhibition. SPE, Dallas, TX, October. Paper SPE 22873

Mayerhofer, M.J., Economides, M.J. and Ehlig-Economides, C.A. 1993. Pressure Transient Analysis of Fracture Calibration Tests Paper SPE 26527 Presented at 68th Annual Technical Conference and Exhibition, Houston , Texas, 3-6 October

McDaniel, R.R., Deysarkar, A.K., Callanan, M.J. and Kohlhaas, C.A. 1985. An Improved Method for Measuring Fluid Loss at Simulated Fracture Conditions. Society of Petroleum Engineers Journal. Vol. 25, No. 4, pp. 482-490 (6 ref.).

McFarland, M.J. 2000. Biosolids Engineering. New York: McGraw-Hill.

Nadeem, M. 2003. Geological Suitability of Most Populated US Metropolitan Areas for Deep Biosolids Injection. Terralog Technologies Inc. Calgary, Canada, pp. 134.

Nadeem, M. 2005. Reservoir Screening Criteria for Deep Slurry Injection. M.Sc. thesis. University of Waterloo, Canada.

National biosolids partnership. 2005a. Annual Report 2004-2005. < http://biosolids.org/docs/nbp_04-05_annrpt_final.pdf>. Accessed Nov 20, 2006.

National biosolids partnership. 2005b. National Manual of Good Practice for Biosolids. Jan, 2005. <http://biosolids.org/docs/MGP_National_Manual_of_Good_Practice_0105.pdf >. Accessed Nov 20, 2006.

NEBRA. 2005. Official usage of the term "biosolids". New England Biosolids & Residuals Association - Information update July 2005. < www.nebiosolids.org/pdf/Biosolids-theWord-Jul05.pdf >. Accessed Nov 20, 2006.

Nordgen, R.P. 1972. Propagation of a Vertical Hydraulic Fracture. Society of Petroleum Engineers Journal. Vol. 12, pp. 306-314. SPE 3009

Obert, L. and Duvall, W.I. 1967. Rock Mechanics and the Design of Structures in Rock. New York: John Wiley & Sons, Inc.

Office of Technology Assessment. 1983. Technologies and Management Strategies for Hazardous Waste Control (Washington, D.C., March 1983), 195.

O'Kelly,B.C. 2005. Mechanical Properties of Dewatered Sewage Sludge. Waste Management, Vol. 25, No. 1, pp. 47-52.

Perkins, T.K. and Kern, L. R. 1961. Width of Hydraulic Fracturing, Journal of Petroleum Technology, Vol. 13, No. 9, pp. 937-949.

Reed, A.C., Mathews, J.L., Bruno, M.S. and Olmstead, S.E. 2001. Chevron Safely Disposes One Million Barrels of NORM in Louisiana Through Slurry Fracture Injection. Paper SPE 71434 presented at the Proc. 2001 Annual Technical. Conference, New Orleans, Louisiana, September 30 - October 3.

Roodhart, L. P. 1985. Fracturing Fluids: Fluid-loss Measurements under Dynamic Conditions. Society of Petroleum Engineers Journal. Vol. 25, Issue: 5, Oct

Roodhart, L.P., Fokker, P.A., Davies, D.R., Shlyapobersky, J and Wong, G.K. 1993. Frac and Pack stimulation: Application, Design, and Field Experience from the Gulf of Mexico to Bomeo, paper SPE 26564 presented at 1993 SPE Annual Technical Conference and Exhibition held in Houston, TX, Oct 3-6.

Schmidt, D.R. and Zoback,M.D. 1989. Poroelasticity Effect in the Determination of Minimum Horizontal Principal Stress in Hydraulic Fracture Test- A Proposed Breakdown Equation Employing a Modified Effective Stress Relation for Tensile Failure. International journal of rock Mechanics, Mining Science & Geomechanic Abstracts Vol. 26, No. 6, pp. 499-506

Schmidt, J.H., Friar, W.L., Bill, M.L. and Cooper, G.D. 1999. Large Scale Injection of North Slope Drilling Cuttings. Paper SPE 52738 presented at the 1999 SPE/EPA Exploration and Production Environmental Conference, Austin, Texas, 28 February-3 March 1999.

Schuh,P.R, Secoy, B.W and Sorrie, E. 1993. Case History: Cuttings Re-injection on the Murdoch Development Project in the Southern Sector of the North Sea. Paper SPE 26680 presented at SPE Offshore European Conference Aberdeen, Scotland, 1993, Vol. 1, pp. 83-98

Settari, A. 1985. A New General Model of Fluid Loss in Hydraulic Fracturing. SPE Journal of Petroleum Technology, Aug, pp. 491-501

Settari, A. 1988. General Model of Fluid Flow (Leakoff) From Fractures Induced in Injection Operations. paper SPE 18197 presented at 1988 SPE Annual Technical Conference and Exhibition held in Houston, TX, Oct 2-5

Shirato, M., Sambuichi, M., Kato, H. and Agagaki, T. 1969. Internal Flow Mechanism in Filter Cake. American Institute of Chemical Engineers Journal. Vol. 15, pp. 405-409

Shirato, M., Murase T., Tokunaga, A. and Yamada, O. 1974. Calculations of Consolidation Period in Expression Operations. Journal of Chemical Engineers. Japan. Vol. 7, pp. 229-231

Skempton, A.W. and Petley, D.J. 1970. Ignition Loss and Other Properties of Peats and Clays from Avonmouth, King's Lynn and Cranberry Moss. Geotechnique, Vol. 20, No. 4, pp. 343-356

Srinivasan, M.M.S., Bruno, M.S., Bilak, R.A. and Danyluk, P.G. 1997. Field Experiences with Oilfield Waste Disposal Through Slurry Fracture Injection. Paper SPE 38254 presented at the 1997 Western Regional Mtg. of SPE, Long Beach, CA, 23-27

Srinivasan, M.M.S., Bruno, M.S., Hejl, K.A., Danyluk, P.G. and Olmstead, S.E. 1998. Disposal of crude contaminated soil through slurry fracture injection at the West Coyote Field in California. SPE 46239, presented at the SPE Western Regional Meeting, Bakersfield, CA, May 10-13.

Terralog Technologies Inc. < http://www.terralog.com/thermal_treatment.asp >. Accessed Nov 20, 2006

Texas Department of Water Resources. 1984. Underground Injection Operations in Texas. December 3-1

Texas Center for Policy Studies and Environmental Defense. 2006. Texas Environmental Profiles – An information and on-line activism resource for the state of Texas. <http://www.texasep.org/html/wst/wst.html>. Accessed Nov 20, 2006.

Tiller, F.M. and Kwon, J.H. 1998. Role of porosity in filtration: XIII. Behavior of Highly Compactible cakes. American Institute of Chemical Engineers Journal. Vol. 44, No. 10, pp. 2159-2167

Tiller, F.M., Lu, R., Kwon, J.H. and Lee, D.J. 1999. Variable Flow Rate in Compactable Filter Cakes. Water Resources. Vol. 33, No. 1, pp. 15-22

Timoshenko, S. and Goodier, N.J. 1951. Theory of Elasticity, 2nd ed. New York: McGraw Hill.

Tsang, C.F. and Apps, J.A. 2005. eds. Section VI Injection of Solids. In Underground Injection Science and Technology. Amsterdam: Elsevier Inc.

USDA (United States Department of Agriculture). 1997. Interagency Agreement between the U.S. EPA and USDA, Agricultural Research Service with Respect to Beneficial Management of Municipal Biosolids and Other Municipal and Agricultural Organic and Inorganic Recyclable Products.

US EPA (US Environmental Protection Agency). 1994. A Plain English Guide to the EPA part 503 Biosolids Rule. EPA 832R93003. Septermber. <http://www.epa.gov/OWM/mtb/biosolids/503pe/index.htm>

US EPA (US Environmental Protection Agency). 1999. Biosolids Generation, Use, and Disposal in the United State. EPA530-R-99-009. < www.epa.gov/epaoswer/non-hw/compost/biosolid.pdf >

US EPA (US Environmental Protection Agency). 2000a. Guide to Field Storage of Biosolids. EPA832-B-00-007. July. < http://www.epa.gov/owm/mtb/biosolids/fsguide/>

US EPA (US Environmental Protection Agency). 2000b. Biosolids Technology Fact Sheet Alkaline Stabilization of Biosolids. EPA 832-F-00-052. September. <http://www.epa.gov/owm/septic/pubs/alkaline_stabilization.pdf>

US EPA (US Environmental Protection Agency). 2000c. Biosolids and Residuals Management Fact Sheet: Odor Control in Biosolids Management. EPA 832-F-00-067, September. <www.epa.gov/owm/mtb/odor_control-biosolids.pdf >

US EPA (US Environmental Protection Agency). 2002a. Protecting Drinking Water Through Underground Injection Control EPA 816-K-02-001. Jan 2002. <http://www.epa.gov/safewater/uic/uicpocket.html>

US EPA (US Environmental Protection Agency). 2002b. Biosolids Technology Fact Sheet Use of Composting for Biosolids Management EPA 832-f-02-024 September. <http://www.epa.gov/owm/mtb/combioman.pdf>

US EPA (US Environmental Protection Agency). 2004. Evaluation of Impacts to Underground Sources of Drinking Water by Hydraulic Fracturing of Coalbed Methane Reservoirs. EPA 816-R-04-003, June. < http://www.epa.gov/safewater/uic/cbmstudy/docs.html>

US EPA, Underground Injection Control (UIC) Program. 2006. UIC Class V Experimental Permit (Biosolids injection) - City of Los Angeles. < http://www.epa.gov/region9/water/groundwater/uic-permits.html>. Accessed Nov 20, 2006.

Valko, P. and Economides, M.J. eds. 1995. Hydraulic Fracture Mechanics. New York: John Wiley& Sons.

Veil, J.A and Dussseault, M.B. 2003. Evaluation of Slurry Injection Technology for Management of Drilling Wastes. Argonne National Laboratory Report for the US Department of Energy, W-31-199-Eng-38, 110 pages.

Wakeman R.J., Sabri M.N. and Tarleton E.S. 1991. Factors Affecting the Formation and Properties of Wet Compacts. Powder Technical. Vol. 65, pp. 283-292.

Walker, J. 1998. Biosolids Management, Use and Disposal. In: Encyclopedia of Environmental Analysis and Remediation. Robert A. Meyers, ed. New York: John Wiley & Sons, Inc.

Water Environment Federation. 1995. Wastewater Residuals Stabilization: Manual of Practice, FD-9.

Wellsbury, P., Goodman, K., Barth, T., Cragg, B.A., Barnes, S.P. and Parkes, R.J. 1997. Deep Marine Biosphere Fuelled by Increasing Organic Matter Availability During Burial and Heating. Nature. Vol. 388, pp. 573-576

Wong, G.K., Fors, R.R., Casassa, J.S., Hite, R.H. and Shlyapobersky, J. 1993. Design, Execution and Evaluation of Frac and Pack (F&P) Treatments in Unconsolidated Sand Formations in the Gulf of Mexico. paper SPE 26563 presented at 1993 SPE Annual Technical Conference and Exhibition held in Houston, TX, Oct 3-6.

Yew, C.H. 1997. Mechanics of Hydraulic Fracturing. Houston: Gulf Publishing.

Yi, T.C. and Penden, J.M. 1993. A Comprehensive Model of Fluid Loss in Hydraulic Fracturing. paper SPE 25493 presented at 1993 Production Operations Symposium held in Oklahoma City, OK, March 21-23.